N°d'ordre: 4670

THÈSE

PRÉSENTÉE À

L'UNIVERSITÉ BORDEAUX 1

ÉCOLE DOCTORALE DES SCIENCES PHYSIQUES ET DE L'INGÉNIEUR

PAR **Carlotta NEGRI**

POUR OBTENIR LE GRADE DE

DOCTEUR

SPÉCIALITÉ: Lasers, Matière et Nanosciences

Controlling electron transport: quantum pumping and single-electron tunneling oscillations

Thèse dirigée par Fabio PISTOLESI

Soutenue le: 14 Décembre 2012

Devant la commission d'examen formée de:

Mme GUICHARD Wiebke	Institut Néel, Grenoble - Professeur, Membre IUF	Rapporteur
M. HOUZET Manuel	INAC/SPSMS, CEA Grenoble - Ingénieur de recherche	Rapporteur
M. PISTOLESI Fabio	LOMA, U. Bordeaux 1 - Directeur de Recherche	Directeur de Thèse
M. PORTIER Fabien	DSM/IRAMIS/SPEC/GNE, Saclay - Ingénieur de recherche	Membre du jury
M. WÜRGER Alois	LOMA, U. Bordeaux 1 - Professeur	Président du Jury

In case of doubt, run it out.

Frank Sacherer

Contents

Overview **1**

Part I : Nonadiabatic dissipative quantum pumping **3**

Introduction **4**

1 A brief introduction to quantum pumping **6**

2 Quantum pumping in a three-site system **9**

3 Solution for the isolated system **13**

4 Coupling to an environment **16**

4.1 The derivation of the Master Equation 17

4.2 The ME approach applied to our system 20

4.3 Numerical simulations 23

4.4 Feasibility and conclusions 25

Part II : Single-electron tunneling oscillations **29**

Introduction **30**

1 Single-electron oscillations at zero temperature **32**

1.1 Charging effects in tunnel junctions 32

1.2 The system and the model 36
1.3 Regimes of current transport 39
1.3.1 Non SETOs regimes 39
1.3.2 SETOs regime 41
1.4 Charge-fluctuation spectrum 46
1.5 Numerical simulations 53
1.6 Summary and conclusions 57

Appendix **58**

1.A SETOs with a Master Equation approach 58
1.B More details about current fluctuations 62

2 Thermal fluctuations **65**

2.1 Finite temperature charge noise 65
2.2 Finite temperature current noise 68
2.3 Numerical results 70
2.4 Analytical estimation of thermal effects 74
2.5 The high-voltage limit 75
2.6 Conclusions 81

3 Effects of the electromagnetic environment **82**

3.1 The $P(E)$ theory and the calculation of the tunneling rates 86
3.2 On the derivation of the classical ME 93
3.3 Combining the ME with the $P(E)$ theory 98
3.3.1 Numerical results 99
3.4 Conclusions and perspectives 103

Appendix **105**

3.A Details of the $P(E)$ numerical implementation 105

3.B Vanishing of the quantum component of the density matrix 106

List of Figures **109**

Index of Notations **112**

Bibliography **114**

Overview

The ongoing progress in the realization of smaller and smaller electronic devices has brought about a deep interest in the study of electrical transport at the nanoscale. Performing transport measurements in systems such as ultra-small junctions, quantum dots, single molecules and similar nanoscale devices, unravels the quantum nature of electrons and its influence on various physical properties such as the conductance and the corresponding current-noise statistics. This is intriguing not only from the point of view of applications but also for the more fundamental and theoretical interest of actually seeing quantum mechanics at play at a macroscopic scale, where macroscopic is to be intended here in the sense more-than-atomic. The possible macroscopic manifestations of quantum mechanics propose a major experimental challenge, and striking breakthroughs as the first experiments of ground-state cooling nanomechanical resonators have been recently achieved [1, 2].

Particularly interesting possibilities arise in this context when external electromagnetic fields influence the electron transport and enable selective electronic excitations. Time-dependent effects can be eventually used in this case to induce, drive, steer and in general control currents through mesoscopic and nanoscopic conductors, at a tolerable, also controllable current-noise level. Thanks to a large amount of theoretical efforts in the field of mesoscopic transport (for just a partial theoretical glimpse see for example Refs. [3–6]), a number of electron transport control schemes can be successfully designed and operated nowadays, from photon-assisted tunneling [7–9] to electron pumping [10–19].

Grasping some of the quantum transport mechanisms which can induce controllable currents in nanoscale systems is the leitmotiv of this dissertation. We will be considering two kinds of systems in which an intriguing mechanism of coupling between excitations by external fields and electron transport is at play. In the first part we will tackle a problem which falls into the category of quantum pumping: we choose a basic three-site model in a ring configuration to analyze the possibility of inducing a direct circulating current in the presence of dissipation and with a time-dependent driving which can also be nonadiabatic. The system is in principle insulating and the current arises as the DC response to a cyclic (AC) perturbation: understanding and controlling this induced current in arbitrary driving regimes is of essential and general interest for applications, for example to quantum dot circuitry. We indeed find an analytical solution for our dissipative model, characterizing the

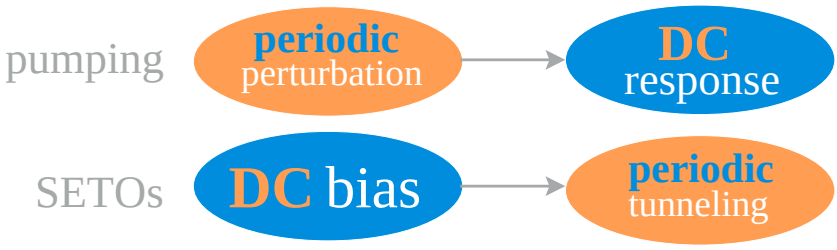

Figure 0.1: Pumping versus SETOs, 'opposite' phenomena.

differences between adiabatic and antiadiabatic regimes and clarifying the dependence of the obtained direct current on the driving frequency. This pumped current will very interestingly turn out to be nonmonotonic for increasing frequency, displaying a temperature-dependent optimal value.

The second part of the dissertation will be instead devoted to a problem which is in some sense the inverse of electron pumping [see the scheme in Fig. 0.1]. Here a time-dependent effect, an almost periodic tunneling of single electrons, will arise in fact through a tunnel junction circuit as a consequence of a DC bias: this phenomenon is known as single-electron tunneling oscillations (SETOs). It is well-established among the single-electron effects and has been widely studied since the 1980s, but it deserves a renewed interest in view of the recent progresses in measuring high-frequencies current noise [20–23]. We will study the charge and current noise spectrum of a tunnel junction in different resistive environments with the aim of determining the boundaries of the SETOs regime and of quantifying their accuracy in terms of periodicity. The possibility of controlling and optimizing the SETOs would provide in practice a one-electron source, with consequent possible applications to nanoscale circuits. The zero-temperature, ideally current-biased case will constitute the bulk of our analysis, but also the extension to finite temperature and to more realistic environments with quantum fluctuations at play will be discussed.

An additional common point of the two parts of the dissertation is the use of the same kind of technical tool. Specifically, in both cases we are considering an open quantum system and we need an equation for the reduced density matrix of the relevant degrees of freedom. We will thus resort to a Master Equation (ME) approach to describe both systems. ME techniques are the state of the art to treat in a simple and convenient way the coupling of quantum systems to a large number of degrees of freedom representing the environment, among which the non-relevant ones can be eliminated. In the first part, the ME for the density matrix will be the very starting point to treat the dissipative coupling of the three-site system with an external bath (the environment). In the second part the ME will be fundamental to treat the finite-temperature case and to address a more realistic environment including effects of quantum fluctuations.

Part I

Quantum pumping in the presence of dissipation in a nonadiabatic regime

Introduction

In this first part of the dissertation we study an interesting nanoscale electronic problem in the presence of dissipation, which can be classified in the category of quantum pumping. In a broad sense, one can refer to quantum pumping whenever a direct current is obtained by driving quantum particles through a system with a cyclic modulation of some of the system parameters. More precisely, in contexts like the one considered in the following, where the pumping involves a ring topology, the effect is also known as quantum *stirring*. In the case of electronic systems, pumping can involve unpaired electrons as well as Cooper pairs [24, 25]. Here we will consider a system of electrons within a three-site model, where the net direct current component is generated through a 'peristaltic' modulation of the transmission amplitudes and gate voltages [26–33]. When the modulation is adiabatic, i.e. when the pumping period is much longer than the intrinsic time-scale of the system, it has long been recognized that the charge pumped over a period has a geometric nature [34–36] and it is in many cases quantized, as we will briefly introduce in chapter 1. These geometrical aspects survive even in the presence of a coupling between the electrons and an external phonon bath, despite the obvious source of inelastic effects [24, 25, 37]. Like in classical pumps, the current in this slow adiabatic regime increases proportionally to the driving frequency $\omega/2\pi$, as long as $\hbar\omega$ is much smaller than all intrinsic energy scales of the system. The opposite antiadiabatic case of fast driving is on the other hand less predictable, especially in the presence of dissipation, and will be found displaying the most interesting features.

A simple three-level model is here considered: three sites in a triangular setup, under the action of a cyclic potential designed to pump current through the ring. Our aim is to focus specifically on the crossover from adiabatic to antiadiabatic quantum pumping [35, 38, 39] analyzing the kind and magnitude of the differences in the two cases: what is the behavior of the DC output as the frequency crosses over beyond the adiabatic and into the antiadiabatic $\omega \to \infty$ regime? For a particular but reasonable choice of coupling to the bath, we find that the dissipative model admits a full analytical solution for the steady state current valid at arbitrary frequency. Through that solution we can analyze and understand the main features of the dependence of the DC response on the pumping frequency. At low frequencies the pumped current tracks the known adiabatic result, namely the direct current increases linearly with frequency, and the pumped charge is as expected geometric in nature (albeit not quantized). However, and this is a surprising outcome, the pumped direct current turns

nonmonotonic for increasing ω, going through a temperature dependent optimal value and then dropping eventually as ω^{-1} for $\omega \to \infty$.

The plan of this part is the following: Chapter 1 gives a brief introduction to pumping. In chapter 2 we present two physical systems which can be described by a three-site model. In chapter 3 we obtain the analytical solution for the isolated three-site model under a harmonic time-dependent perturbation. In chapter 4 we introduce a thermal bath of harmonic oscillators to account for dissipation, finding an analytical solution for the associated Born-Markov Master Equation. We then briefly present the numerical results obtained in Ref. [40] and comment about feasibility and quantitative estimates of the proposed model. The results of this part have been published in Ref. [41].

Chapter 1

A brief introduction to quantum pumping

Before plunging into our specific dissipative quantum pumping problem in a three-site model, we want to put it a little bit into context providing a brief introduction to the broad field of pumping. The analogy between electric current and the flow of water is the most natural way to introduce the concept of pumping [42]: to move water (charge) between two pools (reservoirs) one can either exploit potential difference between the two reservoirs so as to make the water flow through a pipe (wire), or operate a pumping device at some location along the pipe (the scattering region). The 'pumping' is precisely this possibility of moving charge without creating a potential difference. More specifically, quantum pumping differs from classical pumping since it exploits quantum coherent effects to generate a direct current as a response to a cyclic (AC) driving of some external potential.

There are different mechanisms which can lead to this kind of transport. Historically, the idea of quantum pumping has been around since the 1980s, beginning with the preliminary works of Thouless [43] and Niu [44], when it was first realized that a slow cyclic parametric deformation of the confining potential of a mesoscopic system connected to electron reservoirs could lead to a net charge transport. Thouless theoretical argument is fairly clear and allows us to grasp some very basic concepts behind pumping, we refer in the following to the nice summary of Ref. [45]. For simplicity, spinless electron in a 1D channel are considered, subjected to a periodic potential $U(x,t) = U(x+a,t)$; if the number of electrons per period is an integer N, the N lowest energy bands of the spectrum are full and the higher ones are empty. By letting the potential move with a small velocity $U(x,t) = U(x-vt)$, each point in space sees a periodically varying potential: if the electrons follow adiabatically the variation of the potential, a net current $\mathrm{I} = Nev/a$ is induced and over a period $\mathrm{T} = a/v$ a net quantized charge $\mathrm{Q} = \mathrm{IT} = N\mathrm{e}$ is transferred. The Thouless pump can be seen as the electron analog of an Archimedean screw, as shown in Fig. 1.1, taken from Ref. [45]. This very simple idea is at the basis of the adiabatic pumping mechanism: take a phase coherent metallic system

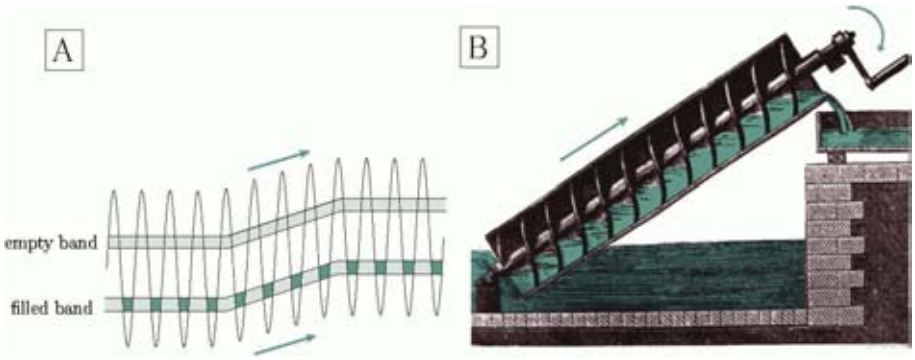

Figure 1.1: Analogy between a Thouless adiabatic electron pump (A) and an Archimedean screw (B).

coupled to reservoirs at the same chemical potentials; the distribution of charge is determined by the eigenmodes of the Hamiltonian and is a represented by a standing wavefunction very sensitive to the configuration of the confining potential. Shape changes in this potential will thus affect the interference pattern of the coherent electrons (thus the name 'interference pumping' sometimes encountered in the literature for this basic kind of pumping): by subjecting the potential landscape to a sufficiently slow parametrical perturbation, the electronic distribution will follow adiabatically, the charge will be redistributed and a total net transfer between the reservoirs becomes possible even if they have the same chemical potential. It is to be noted that the parametrical changes have to involve at least two parameters for the pumping to occur. The reason is deeply related to geometrical considerations, as the work of Berry [46] demonstrated. Let us focus on the Thouless pump for simplicity: after each cycle every potential minimum of the traveling wave $U(x - vt)$ gets shifted by one period a. A single standing wave perturbation would not do the trick, at least two are needed, and $U(x - vt)$ can be seen indeed as a superposition of two standing waves. For example with $U(x) = U_0 \sin(2\pi x/a)$ a good traveling-wave perturbation able to pump the charge would be $U(x - vt) = U_1(t) \sin(2\pi x/a) + U_2(t) \cos(2\pi x/a)$ with $U_{1,2}(t) = U_0 \cos(2\pi t/\mathrm{T} + \varphi_{1,2})$ and $\varphi_{1,2} = \{0, 2\pi\}$. The trajectory of the time evolution of the potential in the plane of the parameters U_1 and U_2, call it ∂U, is in this case a circle. The pumping condition can now be stated in general geometrical terms which extend beyond the specific case of the Thouless pumps: taken two arbitrary adiabatic perturbations $U(x, t) = U_1(t)f_1(x) + U_2(t)f_2(t)$ with nonzero phase difference, the pumping can occur if the trajectory ∂U encircles a nonvanishing area in the parameter space. The pumped charge is determined by the size and the shape of ∂U and can be seen as a 'magnetic flux' of some effective magnetic field defined in the parameter space. It is moreover related also to another kind of magnetic flux, a phase (the Berry phase) acquired by the system wavefunction after an adiabatic cycle of evolution of the parameters $U_i(t)$. This is the exact geometric analogous of the Aharonov-Bohm effect: a particle in a magnetic field following a closed trajectory acquires a phase equal to the magnetic flux through the trajectory in units of h/e. For this reason this kind of adiabatic pumping is often referred to also as 'geometric magnetism'.

A vast amount of theoretical development sprouted from Thouless seminal paper can be found in the literature, we are not interested in giving further details here, we refer for example to the early papers in Refs. [34, 45, 47–49]. In Ref. [34] the total charge adiabatically pumped in a phase-coherent system during a cycle of perturbation of the potential landscape was for the first time directly related to the scattering matrix, with a formula which is the pumping equivalent of the Landauer formula for the conductance. The scattering-based approach has been developed and generalized later for example in Ref. [27] and Ref. [28]. In recent years, thanks to a well-established formalism and more sophisticated theoretical insight, a variety of pumping-related phenomena have been explored, from mesoscopic fluctuations of the pumped current [50, 51], to noise [52, 53] and dissipation [53], to symmetry properties in the presence of magnetic fields [54].

In the adiabatic pumping so far illustrated electron-electron interactions are weak and can be neglected. Other pumping mechanisms exist which on the other hand do require to account for interacting electrons and involve systems such as quantum dots, tunnel junctions and single-electron transistors. Photon-assisted tunneling for example has been investigated in Refs. [55, 56]. The most widely studied pumping approach for these systems is however based on the Coulomb blockade. We refer to the literature for the details, see for example Refs. [57–59]. Single-electron transport in a Coulomb blockaded system will be also studied in part II of this dissertation, but focusing on a phenomenon in some sense opposite to pumping, an AC effect triggered by a DC bias, as sketched in the general overview. From the experimental point of view, nanoscale pumps have been efficiently realized in systems exhibiting strong Coulomb effects [11–15]. In Refs. [16–18] a clever driving scheme which exploits surface acoustic waves was designed to build a single-electron pump. On the other hand, evidence for pumping in the absence of Coulomb blockade has been more elusive so far. The pioneering experiment of Ref. [10] evidenced the difficulty of modulating in time the properties of an open mesoscopic conductor at cryogenic temperatures without side effects due to stray capacitances [60, 61]. One possible solution to this problem is to exploit the AC Josephson effect and use the phases of the superconducting order parameter in superconducting contacts as pumping parameters [62]. Recently in Ref. [19] the experimental detection of a pumped-charge flow in a (SQUID-embedded) unbiased InAs nanowire has been reported: pumping is obtained via the cyclic modulation of the phase of the order parameter of different superconducting electrodes.

This brief outline was intended to provide a general picture of the pumping literature. The adiabatic 'interference' pumping and the Coulomb-blockade-based pumping have been distinguished as the main pumping mechanisms, to roughly classify the possible different approaches. As explained in the introduction, in this part of the thesis we will be interested in a quantum stirring problem in a three-site system, which therefore falls in the first category, with the important difference that we will not stick to the already well-known adiabatic picture, but the nonadiabatic regime will be explored, and also the presence of a dissipative environment, as has only very recently started to be considered [24, 25, 39, 63].

Chapter 2

Quantum pumping in a three-site system

We consider a three-site model in a ring configuration, see Fig. 2.1. We will focus on two categories of systems which can be reduced to this basic structure. The first one is represented by molecular trimers such as H_3, Li_3 and Na_3 [64–66] and it was studied in Ref. [67]. The valence electronic states of these molecules are subjected to degenerate electron-vibration interaction of Jahn-Teller $e \otimes E$ type [68] and the driving, i.e. the pumping, in this case is realized by the excitation of rotating vibrational modes which then act on the electronic structure through this degeneracy. A realistical and simple electronic picture can be obtained in a standard tight-binding (TB) model [69] by considering a basis set consisting only of s-type orbitals on the vertices of a triangle. The corresponding 3×3 Hamiltonian is in the form

$$\mathcal{H}_0 = \begin{pmatrix} \epsilon_a & -\gamma_{ab} & -\gamma_{ac}^* \\ -\gamma_{ab}^* & \epsilon_b & -\gamma_{bc} \\ -\gamma_{ac} & -\gamma_{bc}^* & \epsilon_c \end{pmatrix}, \tag{2.1}$$

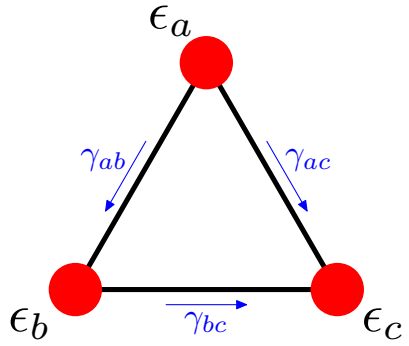

Figure 2.1: Scheme of the three-site model.

where ϵ_i labels the on-site energies and γ_{ij} the TB hopping integrals. A trimer of equal atoms as the molecules here considered has equal on-site energies, which can be taken at zero without loss of generality: $\epsilon_a = \epsilon_b = \epsilon_c = 0$. In the equilateral geometry the hopping integrals are identical $\gamma_{ij} = \gamma_0$ and the Hamiltonian can be easily diagonalized giving a ground state $|0\rangle = (|a\rangle + |b\rangle + |c\rangle)/\sqrt{3}$ with energy $-2\gamma_0$ and a doublet of degenerate excited states with energy γ_0, whose 2×2 subspace is spanned for example by the basis

$$\begin{aligned} |x\rangle =& \frac{|b\rangle - |c\rangle}{\sqrt{2}} \\ |y\rangle =& \frac{2|a\rangle - |b\rangle - |c\rangle}{\sqrt{6}} \,. \end{aligned} \tag{2.2}$$

Under molecular distortion however the hopping terms change, and it can be assumed their dependence on the displacement to be

$$\gamma_{ij} \simeq \gamma_0 e^{-k(d_{ij}-u_0)} \,, \tag{2.3}$$

where d_{ij} is the instantaneous distance between atoms i and j and u_0 is the equilibrium separation in the equilateral geometry (k is a coupling constant). Specifically, such time-dependent overlaps are obtained when the molecule is distorted by the excitation of the vibrational modes. Of the three normal modes of the system one is just an uniform dilation, which fully preserves the D_3 group of the equilateral geometry and can be ignored in studying the coupling to electronic states since it does not split the degeneracy. The other two modes are degenerate and lead to the deformations of the triangle sketched in Fig. 2.2. The displaced atomic positions can be written in terms of the normal coordinates Q_x and Q_y as:

$$\begin{cases} \mathbf{R}_a = (0,1)\frac{u_0}{\sqrt{3}} + \left(\frac{1}{\sqrt{3}}, 0\right) Q_x + \left(0, \frac{1}{\sqrt{3}}\right) Q_y \\ \mathbf{R}_b = -(\frac{\sqrt{3}}{2}, \frac{1}{2})\frac{u_0}{\sqrt{3}} - \left(\frac{1}{2\sqrt{3}}, \frac{1}{2}\right) Q_x + \left(\frac{1}{2}, -\frac{1}{2\sqrt{3}}\right) Q_y \\ \mathbf{R}_c = (\frac{\sqrt{3}}{2}, -\frac{1}{2})\frac{u_0}{\sqrt{3}} + \left(-\frac{1}{2\sqrt{3}}, \frac{1}{2}\right) Q_x - \left(\frac{1}{2}, \frac{1}{2\sqrt{3}}\right) Q_y \end{cases} . \tag{2.4}$$

The modified hopping integrals are obtained by taking $d_{ij} = |\mathbf{R}_i - \mathbf{R}_j|$ in Eq. (2.3). Considering small excitation, we can linearize for small Q_i and obtain the linearized electron-vibration coupling, with overlaps given by:

$$\begin{cases} \gamma_{ab} \simeq \gamma_0 \left(1 - k\frac{\sqrt{3}}{2} Q_x - k\frac{1}{2} Q_y\right) \\ \gamma_{bc} \simeq \gamma_0 \left(1 + k Q_y\right) \\ \gamma_{ac} \simeq \gamma_0 \left(1 + k\frac{\sqrt{3}}{2} Q_x - k\frac{1}{2} Q_y\right) \end{cases} . \tag{2.5}$$

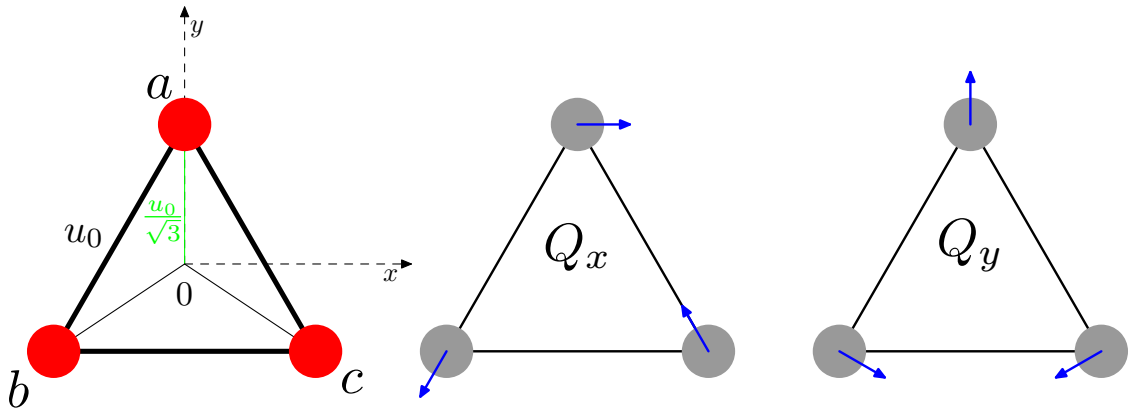

Figure 2.2: Sketch of the vibrational modes of the trimer.

The Hamiltonian for this small perturbation reads in the $|0\rangle$, $|x\rangle$, $|y\rangle$ basis:

$$\mathcal{H}_{\text{lin}} = \gamma_0 \begin{pmatrix} -2 & \frac{1}{\sqrt{2}}kQ_x & \frac{1}{\sqrt{2}}kQ_y \\ \frac{1}{\sqrt{2}}kQ_x & 1+kQ_y & kQ_x \\ \frac{1}{\sqrt{2}}kQ_y & kQ_x & 1-kQ_y \end{pmatrix} . \tag{2.6}$$

The perturbation being small with respect to the gap $3\gamma_0$ between the unperturbed ground state and the doublet, we can safely discard admixtures with the $|0\rangle$ state and restrict to the $|x\rangle$, $|y\rangle$ subspace, where, ignoring the trivial diagonal shift γ_0, the linearized Hamiltonian takes the form:

$$\mathcal{H}^{2\times 2}_{\text{lin}} = k\gamma_0 \begin{pmatrix} Q_y & Q_x \\ Q_x & -Q_y \end{pmatrix} . \tag{2.7}$$

The pumping (or stirring) of the system can then be realized by choosing a rotating combination of the perturbing vibrations with amplitudes:

$$\begin{cases} Q_x = \frac{\hbar\Delta}{2k\gamma_0}\sin(\omega t) \\ Q_y = \frac{\hbar\Delta}{2k\gamma_0}\cos(\omega t) \end{cases} , \tag{2.8}$$

with the parameter Δ representing the coupling strength. $\hbar\Delta$ determines the splitting between $|x\rangle$ and $|y\rangle$. The resulting pumping Hamiltonian can be written in terms of the Pauli matrices as

$$\mathcal{H}_S(t) = \frac{\hbar\Delta}{2}\left(\cos(\omega t)\sigma^z + \sin(\omega t)\sigma^x\right) . \tag{2.9}$$

A second straightforward system described by the three-site model is a triple quantum dot with all the dots connected in a ring structure. The experimental implementation of this kind of geometry has been proven realizable [70, 71]. Considering each site to be a single-orbital dot and indicating as ϵ_i the external bias applied to each dot i and as γ_{ij} the hopping

amplitude for an electron to jump between sites i and j, the Hamiltonian of the system is exactly as in Eq. (2.1). In the fully symmetric case $\epsilon_a = \epsilon_b = \epsilon_b = 0$ and $\gamma_{ij} = \gamma_0$ we get the same ground state and doublet of degenerate states as for the trimer and we can use the $|0\rangle$, $|x\rangle$, $|y\rangle$ basis. When three electrons occupy the three dots two of them fill the state $|0\rangle$ and the third one moves in the $|x\rangle$, $|y\rangle$ subspace which is then again the one relevant for transport and pumping processes. To split the degeneracy an experimentally feasible way is to perturb the bias ϵ_i. We consider the following perturbing Hamiltonian in the $|0\rangle$, $|x\rangle$, $|y\rangle$ basis:

$$\mathcal{H}_{\text{bias}} = \begin{pmatrix} 0 & \frac{1}{\sqrt{6}}(\epsilon_b - \epsilon_c) & \frac{1}{\sqrt{2}}\epsilon_a \\ \frac{1}{\sqrt{6}}(\epsilon_b - \epsilon_c) & -\frac{1}{2}\epsilon_a & \frac{1}{2\sqrt{3}}(\epsilon_c - \epsilon_b) \\ \frac{1}{\sqrt{2}}\epsilon_a & \frac{1}{2\sqrt{3}}(\epsilon_c - \epsilon_b) & \frac{1}{2}\epsilon_a \end{pmatrix} . \tag{2.10}$$

For small perturbations we can again restrict to the doublet subspace:

$$\mathcal{H}^{2\times 2}_{\text{bias}} = -\frac{1}{2\sqrt{3}} \begin{pmatrix} \sqrt{3}\epsilon_a & \epsilon_b - \epsilon_c \\ \epsilon_b - \epsilon_c & -\sqrt{3}\epsilon_a \end{pmatrix} . \tag{2.11}$$

The pumping is in this case realized by cycling the external potentials as follows:

$$\begin{cases} \epsilon_a(t) = -\hbar\Delta \cos\left(\omega t\right) \\ \epsilon_b(t) = -\hbar\Delta \cos\left(\omega t - \frac{2\pi}{3}\right) \\ \epsilon_c(t) = -\hbar\Delta \cos\left(\omega t + \frac{2\pi}{3}\right) \end{cases} , \tag{2.12}$$

and the Hamiltonian reduces precisely to Eq. (2.9).

To study the pumping we need at this point to estimate the current circulating in the ring. The simplest possible way to define a current operator is to consider the transfer of electrons between pairs of sites. The current between e.g. sites a and b is then given by (see Ref. [67])

$$I_{ab} = -iq\gamma_{ab}\left(c_b^\dagger c_a - c_a^\dagger c_b\right) , \tag{2.13}$$

where $c_i^\dagger$ and c_i are the creation and annihilation operators of an electron at site i and q is the charge. In the basis $|0\rangle$, $|x\rangle$, $|y\rangle$ it reads:

$$I_{ab} = iq\gamma_{ab} \begin{pmatrix} 0 & \frac{1}{\sqrt{6}} & \frac{1}{\sqrt{2}} \\ -\frac{1}{\sqrt{6}} & 0 & -\frac{1}{\sqrt{3}} \\ -\frac{1}{\sqrt{2}} & \frac{1}{\sqrt{3}} & 0 \end{pmatrix} , \tag{2.14}$$

which for uniform hoppings γ_0 and restricted to the $|x\rangle$, $|y\rangle$ subspace simply reduces to:

$$I_{ab} = \frac{q\gamma_0}{\sqrt{3}} \begin{pmatrix} 0 & -i \\ i & 0 \end{pmatrix} = I_0\sigma^y , \tag{2.15}$$

with $I_0 = q\gamma_0/\sqrt{3}$. The quantity $\langle\sigma^y(t)\rangle$ will thus estimate the current pumped in the system.

Chapter 3

Solution for the isolated system

A clever change of basis [40] leads to the solution of the Hamiltonian (2.9) in an elegant and simple way. We consider a rotation of frequency ω around the y axis:

$$R_t = e^{-i\omega t\sigma^y/2} = \mathbb{1}\cos(\omega t/2) - i\sigma^y \sin(\omega t/2)\,, \tag{3.1}$$

and apply it to Eq. (2.9), obtaining a new time-independent Hamiltonian:

$$\tilde{\mathcal{H}}_S = R_t^{-1}\mathcal{H}_S(t)R_t = \frac{\hbar\Delta}{2}\sigma^z\,. \tag{3.2}$$

The rotated states $|\tilde{\psi}(t)\rangle = R_t^{-1}|\psi(t)\rangle$ obey now a modified Schrödinger equation with the effective Hamiltonian

$$\tilde{\mathcal{H}}_{\text{eff}} = \tilde{\mathcal{H}}_S - \frac{\hbar\omega}{2}\sigma^y = \frac{\hbar\Delta}{2}\sigma^z - \frac{\hbar\omega}{2}\sigma^y = \frac{\hbar\omega'}{2}\hat{\mathbf{n}}\cdot\vec{\sigma}\,, \tag{3.3}$$

which represents in practice a time-independent field pointing in the direction

$$\hat{\mathbf{n}} = (0, -\omega/\omega', \Delta/\omega')\,, \tag{3.4}$$

with associated Larmor frequency $\omega' = \sqrt{\Delta^2+\omega^2}$. The eigenstates are then simply 'spin' states directed along $\pm\hat{\mathbf{n}}$: $\tilde{\mathcal{H}}_{\text{eff}}|\pm\hat{\mathbf{n}}\rangle = \pm\hbar\omega'/2|\pm\hat{\mathbf{n}}\rangle$. The current operator σ^y being parallel to the rotation axis it is not affected by the rotation and remains time-independent in the rotated frame; the current keeps the form $I(t) = I_0\langle\tilde{\psi}(t)|\sigma^y|\tilde{\psi}(t)\rangle$. The current on the eigenstates is straightforwardly obtained:

$$\langle\pm\hat{\mathbf{n}}|\sigma^y|\pm\hat{\mathbf{n}}\rangle = \mp\frac{\omega}{\omega'}\,. \tag{3.5}$$

Let us choose the initial state at $t = 0$ as for example the ground state of the initial Hamiltonian (2.9), that is $|-\hat{z}\rangle$:

$$|\tilde{\psi}(0)\rangle = |-\hat{z}\rangle = \sin\left(\frac{\theta}{2}\right)|+\hat{\mathbf{n}}\rangle + \cos\left(\frac{\theta}{2}\right)|-\hat{\mathbf{n}}\rangle\,, \tag{3.6}$$

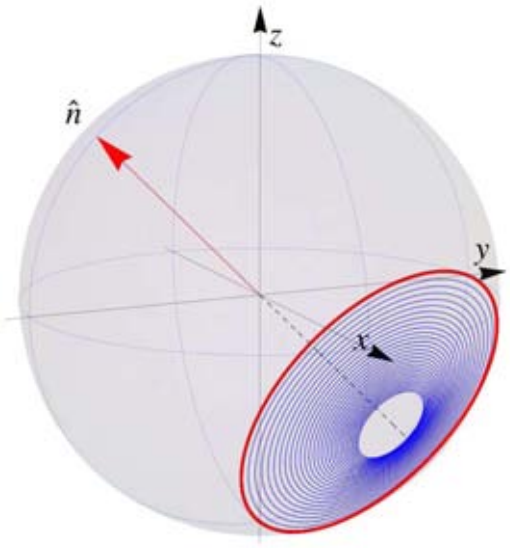

Figure 3.1: The trajectory of a spin initially in $|-\hat{z}\rangle$ in the Bloch sphere. The current $I(t)$ is measured by the instantaneous y-projection of the spin state. The thick circle represents the spin precession around $-\hat{\mathbf{n}}$ in the absence of dissipation. The thin spiral curve represents the relaxing trajectory in the presence of a weak dissipation, which we will introduce in chapter 4.

with $\theta = \arccos(\Delta/\omega')$ (which is the angle between the initial state and the eigenstate). Following the evolution the initial state will then make Rabi oscillations between the eigenstates $|\pm\hat{\mathbf{n}}\rangle$ and the current as a function of time is given by:

$$\begin{aligned}\frac{I(t)}{I_0} = \langle\tilde{\psi(t)}|\sigma^y|\tilde{\psi(t)}\rangle = \sin^2\left(\frac{\theta}{2}\right)\langle+\hat{\mathbf{n}}|\sigma^y|+\hat{\mathbf{n}}\rangle + \cos^2\left(\frac{\theta}{2}\right)\langle-\hat{\mathbf{n}}|\sigma^y|-\hat{\mathbf{n}}\rangle + \\ -\sin\left(\frac{\theta}{2}\right)\cos\left(\frac{\theta}{2}\right)\left(e^{-i\omega' t}\langle+\hat{\mathbf{n}}|\sigma^y|-\hat{\mathbf{n}}\rangle + h.c.\right).\end{aligned} \tag{3.7}$$

Expression (3.7) has a constant and an oscillating part: being interested in the DC pumping we focus then on the former [i.e. the first two terms in Eq. (3.7)], and by defining $\mathrm{J} \equiv I(t)/I_0 = \langle\tilde{\psi}(t)|\sigma^y|\tilde{\psi}(t)\rangle$ we get:

$$\mathrm{J} = \frac{\omega}{\omega'}\cos(\theta) = \frac{\omega}{\omega'}\frac{\Delta}{\omega'}, \tag{3.8}$$

which is just the current on the eigenstate $|\hat{\mathbf{n}}\rangle$ times the cosinus of the angle between the initial state and the eigenstate. In other words, a spin initially in $|-\hat{z}\rangle$ precesses around the $-\hat{\mathbf{n}}$ axis (see the circle in Fig. 3.1), with a projection Δ/ω' along this axis and as a result, the precessing spin carries an oscillating current proportional to its y component.

As shown in Fig. 3.2, the current as a function of the pumping frequency displays a maximum for $\omega = \Delta$. The presence of the maximum is due to the competition of two effects:

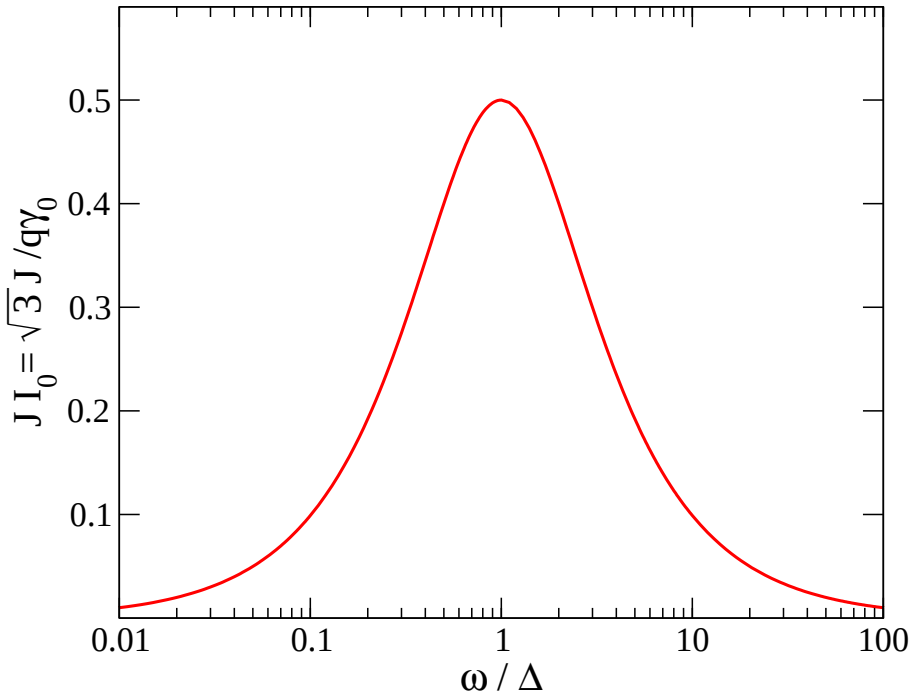

Figure 3.2: Direct current as a function of the pumping frequency as given by Eq. (3.8).

for increasing frequency, $\hat{\mathbf{n}}$ gets closer to the y direction and the current on the eigenstate ω/ω' increases, but at the same time the overlap with the chosen initial state $|-\hat{z}\rangle$ decreases. A different choice of initial condition could lead up to the maximum theoretical current ω/ω'. We can sum up and say that in the absence of any coupling with the environment, any time dependence of the current is in practice determined only by the initial conditions: each of the two eigenvectors of $\mathcal{H}_{\text{eff}}$ produces a pure DC output, while any other initial condition gives also an AC contribution. The DC component can be expressed in terms of the projection of the spin over the eigenstates of $\mathcal{H}_{\text{eff}}$:

$$I = I_0 P \frac{\omega}{\omega'} = -I_0 \,\mathrm{Tr}(\hat{\mathbf{n}} \cdot \vec{\sigma} \tilde{\rho}_S) \,\frac{\omega}{\omega'}\,, \tag{3.9}$$

with $P = -\mathrm{Tr}(\hat{\mathbf{n}} \cdot \vec{\sigma} \tilde{\rho}_S)$ the spin polarization in terms of the density matrix in the rotating frame $\tilde{\rho}_S$. This notation will be clearer in the next section, where we handle explicitly the density matrix of the system.

The same result could be derived also in a different formalism, considering the point of view of the standard quantum pumping literature: the details can be found in Ref. [40], where Eq. (3.8) is shown to be exactly retrievable in the same framework as Ref. [35].

Chapter 4

Coupling to an environment

The solution for the isolated case provides us with a clear understanding of the basics of the pumping mechanism at play in the three-site system. A real physical system however can be hardly considered decoupled from an environment. A minimal interaction with external degrees of freedom is always present and causes an irreversible energy transfer from the system to the environment, which on the other hand exerts a fluctuating force leading to fluctuations of the system observables. A realistic model of a quantum system needs therefore to deal with dissipation and fluctuations. The standard way to proceed is to think the system in contact with a reservoir which has in principle an infinite number of degrees of freedom and has the characteristics of a heat bath. This dissipative medium can be modeled in the simplest effective way as a bosonic environment by introducing an infinite number of harmonic oscillators, as has been proven in the seminal works of Feynman & Vernon and Caldeira & Leggett [72, 73].

We consider thus here the Hamiltonian (2.9) in the presence of dissipation by introducing a bosonic environment as follows:

$$\begin{aligned}\mathcal{H} = &\overbrace{\frac{\hbar\Delta}{2}(\cos(\omega t)\sigma^z + \sin(\omega t)\sigma^x)}^{\mathcal{H}_S} + \\ &+ \underbrace{\sum_{\xi=z,x}\sum_{\nu}\left(\frac{p_{\xi,\nu}^2}{2m} + \frac{m\omega_\nu^2 q_{\xi,\nu}^2}{2}\right)}_{\mathcal{H}_B} + \underbrace{\sum_{\xi=z,x}\sum_{\nu}\sqrt{\frac{2m\omega_\nu}{\hbar}}\lambda_{\xi,\nu}q_{\xi,\nu}\sigma^\xi}_{\mathcal{H}_{SB}},\end{aligned} \tag{4.0.1}$$

where the sum over ξ accounts for two noninteracting baths of harmonic oscillators, labeled z and x and coupled via σ^z and σ^x respectively, with q, p, m and ω the position, momentum, mass and frequency of the oscillators, and λ the coupling constant. In modeling the environment it is customary (see for example Ref. [74]) to go the the continuum limit for the bath, i.e. the description in terms of individual oscillators with discrete frequencies and masses is replaced by a spectral density $J(\omega)$ corresponding to a continuous spectrum of environmental frequencies. The frequency dependence of $J(\omega)$ is assumed to follow a power-law dependence

of the form $J(\omega) \sim \omega^s$. The most common choice for the exponent s is the so-called 'Ohmic' one, i.e. $s = 1$, such that $J(\omega)$ increases linearly with ω. We therefore take Ohmic baths characterized by the following explicit form of the spectral density (see Ref. [40]):

$$J_\xi(\omega) = \sum_\nu \lambda^2_{\xi,\nu}\delta(\omega - \omega_\nu) = \hbar^2\,\alpha_\xi\,\frac{\omega^s}{\omega_c^{s-1}}\,e^{-\omega/\omega_c} = \hbar^2\alpha_\xi\omega e^{-\omega/\omega_c}\,, \tag{4.0.2}$$

with ω_c a cutoff frequency to prevent the distribution of environmental frequencies to grow without bound (which would be physically unreasonable). The coupling α_ξ to the bath is assumed to be weak. In terms of the spectral density (4.0.2) the bath autocorrelation functions $\mathcal{C}(t)$, which will be rigorously defined in the following, can be expressed as (see [40] for details):

$$\mathcal{C}(t) = \int_0^\infty d\omega J(\omega)\cos(\omega t)\coth\left(\frac{\beta\hbar\omega}{2}\right) - i\int_0^\infty d\omega J(\omega)\sin(\omega t)\,. \tag{4.0.3}$$

Since we saw in the previous section that the Hamiltonian of the system is fairly easy to handle in the rotating frame of reference defined by (3.1), we will also adopt the same frame of reference for the total Hamiltonian (4.0.1), which becomes

$$\tilde{\mathcal{H}} = \tilde{\mathcal{H}}_{\text{eff}} + \mathcal{H}_B + \tilde{\mathcal{H}}_{SB}(t) \tag{4.0.4}$$

with the first term given by Eq. (3.3) and the last one displaying the rotated spin operators:

$$\begin{aligned}\tilde{\sigma}^z(t) =& R_t^{-1}\sigma^z R_t = \sigma^z\cos(\omega t) - \sigma^x\sin(\omega t)\\ \tilde{\sigma}^x(t) =& R_t^{-1}\sigma^x R_t = \sigma^x\cos(\omega t) + \sigma^z\sin(\omega t)\,.\end{aligned} \tag{4.0.5}$$

In the following the tildes will be dropped to keep the notation light but all operators are to be intended in the rotated frame of reference. We will approach this system with the standard Master Equation formalism of the quantum dissipation literature: we will first derive the general Master Equation in the Born-Markov approximation and then specialize it to our system.

4.1 The derivation of the Master Equation

We present here a brief derivation of the standard Master Equation (ME) for a quantum dissipative system, following mainly the book of Schlosshauer [74]. We consider an Hamiltonian in the form (4.0.1):

$$\mathcal{H} = \mathcal{H}_S + \mathcal{H}_B + \mathcal{H}_{SB}\,. \tag{4.1.1}$$

The system–bath Hamiltonian can be factorized in the two system and bath contributions separately [1]

$$\mathcal{H}_{SB} = \sum_\alpha S_\alpha \otimes B_\alpha\,. \tag{4.1.2}$$

1. it is always possible to write an arbitrary interaction Hamiltonian in the form of a diagonal decomposition of (unitary but not necessarily Hermitian) system and environment operators [74].

We will work in interaction representation with respect to $\mathcal{H}_0 = \mathcal{H}_S + \mathcal{H}_B$, with the correspondent evolution operator given by:

$$U_0(t,0) = T \exp\left(-\frac{i}{\hbar}\int_0^t dt' \mathcal{H}_0(t')\right) = U_0^S(t,0) \otimes U_0^B(t,0)\,. \tag{4.1.3}$$

Given $\rho(t)$ the density matrix of the system, the evolution equation for its interaction representation $\rho^I(t) = U_0^\dagger(t,0)\rho(t)U_0(t,0)$ reads then:

$$i\hbar\frac{d}{dt}\rho^I(t) = \left[\mathcal{H}_{SB}^I(t), \rho^I(t)\right]\,, \tag{4.1.4}$$

where $\mathcal{H}_{SB}^I(t) = U_0^\dagger(t,0)\mathcal{H}_{SB}U_0(t,0)$ is the system–bath Hamiltonian part in interaction representation. Integration of (4.1.4) gives

$$\rho^I(t) = \rho^I(0) + \frac{1}{i\hbar}\int_0^t dt' \left[\mathcal{H}_{SB}^I(t'), \rho^I(t')\right]\,, \tag{4.1.5}$$

and inserting this expression back into the right-hand side of (4.1.4) leads to

$$\begin{aligned} i\hbar\frac{d}{dt}\rho^I(t) &= \left[\mathcal{H}_{SB}^I(t)\,,\, \rho^I(0) + \frac{1}{i\hbar}\int_0^t dt' \left[\mathcal{H}_{SB}^I(t'), \rho^I(t')\right]\right] = \\ &= \left[\mathcal{H}_{SB}^I(t), \rho^I(0)\right] + \frac{1}{i\hbar}\int_0^t dt' \left[\mathcal{H}_{SB}^I(t), \left[\mathcal{H}_{SB}^I(t'), \rho^I(t')\right]\right]\,. \end{aligned} \tag{4.1.6}$$

To get rid of the explicit dependence on the bath degrees of freedom we trace them out and obtain Eq. (4.1.6) for the reduced density matrix $\rho_S^I(t) = \mathrm{Tr}_B\left\{\rho^I(t)\right\}$:

$$i\hbar\frac{d}{dt}\rho_S^I(t) = \mathrm{Tr}_B\left[\mathcal{H}_{SB}^I(t), \rho^I(0)\right] + \frac{1}{i\hbar}\int_0^t dt' \,\mathrm{Tr}_B\left[\mathcal{H}_{SB}^I(t), \left[\mathcal{H}_{SB}^I(t'), \rho^I(t')\right]\right]\,. \tag{4.1.7}$$

Without loss of generality we can assume $\mathrm{Tr}_B\left[\mathcal{H}_{SB}^I(t), \rho^I(0)\right] = 0$ (this can always be achieved by a formal redefinition of the Hamiltonian $\mathcal{H}_{SB}^I$), thus

$$i\hbar\frac{d}{dt}\rho_S^I(t) = \frac{1}{i\hbar}\int_0^t dt' \,\mathrm{Tr}_B\left[\mathcal{H}_{SB}^I(t), \left[\mathcal{H}_{SB}^I(t'), \rho^I(t')\right]\right]\,. \tag{4.1.8}$$

In order to eliminate any terms pertaining to a time-dependent state of the environment [i.e. express our Master Equation entirely in terms of the reduced density operator $\rho_S^I(t)$] and also to eliminate any dependences of the change of $\rho_S^I(t)$ at time t on $\rho_S^I(t')$ evaluated at times $t' < t$, we will perform now the *Born and Markov approximations* on Eq. (4.1.8). The former assumes that the system–environment coupling is sufficiently weak and the environment large for the changes of the density operator of the environment to be negligible and the system–environment state to remain in an approximate product state at all times: $\rho(t) \approx \rho_S(t) \otimes \rho_B$. The latter states that memory effects of the environment are negligible, that is any self-correlations within the environment created by the coupling to the system

decay rapidly compared to the characteristic timescale over which the state of the system varies noticeably. Using the Born approximation in interaction picture

$$\rho^I(t) \approx \rho_S^I(t) \otimes \rho_B \quad \forall\, t \geq 0\,, \tag{4.1.9}$$

we can rewrite Eq. (4.1.8) as:

$$i\hbar \frac{d}{dt}\rho_S^I(t) \approx \frac{1}{i\hbar}\int_0^t dt'\, \mathrm{Tr}_B\left[\mathcal{H}_{SB}^I(t), \left[\mathcal{H}_{SB}^I(t'), \rho_S^I(t') \otimes \rho_B\right]\right]\,. \tag{4.1.10}$$

We now proceed by exploiting the diagonal form (4.1.2) of the system–bath Hamiltonian in interaction picture:

$$\begin{aligned}\mathcal{H}_{SB}^I(t) =& U_0^\dagger(t,0)\mathcal{H}_{SB}U_0(t,0) = \\ =& \sum_\alpha \left(U^{S\dagger}{}_0(t,0) S_\alpha U_0^S(t,0)\right) \otimes \left(U^{B\dagger}{}_0(t,0) B_\alpha U_0^B(t,0)\right) = \\ =& \sum_\alpha S_\alpha(t) \otimes B_\alpha(t)\,,\end{aligned} \tag{4.1.11}$$

obtaining:

$$i\hbar \frac{d}{dt}\rho_S^I(t) \approx \frac{1}{i\hbar}\int_0^t dt' \sum_{\alpha\beta} \mathrm{Tr}_B\left[S_\alpha(t) \otimes B_\alpha(t), \left[S_\beta(t') \otimes B_\beta(t'), \rho_S^I(t') \otimes \rho_B\right]\right]\,. \tag{4.1.12}$$

We now define the bath autocorrelation functions:

$$\mathcal{C}_{\alpha\beta}(t,t') = \mathrm{Tr}_B\left\{B_\alpha(t) B_\beta(t') \rho_B\right\} = \langle B_\alpha(t) B_\beta(t')\rangle\,. \tag{4.1.13}$$

Assuming that the bath is in equilibrium, i.e. $[\mathcal{H}_B, \rho_B] = 0$, we have

$$\mathcal{C}_{\alpha\beta}(t,t') = \mathrm{Tr}_B\left\{B_\alpha(t-t') B_\beta \rho_B\right\} \equiv \mathcal{C}_{\alpha\beta}(t-t')\,, \tag{4.1.14}$$

which substituted back in Eq. (4.1.12) leads to:

$$\begin{aligned}i\hbar \frac{d}{dt}\rho_S^I(t) \approx \frac{1}{i\hbar}\int_0^t dt' \sum_{\alpha\beta} \Big\{ & \mathcal{C}_{\alpha\beta}(t-t')\Big(S_\alpha(t) S_\beta(t') \rho_S^I(t') - S_\beta(t') \rho_S^I(t') S_\alpha(t)\Big) + \\ & + \mathcal{C}_{\beta\alpha}(t'-t)\Big(\rho_S^I(t') S_\beta(t') S_\alpha(t) - S_\alpha(t) \rho_S^I(t') S_\beta(t')\Big)\Big\}\,.\end{aligned} \tag{4.1.15}$$

We are now ready to use Markov approximation as stated before, meaning practically that the environment self-correlations functions $\mathcal{C}_{\alpha\beta}(t-t')$ are assumed sharply peaked around $(t-t') = 0$ and decay on a timescale much shorter than the timescale set by the changes of $\rho_S^I(t)$. This is equivalent to saying that $\rho_S^I(t)$ changes only insignificantly during the typical time interval over which the environment self-correlations functions vanish, so that we can replace $\rho_S^I(t')$ by $\rho_S^I(t)$ in Eq. (4.1.15). Moreover it implies also that we can safely extend the

lower limit of the integration to $-\infty$. With the definition $\tau \equiv t - t'$ the final Master Equation reads:

$$i\hbar\frac{d}{dt}\rho_S^I(t) \approx \frac{1}{i\hbar}\int_0^\infty d\tau \sum_{\alpha\beta}\Big\{\mathcal{C}_{\alpha\beta}(\tau)\Big(S_\alpha(t)S_\beta(t-\tau)\rho_S^I(t) - S_\beta(t-\tau)\rho_S^I(t)S_\alpha(t)\Big) + \\ + \mathcal{C}_{\beta\alpha}(-\tau)\Big(\rho_S^I(t)S_\beta(t-\tau)S_\alpha(t) - S_\alpha(t)\rho_S^I(t)S_\beta(t-\tau)\Big)\Big\}. \tag{4.1.16}$$

To transform back to the Schrödinger picture we remind:

$$\begin{aligned}
&\rho_S^I(t) = U_0^{S\dagger}(t,0)\rho_S(t)U_0^S(t,0) \\
&i\hbar\,\frac{d}{dt}\rho_S^I(t) = -\left[\mathcal{H}_S, \rho_S^I(t)\right] + U_0^{S\dagger}(t,0)\left(i\hbar\frac{d}{dt}\rho_S(t)\right)U_0^S(t,0) \\
&i\hbar\,\frac{d}{dt}\rho_S(t) = \left[\mathcal{H}_S, \rho_S(t)\right] + U_0^S(t,0)\left(i\hbar\frac{d}{dt}\rho_S^I(t)\right)U_0^{S\dagger}(t,0)\,,
\end{aligned} \tag{4.1.17}$$

which we use to handle the interaction-picture Master Equation, getting:

$$i\hbar\frac{d}{dt}\rho_S(t) \approx \left[\mathcal{H}_S, \rho_S(t)\right] + \frac{1}{i\hbar}\int_0^\infty d\tau \sum_{\alpha\beta}\Big\{\mathcal{C}_{\alpha\beta}(\tau)\Big(S_\alpha S_\beta(-\tau)\rho_S(t) - S_\beta(-\tau)\rho_S(t)S_\alpha\Big) + \\ + \mathcal{C}_{\beta\alpha}(-\tau)\Big(\rho_S(t)S_\beta(-\tau)S_\alpha - S_\alpha\rho_S(t)S_\beta(-\tau)\Big)\Big\}. \tag{4.1.18}$$

4.2 The ME approach applied to our system

Eq. (4.1.18) specialized to our Hamiltonian [given in Eq. (4.0.4)] reads:

$$\frac{\partial}{\partial t}\rho_S(t) \approx -i\left[\mathcal{H}_{\text{eff}}, \rho_S(t)\right] - \frac{1}{\hbar^2}\int_0^\infty d\tau \sum_{\xi\eta}\Big\{\mathcal{C}_{\xi\eta}(\tau)\left[\sigma^\xi, U^\dagger(-\tau)\sigma^\eta(t-\tau)U(-\tau)\rho_S(t)\right] + \\ + \mathcal{C}^*_{\xi\eta}(-\tau)\left[\rho_S(t)U^\dagger(-\tau)\sigma^\eta(t-\tau)U(-\tau), \sigma^\xi(t)\right]\Big\}. \tag{4.2.1}$$

Note that there are two kinds of time-dependence in the system operators: one given by the rotation R_t (σ^ξ(t)) and one given by the ME [$U^\dagger(-\tau)\sigma^\eta(t-\tau)U(-\tau)$], here explicitly outlined by the presence of the operator $U(t) = \exp\{i\omega'\hat{\mathbf{n}}\cdot\vec{\sigma}t/2\}$.

The baths being independent and identical we have $\mathcal{C}_{\xi\eta}(\tau) = \delta_{\xi,\eta}\mathcal{C}(\tau)$, with $\mathcal{C}(\tau)$ defined in Eq. (4.0.3). To introduce a convenient notation we list the following useful integrals:

$$\begin{aligned}
C_{cc} &= \int_0^\infty d\tau\, \mathcal{C}(\tau)\cos(-\omega\tau)\cos(-\omega'\tau) \\
C_{sc} &= \int_0^\infty d\tau\, \mathcal{C}(\tau)\sin(-\omega\tau)\cos(-\omega'\tau) \\
C_{cs} &= \int_0^\infty d\tau\, \mathcal{C}(\tau)\cos(-\omega\tau)\sin(-\omega'\tau)
\end{aligned}$$

$$
\begin{aligned}
C_{ss} &= \int_0^\infty d\tau\ \mathcal{C}(\tau)\sin(-\omega\tau)\sin(-\omega'\tau) \\
C_{c0} &= \int_0^\infty d\tau\ \mathcal{C}(\tau)\cos(-\omega\tau) \\
C_{s0} &= \int_0^\infty d\tau\ \mathcal{C}(\tau)\sin(-\omega\tau)\,.
\end{aligned}
\tag{4.2.2}
$$

We also define a new basis for the spin operators in the rotated frame of reference, oriented along the axes $\hat{\mathbf{x}} = (1,0,0)$, $\hat{\mathbf{n}} = (0, -\omega/\omega', \Delta/\omega')$ and, perpendicular to both, $\hat{\mathbf{m}} = (0, \Delta/\omega', \omega/\omega')$:

$$
\begin{aligned}
\sigma^x &= \hat{\mathbf{x}}\cdot\vec{\sigma} \\
\sigma^m &= \hat{\mathbf{m}}\cdot\vec{\sigma} \\
\sigma^n &= \hat{\mathbf{n}}\cdot\vec{\sigma}\,.
\end{aligned}
\tag{4.2.3}
$$

In terms of these quantities the ME (4.2.1) reads:

$$
\frac{\partial}{\partial t}\rho_S(t) = -i\frac{\omega'}{2}\left[\sigma^n, \rho_S\right] - \Big[\,\mathrm{T}_1\,,\,\mathrm{T}_2\rho_S\,\Big] + \text{c.c.} + \Big[\,\mathrm{T}_3\,,\,\mathrm{T}_4\rho_S\,\Big] + \text{c.c.}\,,
\tag{4.2.4}
$$

where

$$
\begin{aligned}
\mathrm{T}_1 &= +\cos(\omega t)\sigma^x + \sin(\omega t)\left(\frac{\Delta}{\omega'}\sigma^n + \frac{\omega}{\omega'}\sigma^m\right) \\
\mathrm{T}_3 &= -\sin(\omega t)\sigma^x + \cos(\omega t)\left(\frac{\Delta}{\omega'}\sigma^n + \frac{\omega}{\omega'}\sigma^m\right)\,,
\end{aligned}
\tag{4.2.5}
$$

and

$$
\begin{aligned}
\mathrm{T}_2 \;=\; & \frac{\Delta}{\omega}\Big(\sin(\omega t)C_{c0} + \cos(\omega t)C_{s0}\Big)\sigma^n + \\
& + \Big(\cos(\omega t)C_{cc} - \sin(\omega t)C_{sc} + \frac{\omega}{\omega'}\sin(\omega t)C_{cs} + \frac{\omega}{\omega'}\cos(\omega t)C_{ss}\Big)\,\sigma^x + \\
& + \Big(\sin(\omega t)C_{ss} - \cos(\omega t)C_{cs} + \frac{\omega}{\omega'}\sin(\omega t)C_{cc} + \frac{\omega}{\omega'}\cos(\omega t)C_{sc}\Big)\,\sigma^m \quad , \\
\mathrm{T}_4 \;=\; & \frac{\Delta}{\omega}\Big(\cos(\omega t)C_{c0} + \sin(\omega t)C_{s0}\Big)\sigma^n + \\
& + \Big(-\sin(\omega t)C_{cc} - \cos(\omega t)C_{sc} + \frac{\omega}{\omega'}\cos(\omega t)C_{cs} - \frac{\omega}{\omega'}\sin(\omega t)C_{ss}\Big)\,\sigma^x + \\
& + \Big(\sin(\omega t)C_{cs} + \cos(\omega t)C_{ss} + \frac{\omega}{\omega'}\cos(\omega t)C_{cc} - \frac{\omega}{\omega'}\sin(\omega t)C_{sc}\Big)\,\sigma^m \quad .
\end{aligned}
\tag{4.2.6}
$$

We consider now the density matrix to be in the generic form

$$
\bar{\rho}_S = \frac{1}{2}(\mathbb{1} + a\sigma^x + b\sigma^m + c\sigma^n)\,,
\tag{4.2.7}
$$

and after straightforward manipulations we get Eq. (3.40) of [40]:

$$
\frac{\partial}{\partial t}\bar{\rho}_S(t) = -2\Bigg\{\left(\frac{\Delta^2}{\omega'^2}\mathfrak{Re}\{C_{c0}\} + \frac{\omega}{\omega'}\mathfrak{Re}\{C_{ss}\} + \frac{\omega^2}{\omega'^2}\mathfrak{Re}\{C_{cc}\}\right)a +
$$

$$
\begin{aligned}
&+\left(\frac{\omega'}{4}+\frac{\omega}{\omega'}\mathfrak{Re}\{C_{sc}\}-\frac{\omega}{\omega'^2}\mathfrak{Re}\{C_{cs}\}\right)b+\\
&+\frac{\Delta}{\omega'}\left(\mathfrak{Re}\{C_{sc}\}-\frac{\omega}{\omega'}\mathfrak{Re}\{C_{cs}\}\right)c+\\
&+\frac{\Delta}{\omega'}\left(-\frac{\omega}{\omega'}\mathfrak{Im}\{C_{c0}\}+\mathfrak{Im}\{C_{ss}\}+\frac{\omega}{\omega'}\mathfrak{Im}\{C_{cc}\}\right)\Big\}\sigma^x+\\
-2\Big\{&\left(-\frac{\omega'}{4}-\frac{\omega}{\omega'}\mathfrak{Re}\{C_{sc}\}+\mathfrak{Re}\{C_{cs}\}\right)a+\\
&+\left(\frac{\Delta^2}{\omega'^2}\mathfrak{Re}\{C_{c0}\}+\mathfrak{Re}\{C_{cc}\}+\frac{\omega}{\omega'}\mathfrak{Re}\{C_{ss}\}\right)b+\\
&-\frac{\Delta}{\omega'}\left(\frac{\omega}{\omega'}\mathfrak{Re}\{C_{cc}\}+\mathfrak{Re}\{C_{ss}\}\right)c+\\
&+\frac{\Delta}{\omega'}\left(\mathfrak{Im}\{C_{s0}\}+\mathfrak{Im}\{C_{sc}\}-\frac{\omega}{\omega'}\mathfrak{Im}\{C_{cs}\}\right)\Big\}\sigma^m+\\
-2\Big\{&-\frac{\Delta}{\omega'}\mathfrak{Re}\{C_{s0}\}a-\frac{\omega}{\omega'}\frac{\Delta}{\omega'}\mathfrak{Re}\{C_{c0}\}b+\\
&+\left(\frac{\omega^2+\omega'^2}{\omega'^2}\mathfrak{Re}\{C_{cc}\}+2\frac{\omega}{\omega'}\mathfrak{Re}\{C_{ss}\}\right)c+\\
&+\left(-2\frac{\omega}{\omega'}\mathfrak{Im}\{C_{sc}\}+\frac{\omega^2+\omega'^2}{\omega'^2}\mathfrak{Im}\{C_{cs}\}\right)\Big\}\sigma^n\,. \qquad (4.2.8)
\end{aligned}
$$

The equilibrium state of the system is found by setting the time derivative to zero: since the theory is valid in the weak coupling limit $\alpha_\xi \to 0$ [where $\alpha_\xi \to$ is the coupling appearing in Eq. (4.0.2)], and all the C's are of order α, only the term with the c coefficient in Eq. (4.2.7) goes to a finite value:

$$
c_{\rm eq}=\frac{(\omega'-\omega)^2J(\omega'+\omega)+(\omega'+\omega)^2J(\omega'-\omega)}{(\omega'-\omega)^2J(\omega'+\omega)\coth\left(\frac{\hbar(\omega'+\omega)}{2k_BT}\right)+(\omega'+\omega)^2J(\omega'-\omega)\coth\left(\frac{\hbar(\omega'-\omega)}{2k_BT}\right)}\,. \qquad (4.2.9)
$$

The current is then given by projecting this state over the y direction, which adds a factor ω/ω', and multiplying by the I_0 prefactor to get a proper charge current: $I = I_0 J = I_0 c_{\rm eq}\omega/\omega'$. In terms of the formalism of Eq. (3.9), we see that $c_{\rm eq}$ is exactly the spin polarization $P = -\mathrm{Tr}(\hat{\mathbf{n}}\cdot\vec{\sigma}\tilde{\rho}_S)$.

We will now analyze the behavior of the system in different limits, finding that it is actually quite simple. For $T \to 0$, with any value of ω/Δ and any form of the spectral density, the stationary result of the ME is a projector onto the ground state $|-\hat{\mathbf{n}}\rangle$ of $\mathcal{H}_{\rm eff}$ and we get the (maximum) current given by Eq. (3.5). This extends the result of Ref. [24] to the nonadiabatic limit. For finite temperature we distinguish between the low-frequency, adiabatic limit $\omega \ll \Delta$ and the high-frequency antiadiabatic one $\omega \gg \Delta$. In the former pumping effects should be minimal and we correctly find the appropriate result for thermal equilibrium

$$
\mathrm{J} \simeq \frac{\omega}{\omega'}\tanh\left(\frac{\hbar\Delta}{2k_BT}\right)\,, \qquad (4.2.10)
$$

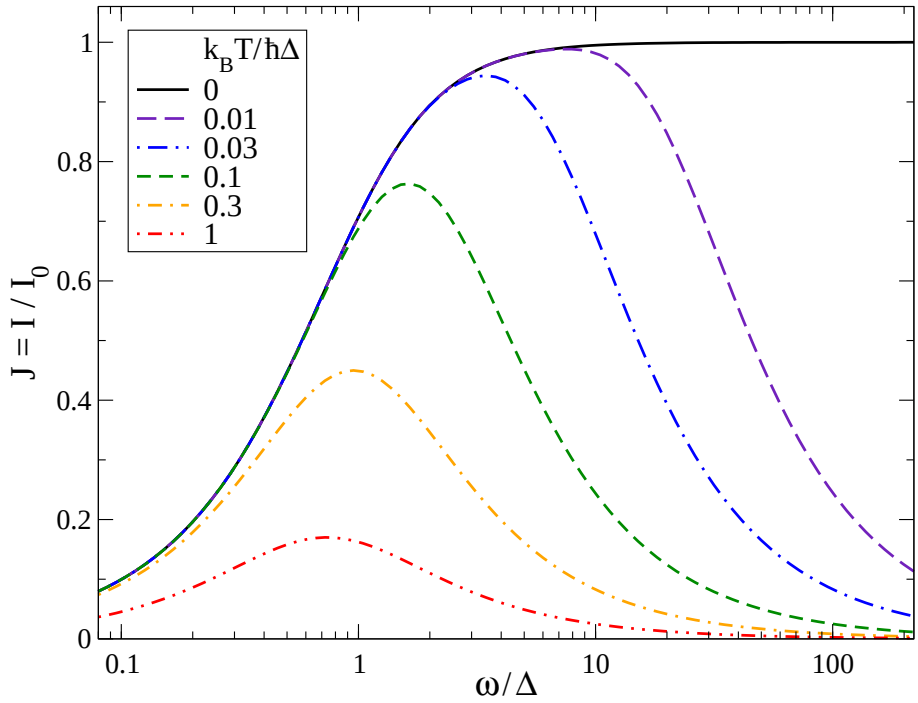

Figure 4.2.1: The DC component J as a function of the pumping frequency ω for $T = 0$ (solid line), as obtained from Eq. (3.5), and for several temperatures (dashed and dot-dashed lines), as obtained by Eq. (4.2.9) .

while in the latter we find

$$\mathrm{J} \simeq \frac{\omega}{\omega'} \tanh\left(\frac{\hbar(\omega'-\omega)}{2k_B T}\right) . \tag{4.2.11}$$

Eq. (4.2.11) states that for fast driving the result is again the thermal equilibrium of a static spin Hamiltonian but this time with the effective frequency

$$(\omega'-\omega) = \Delta\left[\frac{\Delta}{2\omega} + \mathcal{O}\left(\frac{\Delta}{\omega}\right)^3\right] , \tag{4.2.12}$$

vanishing for large ω. As Fig. 4.2.1 shows, at any finite T the current decays for large enough drive. Increasing the driving frequency ω at finite temperature at first increases the pumped current up to $\omega \simeq \hbar\Delta^2/k_B T$, but then for faster driving thermal fluctuations eventually cause the pumped current to drop.

4.3 Numerical simulations

To test the generality of the obtained analytical results the ME (4.2.4) has been solved numerically in Ref. [40] by means of Runge-Kutta integration to obtain $\rho_S(t)$ and from that $I(t) = I_0 \mathrm{Tr}[\sigma^y \rho_S(t)]$. It has been first of all checked that the numerical simulations actually lead to the predicted analytic asymptotic state. Fig. 4.3.1 shows a very good match

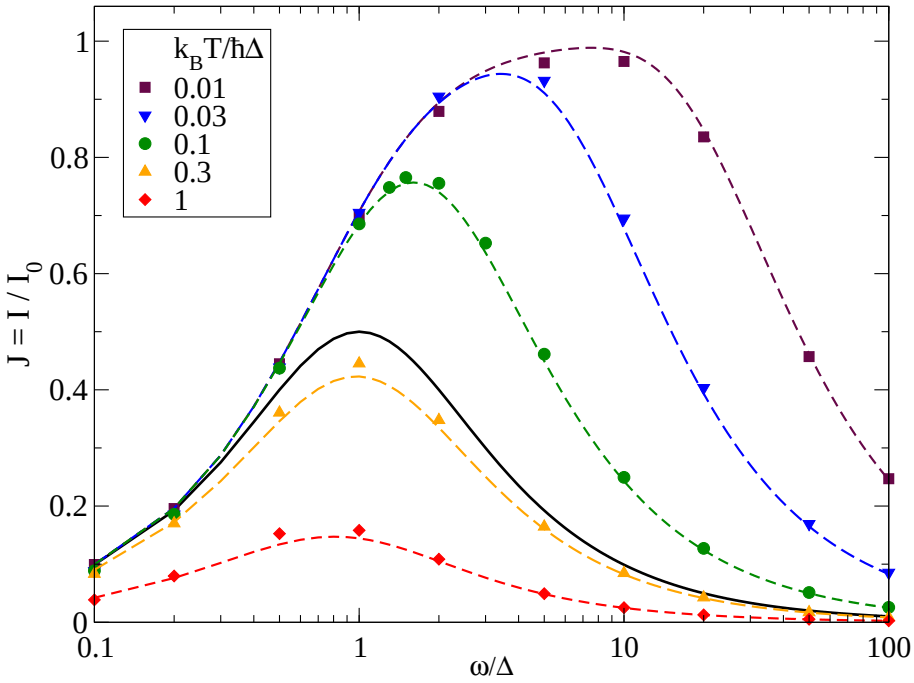

Figure 4.3.1: Asymptotic current J resulting from numerical simulations (points) compared to the analytical results of Eq. (4.2.9) (curves), already showed in Fig. 4.2.1.

between simulations and the analytical results. Secondly, the numerical approach has allowed us to explore the transient approach to the stationary state. Fig. 4.3.2 shows the full time evolution of the current compared to the pure quantum evolution in the absence of dissipation. The presence of the baths leads to damped oscillations towards the asymptotic state. The relaxation time needed to reach it is decreasing with α, but also depends on the temperature, with baths at lower temperature taking a longer time to equilibrate the system.

Finally, the effect of unequal environments in the x and z directions, in which case the simplifications leading to Eq. (4.2.9) do not hold, has been investigated thanks to the numerical simulations. In particular, the case $\alpha_x \neq \alpha_z$ (by symmetry, it does not matter which one is larger) has been considered. At finite (but small) α_ξ the solution is no longer stationary even in the rotating reference frame chosen, and small oscillations of the density matrix and of the current at frequency 2ω remain undamped in the long-time limit. Nevertheless for $\alpha_\xi \to 0$, the amplitude of these oscillating density-matrix terms vanishes linearly with α_ξ, and the constant part of the density matrix at low temperature converges to the symmetric-environment case. In particular at $T = 0$ J again saturates to ω/ω'. In this asymmetric case the behavior for $\alpha_\xi \to 0$ can be recovered also analytically by applying a rotating wave approximation to the asymmetric equivalent of Eq. (4.2.4), i.e. by neglecting all the terms oscillating with frequency ω or ω'. Remarkably, the resulting equation again coincides without approximations with the one appropriate to the symmetric environment. We can thus conclude that the results obtained for the symmetric environment are indeed representative

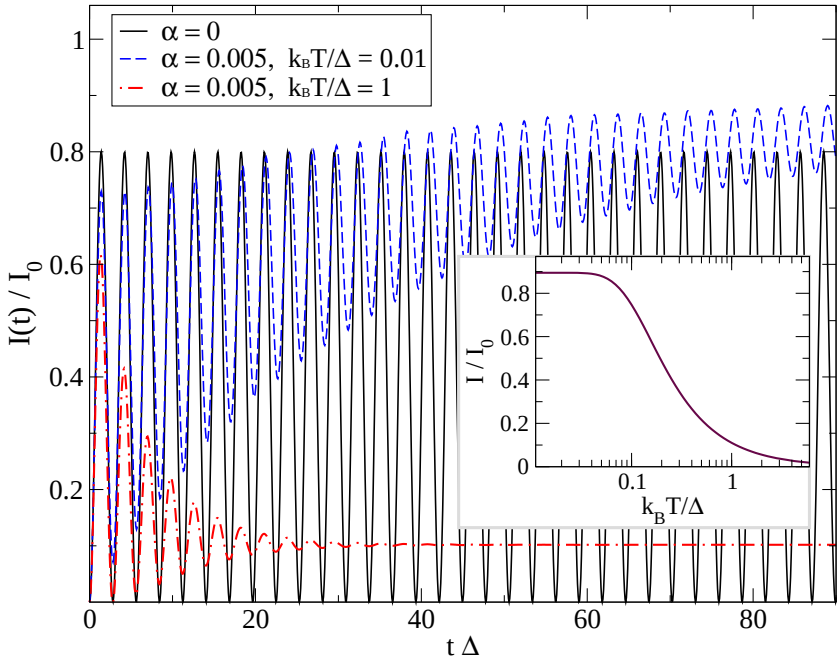

Figure 4.3.2: Time evolution of the current $I(t) = I_0 \mathrm{Tr}[\sigma^y \rho_S(t)]$ for $\omega = 2\Delta$, in the dissipationless case ($\alpha = 0$, solid curve), and in the transient induced by weak dissipation ($\alpha = 0.005$), at low (dashed) and intermediate temperature (dot-dashed), starting from the initial $|-\hat{z}\rangle$ state. Inset: temperature dependence of the steady-state DC output I.

of those expected in the more general asymmetric coupling case, provided the limit of weak coupling to the environment holds. In particular, Eq. (4.2.9) remains valid.

4.4 Feasibility and conclusions

Triple quantum dot systems have been recently realized experimentally [70, 75], and could be used to implement the pumping effect proposed. In Fig. 4.4.1 we reproduce for example the setup of Ref. [70]. To assess typical values for the pumped current, we adopt the parameters characteristic of a triple quantum dot arrangement realized experimentally as described in Ref. [70]. Hopping amplitudes between neighboring dots were in the $10 - 70$ μeV range: we assume a more symmetric arrangement with all hopping amplitudes $\gamma_0 \simeq 50$ μeV, and with gate electrodes apt to control the bias ϵ_i of each individual dot. The electric potentials of such electrodes are to be changed cyclically at frequency $\omega/(2\pi)$, with the appropriate phase relations, as described after Eq. (2.11). Provided that temperature is much smaller than the splitting scale $\hbar\Delta/k_\mathrm{B}$, our theory predicts an optimal current close to $I_0 = 0.05$ meV e$/(\sqrt{3}\hbar) \simeq 8.0\,10^{-24}$ J $\times\, 1.6\,10^{-19}$ C $/\,(1.8\,10^{-34}$ J s$) \simeq 7.0$ nA. Such a current is not especially small, and it should be possible to detect it, e.g. by means of the magnetic field it generates. The setup of Ref. [70] had the three quantum dots scattered over a region

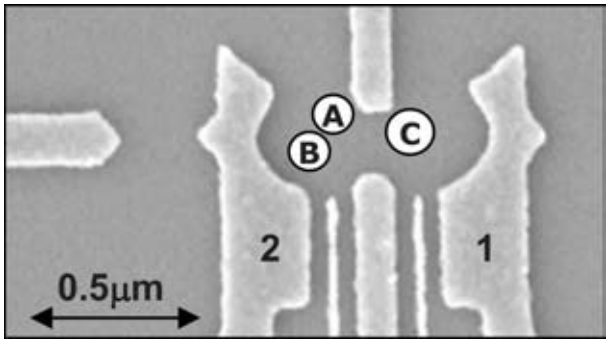

Figure 4.4.1: Experimental setup of a triple quantum dot, taken from Ref. [70].

of linear size $\sim$0.3 μm. We assume that the tunneling current circulating around a similar dot-ring arrangement could produce the same magnetic field as if in a ring wire of effective radius $r_{\rm eff} \simeq 0.2$ μm. With this simplification, we solve the equations of magnetism to compute the magnetic field flux intercepted by a detecting ring placed above the plane containing the quantum dots and parallel to it. We find that a ring-shaped SQUID of $5\,\mu$m radius placed $\sim 5\,\mu$m above the quantum dots intercepts a flux of order $0.02\,\Phi_0$ (here $\Phi_0 = \pi\hbar/{\rm e}$ is the flux quantum), a value routinely detectable.

The frequency and temperature regions where nonadiabatic effects on current could be detected are determined by the energy scale $\hbar\Delta$ of the effective spin-1/2 model, which in turn is the amplitude of the oscillating gate potentials acting on the dots, and is therefore under experimental control. However, the effective 2-level model is meaningful only for $\hbar\Delta \ll \gamma_0$ (otherwise all three states should be included in the calculation). Assuming $\Delta \simeq 0.1\gamma_0/\hbar \simeq$ 8 GHz, the predicted frequency-dependent dissipative effects on current should be observed near and mainly above this resonant angular frequency at temperature $T \lesssim 0.2\hbar\Delta/k_{\rm B}$. For the assumed parameters in the three-dot setup, this temperature amounts to $T \lesssim 10$ mK, which is reachable e.g. by continuous-cycle dilution refrigerators.

There are actually even more promising steps on the way of a possible experimental realization. Unpublished work [71] reveals that a perfectly symmetric and controllable triple quantum dot setup can be fabricated. Thanks to a private communication with Y. Chung we can reproduce Fig. 4.4.2, which shows a SEM image of a symmetric triangular triple quantum dot on a GaAs/AlGaAs 2DEG wafer, where the interdot tunneling is controlled by coupling gates (M1, M2 and M3 in the figure) and each dot is coupled (via the gates QPC1, QPC2 and QPC3) to a reservoir in the tunneling regime. Differently to Ref. [70], hopping amplitudes in Ref. [71] are effectively symmetric with $\gamma_0 \simeq 60$ μeV, and the dots are scattered over a larger region $\sim$0.65 μm. For such a setup, the possibility of variating cyclically the gate potentials with the suitable phases as proposed in chapter 2 and a SQUID-based measurement of the induced current should be straightforwardly available.

In summary, we presented an analytical solution for the time-dependent pumping of direct

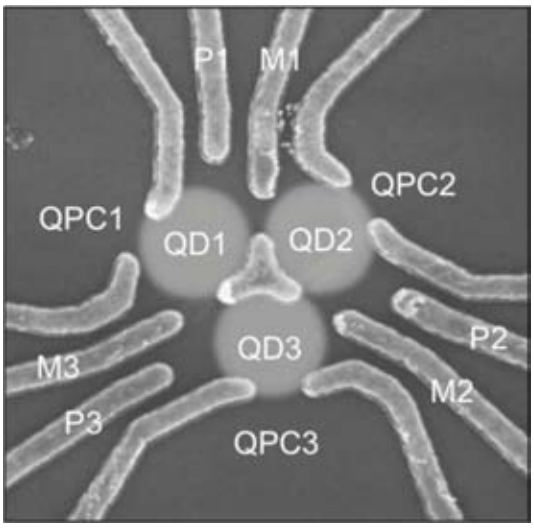

Figure 4.4.2: Experimental setup of a perfectly symmetric triple quantum dot, courtesy of Y. Chun, unpublished [71].

current in a quantum model with dissipation, valid in the weak dissipation limit. The solution fully covers the crossover from the well-known adiabatic limit to the antiadiabatic regime. In Ref. [24] an investigation was attempted of nonadiabaticity, with numerical evidence that a stronger dissipation might somehow compensate for the weak-coupling nonadiabatic current reduction relative to the geometric value of the adiabatic limit. Our exact solution clarifies that nonadiabaticity is fundamentally associated to such a radical current suppression that eventually, for large frequency, the charge pumped in one period drops as the frequency to the power of -2. The method introduced in a very recent work [25] also can deal with the nonadiabatic regime and represents a more general approach to pumping problems in the presence of weak dissipation. However in that work intermediate frequencies were studied only in the absence of dissipation: the present model seems unique in affording an explicit analytic expression for the density matrix and current in the presence of dissipation for arbitrarily high frequency. The main physical surprise of our results is that the frequency dependence of current is nonmonotonic, with an optimal value that moves from Δ upwards to infinity as temperature is reduced. This effect, on the whole reminiscent of magnetic-resonance physics, appears to be directly detectable for example in proven experimentally realizable multi-dot arrangements.

Part II

Single-electron tunneling oscillations

Introduction

Tunnel junctions and single-electron effects have been widely studied over the last four decades since a seminal paper by Averin and Likharev [76], who developed a perturbation theory to describe single-electron tunneling in a current-biased tunnel junction. The first famous experimental work on the observability of single-electron charging effects by Fulton and Dolan [77] boosted a large amount of both experimental and theoretical interest. A good summary of the main achievements is for example the collection of review articles titled *Single Charge Tunneling* [78], and notably the one by Nazarov and Ingold describing the theory of single-electron tunneling under the influence of an electromagnetic environment, to which we will often refer in the following.

This part is devoted to the study of one of the most appealing single-charge effect appearing in a normal-metal tunnel junction, namely the single-electron tunneling oscillations (SETOs), predicted in the 1980s [76, 79–81]. They manifest as an almost periodic fluctuation of the charge at the junction due to the interplay between the tunneling of electrons and the continuous biasing of the junction; in this sense they can be considered as an AC effect induced by a DC bias. Referring explicitly to the original paper by Averin and Likharev [76], we will focus on the junction charge-noise spectrum as a mean to trace and quantify the SETOs. The general plan is as follows: after a brief introduction on charging-effects and the so-called 'orthodox theory' of transport in small tunnel junctions, chapter 1 will present the bulk of our work, which has been devoted to the analytical and numerical study of SETOs at zero temperature and in absence of quantum fluctuations. In chapters 2 and 3 we will extend the analysis to thermal and quantum fluctuations effects respectively, considering the environment from a more general point of view via the so-called '$P(E)$ theory'.

Here we want to provide a brief introductory explanation about this phenomenon: what are in practice SETOs? Consider a tunnel junction with tunneling resistance $R_t \gg R_Q$ and capacitance C (typically $\sim$pF) placed in an environment with resistance R and biased with voltage V_b. As we will discuss in Sec. 1.1, it has been shown that if R is larger than the quantum of resistance R_Q the current is suppressed for bias voltage V_b smaller than the Coulomb gap $e/2C$ associated with the capacitance, and this effect can be visible for temperatures lower than the Coulomb charging energy $e^2/2C$. The idea behind SETOs can be understood in the simplest way in the limit $R, V_b \to \infty$ with $V_b/R = I_b$, i.e. the

purely current-biased junction regime. The current slowly charges the capacitance. When the voltage at the junction $V = Q/C$ reaches the threshold $e/2C$ one electron crosses the junction. If $I_b \ll e/R_tC$ this will happen just after V has reached the threshold. The charge on the capacitance after the tunneling event will be $Q = -e/2$, and Q will start to increase slowly again. A time e/I_b is needed before a new electron can cross the junction and the sequence can start again. The voltage at the junction will thus be periodically modulated at a tunable frequency I_b/e.

In practice, realizing a high-impedance environment with a flat frequency response till frequencies of the order of $e^2/2C\hbar$ is a challenging experimental problem, as discussed in detail in chapter 3. Most experimental observations of Coulomb blockade phenomena in *single* tunnel junctions have actually been done in an intermediate-impedance situation ($R \sim R_Q$), which leads at least to clearly nonlinear characteristics of the junction, see for example Refs. [82, 83]. Nevertheless, it is feasible to realize impedances of the order of some hundreds of kΩ; for instance in Ref. [84] a resistance $R \sim 0.4$ MΩ has been realized. For these values not only the suppression of the current at low-bias voltage, but also SETOs should be visible. Interestingly, in Ref. [85] a resistive environment yielding to Coulomb blockade has been obtained by exploiting weak localization in a multiwalled carbon nanotube.

Observation of SETOs remains however experimentally challenging. The implementation of the required strong-impedance environment has been realized by different authors using for example on-chip resistors [86–91]. To avoid heating problems an alternative approach has also been tried by designing the environment with tunnel-junction arrays [92, 93]; The stochastic nature of the current is reduced by the presence of a large number of arrays [94]; recently an observation of soliton-like single electron oscillations with this method has been reported [95]. A similar phenomenon for superconducting Josephson junctions has been predicted (Bloch oscillations) [96] and investigated by many authors [97–100]. Arrays of DC SQUIDs have also been exploited in this case to build up the proper environment to obtain Coulomb blockade of Cooper pairs [101–103]. Reports on the observation of Shapiro-step-like structures in microwave/RF-irradiated junctions constitute the present state of the art for the experimental probe of this effect [90, 98, 104, 105]. Progress in the detection of high-frequency current fluctuations [20–23] can open new possibilities of observation, and especially of the crossover region, where the oscillations are not completely established. At the same time the possibility of generating a periodic and frequency-tunable electric signal without any oscillating source is an interesting opportunity and could have applications, for instance, as actuation of motion in nanomechanical systems or as controlled single-electron source.

Chapter 1

Single-electron oscillations at zero temperature

In this chapter we investigate how accurate the SETOs can be as a function of the impedance and of the bias conditions, at zero temperature and in a strict current-biasing scheme in a limit for which quantum fluctuations are negligible. To this purpose we study the charge-fluctuation spectrum at the junction capacitance (or equivalently the current-fluctuation spectrum through the resistance load), and in particular the width of the peak at frequency $\sim I_b/\mathrm{e}$. Notwithstanding the relatively large number of papers on this subject, some specifically addressing the dynamics of arbitrarily biased mesoscopic tunnel junctions with an analytical approach [106–108], a consistent and simple calculation of these quantities is not available. It can be useful in order to evaluate the expected effect in view of measuring current fluctuations in this kind of device. We find that the width of the peak scales as the inverse of the impedance for large R/R_t. The peak remains observable till values of R/R_t of the order of 5. This chapter can be considered as the bulk of the SETOs part and is organized as follows: in section 1.1 we introduce the basic assumptions underlying our treatment of the transport through the junction; in 1.2 we present the model of the junction circuit; in 1.3 we discuss the different regimes that the system undergoes by varying the bias current and the environment resistance, obtaining in particular an analytical expression for the the I-V characteristic in the SETOs regime; in 1.4 we calculate analytically the charge spectrum; the results are discussed and compared with numerical Monte Carlo simulations in section 1.5; section 1.6 gives our conclusions. The results have been published in Ref. [109].

1.1 Charging effects in tunnel junctions

A tunnel junction can be generally defined as a barrier, for example a thin layer of insulating material, interposed between conductors (see Fig. 1.1.1), through which electrons can

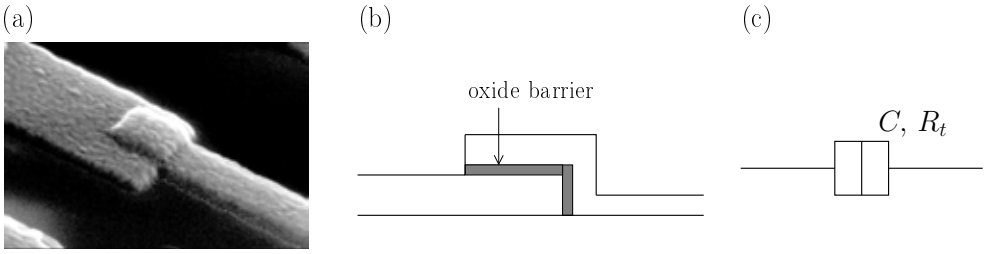

Figure 1.1.1: (a) a real evaporated overlap junction; (b) schematic example of an overlap junction with an insulating layer; (c) circuit representation of a tunnel junction element.

only pass by quantum tunneling. We will be interested here only in the case where the conductors, which we can call electrodes, are normal metals, thus disregarding superconducting tunnel junctions in the following. It is by now well-known that with very small junctions and at low temperatures, the result of a recharging of the junction capacitance by the tunneling of a single electron can give rise to charging effects. The conditions for such a direct manifestation of the discreteness of the charge are however not so straightforwardly realized. A tunnel barrier alone in fact is not enough to observe the effects of single charge quanta on macroscopic quantities (currents and voltages). It is primarily needed Coulomb interaction between electrons to be strong enough to act against thermal charge fluctuations. Secondly, also quantum electromagnetic fluctuations play an essential role in determining the tunneling rates of electrons across the junction. We shall stress that single-electron effects are washed out in a *single* tunnel junction unless a proper biasing scheme is implemented, while they are not prevented to occur in systems composed of at least one 'island' (as is obtained for example by placing two tunnel junctions in series).

From the semiclassical point of view we will be adopting here, a junction or generically a tunnel barrier can be represented by a capacitance C and a tunneling resistance R_t. The basic conditions for single-electron effects which arise in the presence of tunnel barriers not to be masked by thermal and quantum fluctuations are

1. the tunneling resistance R_t must be much greater that the quantum resistance $R_Q = h/\mathrm{e}^2 \simeq 25.8\ \mathrm{k}\Omega$, to ensure the wave function of an electron to be well-localized on one side or the other of the barrier, so that we can meaningfully speak about a 'tunneled electron':
$$R_t \gg R_Q\,, \tag{1.1.1}$$

2. the capacitance C associated to the barrier must be small enough and the temperature low enough for the energy scale of thermal fluctuations to be exceeded by the charging energy $E_c = \frac{\mathrm{e}^2}{2C}$, that is the energy required to charge the capacitance with an electron:
$$E_c \gg k_B T\,. \tag{1.1.2}$$

If these conditions are realized the charging energy dominates the transport process and this

is enough for Coulomb blockade to occur in circuits with at least one island, i.e. if they are contacted to a voltage source there is a threshold for the passage of current through the island $V > \mathrm{e}/2C$. Consider instead just a single tunnel junction contacted to an ideal voltage source (or 'ideally voltage biased'): an electron which tunnels through the barrier from one side of the capacitance to the other is immediately removed from the junction and the only energy scale involved is $\mathrm{e}V$, the work done by the voltage source; the charge on the junction capacitor is in other words kept fixed at all times. This results in a linear current-voltage characteristics without Coulomb blockade. On the other hand, consider adding an ideal resistive environment, say a resistor $R > R_Q$ in series with the voltage source for simplicity: this prevents the immediate removal of the tunneled charge since the junction capacitance is now being slowly charged with time constant RC. Coulomb blockade thus does occur and the transport through the junction is blocked until its voltage is enough for the charging energy to be exceeded $V = Q/C > \mathrm{e}/2C$; at this point an electron can tunnel through the junction changing the capacitor charge by e and the process of slow charging continues. The result is the well-known offset in the current-voltage characteristics given by $\mathrm{e}/2C$ known as 'Coulomb gap'. In Fig. 1.1.2 we show schematically how the resistive environment is essential for single-charge effects to show off in a tunnel-junction circuit without an island. We want to clarify here a matter of nomenclature in the literature for single tunnel junctions which may otherwise generate some confusion: in the zero-impedance limit of Fig. 1.1.2, i.e. when no single-charge effects are displayed [even in the presence of conditions (1.1.1) and (1.1.2)] the junction is referred to as ideally 'voltage biased' and the *global rule* is said to apply, while the opposite $R \to \infty$ limit is the ideally 'current biased' case and the *local rule* is said to apply. These definitions label the two opposite limiting behaviors of any tunnel junction and apply independently from the effective biasing scheme of the circuits considered.

In this chapter we will work in the limit of $R \gg R_Q$, so that we can neglect quantum fluctuations and study the phenomenon of the single-electron tunneling oscillations in the tunnel junction as a function of the ratio R/R_t. A semiclassical theory describing this regime, the so-called 'orthodox theory' has been developed in Ref. [76], to which we refer in the following. We will then relax this assumption in chapter 3 and see the crossover to a low-impedance case where Coulomb blockade starts to be washed out and the global rule applies. This will require taking into account the environment properly, as is done by the $P(E)$ theory by Ingold and Nazarov (Ref. [110]).

We now recall the derivation of the tunneling rates expression in the orthodox theory framework, as is very clearly done for example in Ref. [111]. Following the local rule, the rates are calculated taking into account only the change in the electrostatic energy of the junction before and after the electron has tunneled ΔE. Using Fermi's golden rule the tunnel rate from an initial state i to a final state f can be generically expressed as

$$\Gamma_{i\to f}(\Delta E) = \frac{2\pi}{\hbar}|M_{if}|^2\delta(E_i - E_f - \Delta E)\,, \tag{1.1.3}$$

where M_{if} is the tunnel transmission coefficient from the state i with momentum k_i to the state f with momentum k_f, E_i and E_f are the initial and final energies of the tunneling

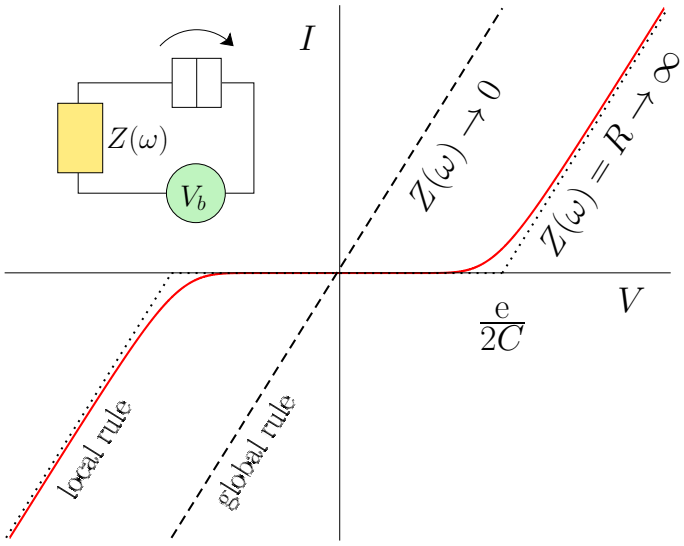

Figure 1.1.2: Basic scheme of the influence of the environment [here represented generically as an impedance $Z(\omega)$] on single-charge effects for a single tunnel junction. I and V are the current and the voltage at the junction. In the case of ideal pure voltage bias, i.e. $Z(\omega) \to 0$, single-charge effects are washed out (dashed line). In the case of ideal current bias, i.e. the impedance is an infinite resistance $Z(\omega) = R \to \infty$, there is an offset in the I-V curve due to Coulomb Blockade (dotted line).

electron. The total rate from occupied states at one side of the tunnel barrier to unoccupied states on the other side is given by the summation over possible initial and final states:

$$\Gamma(\Delta E) = \frac{2\pi}{\hbar} \sum_i \sum_f |M_{if}|^2 f(E_i)(1 - f(E_f))\delta(E_i - E_f - \Delta E)\,, \tag{1.1.4}$$

where $f(E)$ is the Fermi function

$$f(E) = \frac{1}{1 + e^{(E-E_F)/(k_B T)}}\,. \tag{1.1.5}$$

The transmission probability can reasonably be treated as a constant $|M_{if}|^2 \simeq |M|^2$, and by using the density of states $D(E)$ we can convert the summations into integrals:

$$\Gamma(\Delta E) = \frac{2\pi}{\hbar}|M|^2 \int_{E_{ci}}^{\infty} dE_i \int_{E_{cf}}^{\infty} dE_f\; D_i(E_i) D_f(E_f) f(E_i)(1 - f(E_f))\delta(E_i - E_f - \Delta E)\,, \tag{1.1.6}$$

where E_{c_i} and E_{c_f} are the conduction band edges of the sides the electron is tunneling from and to respectively. The product of the Fermi functions in Eq. (1.1.6) is nonvanishing in a window defined by the Fermi energies of the initial and final sides (E_{F_i} and E_{F_f}), over which the densities of states can be taken constant. We thus get

$$\Gamma(\Delta E) = \frac{2\pi}{\hbar}|M|^2 D_i D_f \int_{E_c}^{\infty} dE\; f(E)(1 - f(E))\delta(E - \Delta E)\,, \tag{1.1.7}$$

with $E_c = max(E_{c_i}, E_{c_f})$. In absence of charging effects we know that the tunnel junction has Ohmic I-V characteristics, with the current proportional to the applied bias through the tunneling resistance R_t. We can thus phenomenologically define the tunneling resistance incorporating the transmission matrix element and the densities of states:

$$R_t = \frac{\hbar}{2\pi \mathrm{e}^2 |M|^2 D_i D_f} \,. \tag{1.1.8}$$

For metal junctions we have $E_F \gg E_c$ and we can safely take the integration from $-\infty$:

$$\Gamma(\Delta E) \simeq \frac{1}{\mathrm{e}^2 R_t} \int_{-\infty}^{\infty} dE\, f(E)(1-f(E))\delta(E-\Delta E) \;\simeq\; \frac{1}{\mathrm{e}^2 R_t}\; \frac{\Delta E}{e^{\Delta F/(k_B T)}-1}\,, \tag{1.1.9}$$

or at zero temperature

$$\Gamma(\Delta E) \simeq \begin{cases} 0 & \Delta E \geq 0 \\ -\Delta E/(\mathrm{e}^2 R_t) & \Delta E < 0 \end{cases} \quad . \tag{1.1.10}$$

The difference in the electrostatic energy before and after tunneling reads explicitly:

$$\Delta E = \frac{(Q \pm \mathrm{e})^2}{2C} - \frac{Q^2}{2C} = \frac{\mathrm{e}}{C}\left(\frac{\mathrm{e}}{2} \pm Q\right) . \tag{1.1.11}$$

Apart from the above mentioned condition $R_t \gg R_Q$ (about the required opacity of the tunnel barriers to speak consistently of localized electrons), a few other basic assumptions underlie this result: dimensions and shapes of electrodes and junction are ignored, the orthodox theory is a $0D$ model; the tunneling process is assumed to be almost instantaneous, the barrier traversal time of tunneling electron is the shortest timescale of the system and in particular is much shorter than the time between consecutive tunnel events; the electric charge redistribution inside the electrodes after the tunneling is assumed to be instantaneous; the energy quantization in the electrodes is ignored.

1.2 The system and the model

Let us consider a tunnel junction with tunneling resistance $R_t \gg R_Q$ and associated capacitance C. The circuit is voltage-biased (at voltage V_b) at zero temperature ($T = 0$) in the presence of a resistor of resistance R in series with the junction [see. Fig. (1.2.1) left side]. This circuit is equivalent to one with a current source I_b and a shunt resistor R_s in parallel to the junction, provided $I_b = V_b/R$ and $R = R_s$ [see. Fig. (1.2.1) right side]. We will thus use the parallel configuration to describe the device in analogy with the previous literature [76]. It is clear that the results can be readily converted to the voltage bias case. In particular note that the limit $R_s \to \infty$ (specifically $R_s \gg R_t$) describes the ideal current source.

Since we are interested in studying SETOs we need $R_s \gtrsim R_t \gg R_Q$, as we will explain in detail. We thus assume from the outset that $R_s \gg R_Q$, which allows us to neglect quantum

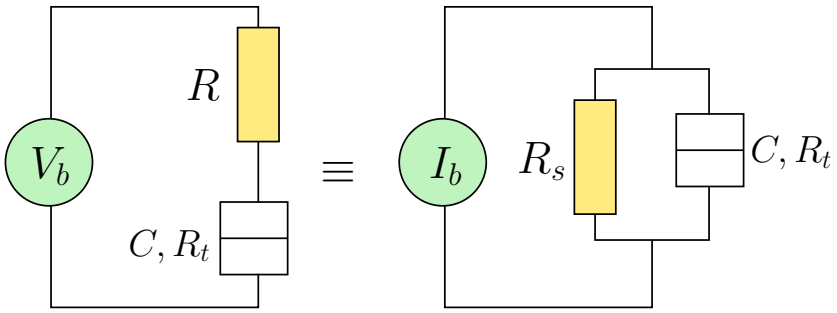

Figure 1.2.1: Circuit scheme of the system considered: a tunnel junction with capacitance C and tunneling resistance R_t, biased by the constant current I_b and shunted by a resistance R_s in parallel.

fluctuations and treat the charge degrees of freedom classically [76]. We also assume that the environment has a flat frequency response $Z(\omega) = R_s$ up to frequencies $\hbar\omega \approx \mathrm{e}^2/2C$. This hypothesis, though not easy to fulfill in practice (see chapter 3 for more details), is the common assumption in the literature about this problem, and allows a simpler and more transparent approach. As introduced in section 1.1, in this regime the transport through the junction is described by the orthodox Coulomb blockade theory. We rewrite the expression for the electron-tunneling rate (1.1.10) in terms of the voltage at the junction (V_J) as follows:

$$\Gamma(V_J) = \theta(V_J - \mathrm{e}/2C)(V_J - \mathrm{e}/2C)/\mathrm{e}R_t\,, \tag{1.2.1}$$

where θ is the Heaviside function. If ($R_Q \ll$) $R_s \ll R_t$ the standard picture of Coulomb blockade applies to the degrees of freedom of the environment: they have the time to relax to thermal equilibrium between two electron-tunneling events. The current-voltage characteristic in this case is then given by $\langle I_J(V_J)\rangle = R_t^{-1}(\langle V_J\rangle - \mathrm{e}/2C)\theta(\langle V_J\rangle - \mathrm{e}/2C)$, exposing a linear monotonic behavior and a clear Coulomb gap for the current I_J through the junction. But if $R_s \sim R_t$ or larger (for moderate values of the bias voltage) the resistive environment (described for instance by a large collection of bosonic modes) reaches thermal equilibrium, but not the charge on the capacitance $Q(t)$, which needs a time $\tau_s = R_sC$ to relax to its stationary state. Formula (1.2.1) still holds, but with a time-dependent voltage $V_J(t) = Q(t)/C$. The time dependence of the charge is given by the solution of the differential equation:

$$\dot{Q} = -Q/R_sC + I_b\,, \tag{1.2.2}$$

which for an initial condition Q_0 at $t = 0$ reads

$$Q_f(Q_0, t) = (Q_0 - I_b\tau_s)e^{-t/\tau_s} + I_b\tau_s\,. \tag{1.2.3}$$

With Eq. (1.2.3) and the tunneling rate (1.2.1) the stochastic problem of transport through the junction is then completely formulated. In the remainder of the chapter we discuss the behavior of the current and of the charge as a function of the two relevant dimensionless parameters of the problem:

$$\rho = \frac{R_s}{R_t} \tag{1.2.4}$$

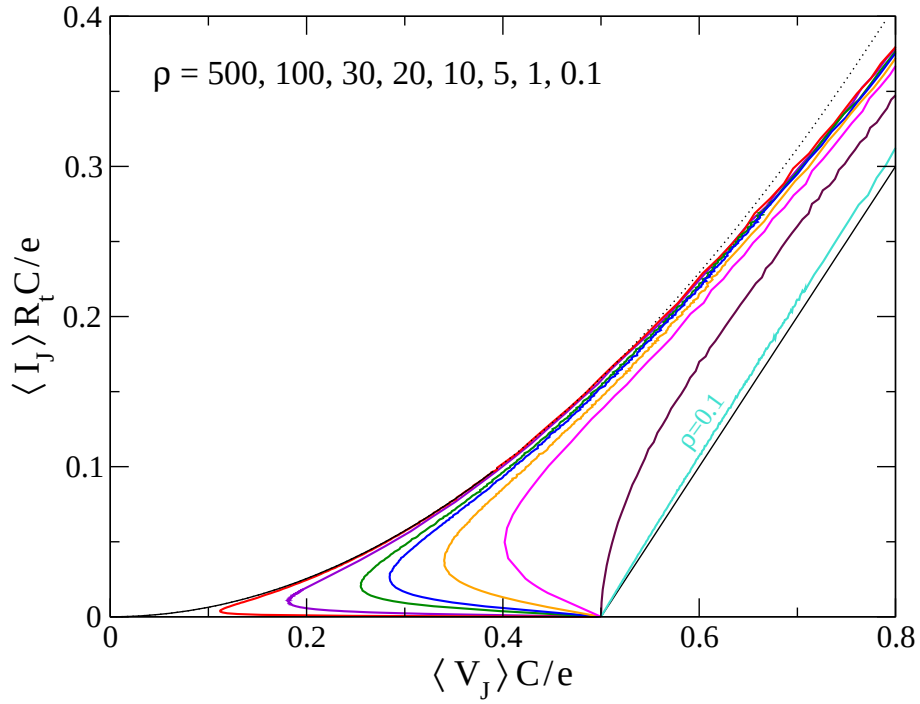

Figure 1.2.2: Average current through the junction versus average voltage for different values of the ratio $\rho = R_s/R_t$. The curves evolve from the standard Coulomb blockade suppression (rightmost line corresponding to $\rho = 0.1$) to a square root behavior (leftmost line $\rho = 500$). The dotted line is the large-ρ limit of Eq. (1.2.6).

and

$$\kappa = (I_b - I_{\rm th})/I_{\rm th}\,, \tag{1.2.5}$$

with $I_{\rm th} = {\rm e}/(2\tau_s)$ the threshold for the current to start flowing through the tunnel junction.

The current through the junction has already been calculated numerically in the very early literature [80]. We obtained the same results by Monte Carlo simulations and for convenience we show the curves in Fig. 1.2.2. The limit of infinite R_s, or ideal current source, was discussed in details in Refs. [76, 112]. There it was shown in particular that in this limit the system is in the ideal SETOs regime with frequency $I_b/{\rm e}$, and with an average voltage at the junction given by (see [76])

$$\langle V_J\rangle = \sqrt{\frac{\pi {\rm e} R_t \langle I_J\rangle}{2C}}\,. \tag{1.2.6}$$

In the next section we will discuss the behavior of the system for the intermediate regimes appearing when R_s/R_t is not infinite, giving in particular analytical expressions for the SETOs frequency and I-V characteristics.

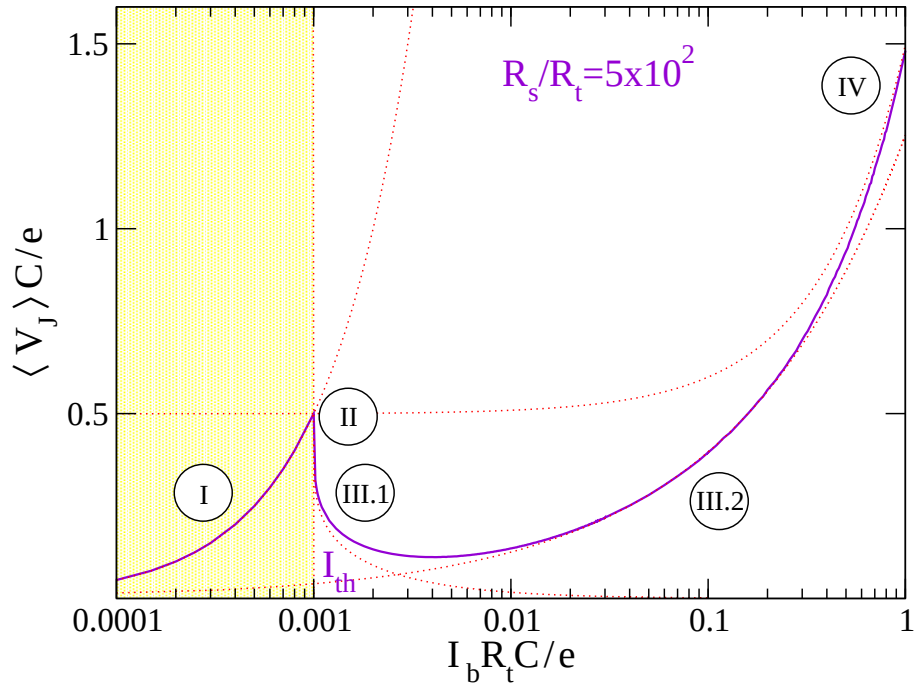

Figure 1.3.1: Average voltage through the junction versus bias current in logarithmic scale ($\rho = 5 \times 10^2$): four different transport regimes can be outlined. Solid line is the numerical simulation, while dashed lines represent the analytical curves given in Sec. 1.3.

1.3 Regimes of current transport

In this section we study the evolution of the current through the junction as a function of the current bias for different values of the external resistance. The most interesting case is when R_s/R_t is very large, we thus plot in Fig. 1.3.1 the current on a logarithmic scale for the extreme value of $R_s/R_t = 5 \times 10^2$. Fig. (1.3.1) will be used as a map for the rest of the section, where we will discuss how the junction evolves through the four different regimes of transport indicated in the figure with roman numbers from (I) to (IV). Fig. (1.3.2) shows the behavior of $Q(t)$ in the different regimes.

1.3.1 Non SETOs regimes

Let us begin with the region indicated with (I) in Fig. 1.3.1. For $I_b < I_{\rm th}$ the whole current flows through the shunting resistance and the voltage at the junction

$$\langle V_J \rangle_{\rm I} = R_s I_b \tag{1.3.1}$$

remains below the threshold of the Coulomb blockade: e/2C. Note that this first branch of the I-V characteristic in Fig. 1.2.2 is flattened on the $I_J = 0$ value and it is thus not visible.

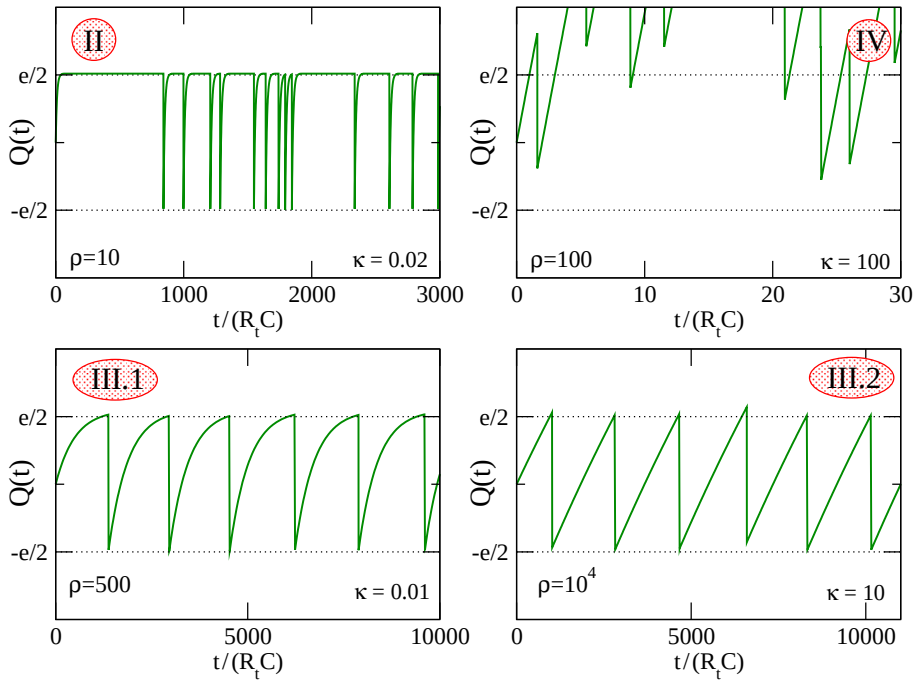

Figure 1.3.2: The time behavior of the charge in the different regimes. Extreme values of the parameters ρ and κ have been chosen to best outline the differences.

For $I_b > I_{\rm th}$ transport through the junction becomes possible. For $I_b - I_{\rm th} \to 0^+$ one can identify a poissonian regime of transport [region (II) in Fig. 1.3.1], where the time between tunneling events fluctuates strongly. This is due to the fact that $\Gamma(V)$ as given by Eq. (1.2.1) vanishes linearly near the threshold, and for very small $I_b - I_{\rm th}$ the charge has always the time (typically τ_s) to reach the saturation value $Q_{\rm s} = I_b \tau_s$. We thus have that the typical inverse time between two tunnel events is

$$\frac{1}{\tau_{\rm eff}} = \Gamma(Q_{\rm s}) = \frac{R_s}{R_t}\,\frac{I_b - I_{\rm th}}{\rm e} \ll \frac{1}{\tau_s}\,. \tag{1.3.2}$$

The last inequality sets also the region of existence of the regime (II) i.e. $0 < \kappa \ll 1/\rho$. The average of V_J can be readily evaluated by averaging the oscillations of the charge $Q(t) = Q_{\rm s} - {\rm e}\, e^{-t/\tau_s}$ on the average time between two tunneling events $\tau_{\rm eff} + \tau_s \approx \tau_{\rm eff}$. This gives:

$$\langle V_J \rangle_{\rm II} = R_s \left[I_b \left(1 - \frac{R_s}{R_t} \right) + I_{\rm th}\, \frac{R_s}{R_t} \right] \tag{1.3.3}$$

and the curve is shown dashed in Fig. 1.3.1 (appearing almost a vertical line at the chosen scale). Note that the slope changes sign at $R_s/R_t = 1$. We will see that for $R_s \ll R_t$ this region joins continuously region (IV) without the appearance of region (III).

It is thus convenient to discuss now the region (IV) defined as the limit of large I_b. In this limit the junction has the I-V characteristic of a normal resistor shifted by the Coulomb

gap. The average V_J reads then

$$\langle V_J \rangle_{\rm IV} = \frac{R_s R_t}{R_s + R_t} \left(I_b + \frac{\rm e}{2R_t C} \right) . \tag{1.3.4}$$

This expression holds for $\langle V_J \rangle \gg {\rm e}/2C$, i.e. for $I_b/I_{\rm th} \gg (R_t + R_s)/R_s$. For $R_s \gg R_t$ it is then clear that a large region defined by the condition

$$1/\rho \ll \kappa \ll \rho \tag{1.3.5}$$

exists between region (II) and region (IV). This is the SETOs region, (III) in Fig. (1.3.1), which will be discussed below. On the other side, for $R_s \ll R_t$, one sees that region (II) and region (IV) overlap at $\kappa \approx 1$. Actually it is straightforward to check that Eq. (1.3.4) expanded to first order in R_s/R_t coincides with Eq. (1.3.3).

1.3.2 SETOs regime

Let us now discuss the single-electron oscillations regime, defined as region (III) in Fig. 1.3.1. This region is present only if $R_s \gg R_t$ and is characterized by nearly periodic electron tunneling events, since the time between two events is dominated by the deterministic charging time of the capacitance. This time is typically of the order of $t_\star$, defined as the time needed to charge the capacitance from $Q = -{\rm e}/2$ to $Q = {\rm e}/2$:

$$t_\star/\tau_s = \ln \left(\frac{I_b + I_{\rm th}}{I_b - I_{\rm th}} \right) = \ln \left(\frac{2+\kappa}{\kappa} \right) . \tag{1.3.6}$$

The electrons hop just after the threshold voltage has been reached.

A general statistical theoretical framework is presented in Ref. [76] (and recalled in appendix 1.A), but its analytical solution is given there only in the ideal current source limit ($R_s/R_t \to \infty$). Actually a simple approach happens to be available for the SETOs regime and further progress is possible. In order to obtain these results and for the calculation of the correlation function of the next section it is convenient to introduce a few concepts.

In Fig. (1.3.3) the typical time dependence of the charge $Q(t)$ in the SETOs regime is shown. We can associate a number n to each hopping event and define t_n and $\tau_n = t_n + \delta\tau_n$ as the instant of time when $Q(t) = {\rm e}/2$ and when the hopping event takes places, respectively. These quantities fluctuate randomly, but a correlation between t_n and t_{n-1} exists. Inversion of Eq. (1.2.3) gives the time needed to reach the border of the Coulomb blockade region starting from a charge Q_0:

$$\Xi(Q_0) = -\tau_s \ln \left(\frac{I_b \tau_s - {\rm e}/2}{I_b \tau_s - Q_0} \right) . \tag{1.3.7}$$

We thus have the following relation between successive times t_n:

$$t_n - t_{n-1} \equiv \mathfrak{F}(\delta\tau_{n-1}) , \tag{1.3.8}$$

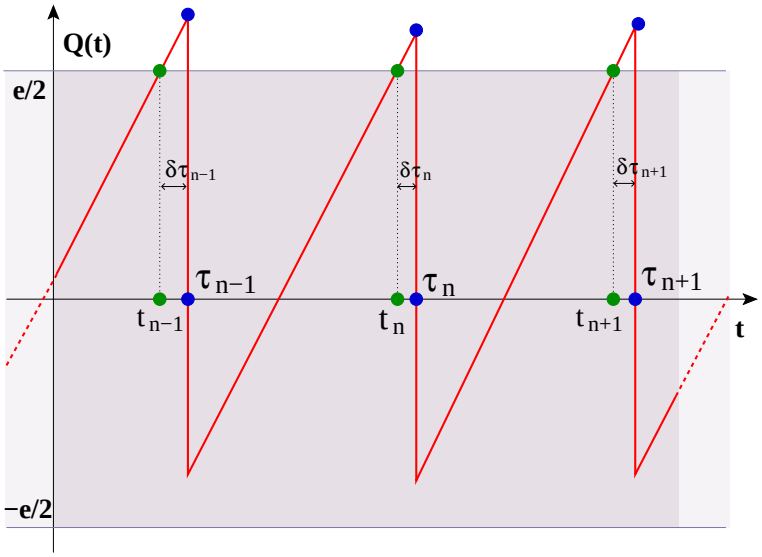

Figure 1.3.3: Details of the tunneling process: t_n is the time at which the charge reaches the blockade region border after the $(n-1)$th tunneling event and $\delta\tau_n$ is the time it stays outside the border before the nth event.

with

$$\mathfrak{F}(\delta\tau) = \delta\tau + \Xi\left(Q_f\left(\frac{\mathrm{e}}{2}, \delta\tau\right) - \mathrm{e}\right) = \delta\tau - \tau_s \ln\left(\frac{\kappa}{2 + \kappa e^{-\delta\tau/\tau_s}}\right). \tag{1.3.9}$$

Let us now introduce the probability $P_n(t)$ that n electrons have tunneled through the junction at the time t. Within the SETOs region, this quantity is different from zero only in a small time region of the order of $t_\star$, and, in particular, the above-mentioned condition on the typical hopping time implies that $P_n(t)$ will reach 1 and then vanish in a time much shorter than $t_\star$, just after $Q(t)$ crosses the threshold e/2. The rate equation for $t \geq t_n$ $[Q(t_n) = \mathrm{e}/2]$ takes the simple form

$$\frac{dP_n(t)}{dt} = -\Gamma\left(\frac{Q_f(\mathrm{e}/2, t)}{C}\right) P_n(t)\,, \tag{1.3.10}$$

with the initial condition $P_n(t_n) = 1$. The solution reads

$$P_n(t) = \exp\left\{-\frac{(I_b\tau_s - \mathrm{e}/2)}{\mathrm{e}R_tC}\,\tau_s\left(\frac{t-t_n}{\tau_s} + e^{-\frac{t-t_n}{\tau_s}} - 1\right)\right\}. \tag{1.3.11}$$

For short times $(t - t_n \ll \tau_s)$ it has a Gaussian form

$$P_n(t) \approx \exp\left\{-\frac{I_b\tau_s - \mathrm{e}/2}{2\mathrm{e}R_tC\tau_s}(t-t_n)^2\right\} = \exp\left\{-\frac{(t-t_n)^2\kappa\rho}{(4\tau_s^2)}\right\} \tag{1.3.12}$$

that has a decay time scale $\sim \tau_s/\sqrt{\kappa\rho} \ll t_\star$ in region (III). The Gaussian form will thus be used in the following for the analytical calculations.

From the knowledge of $P_n(t)$ it is possible to obtain the probability density that a hopping event takes places at time t: $\mathcal{P}(t) = -dP_n/dt$, for $t \geq t_n$. This allows us to calculate the

average delay time $\langle\delta\tau\rangle$ for an electron to hop after the threshold e/2 has been crossed by the charge $Q(t)$:

$$\langle\delta\tau\rangle = \int_0^\infty dt\ t\ \mathcal{P}(t)\,. \tag{1.3.13}$$

In particular, when P_n can be approximated by the Gaussian (1.3.12) one obtains

$$\mathcal{P}_{\rm gauss}(\delta\tau) = -\frac{{\rm e}/2 - I_b\tau_s}{{\rm e}R_tC\tau_s}\ \delta\tau\ \exp\left\{\frac{{\rm e}/2 - I_b\tau_s}{2{\rm e}R_tC\tau_s}\ \delta\tau^2\right\} = \frac{\kappa\rho}{2\tau_s^2}\ \delta\tau\ \exp\left\{-\frac{\kappa\rho}{4\tau_s^2}\ \delta\tau^2\right\}, \tag{1.3.14}$$

We can therefore explicitly calculate all the moments $\langle\delta\tau^n\rangle$:

$$\langle\delta\tau^n\rangle = \int_0^\infty d(\delta\tau)\ \frac{\kappa\rho}{2\tau_s^2}\ \delta\tau^{n+1}\ \exp\left\{-\frac{\kappa\rho}{4\tau_s^2}\ \delta\tau^2\right\} = \left(\frac{4\tau_s^2}{\kappa\rho}\right)^{n/2}\Gamma\left(1+\frac{n}{2}\right), \tag{1.3.15}$$

where we have the Gamma function $\Gamma(1+n/2) = \sqrt{\pi}(n)!!/2^{(n+1)/2}$. In the following we will need only the first two:

$$\begin{aligned}\langle\delta\tau\rangle &= \int_0^\infty d(\delta\tau)\ \delta\tau\ \mathcal{P}_{\rm gauss}(\delta\tau) = \sqrt{\frac{{\rm e}\pi R_tC\tau_s}{2(I_b\tau_s - {\rm e}/2)}} = \tau_s\sqrt{\frac{\pi}{\kappa\rho}}\\ \left\langle\delta\tau^2\right\rangle &= \int_0^\infty d(\delta\tau)\ \delta\tau^2\ \mathcal{P}_{\rm gauss}(\delta\tau) = \frac{4{\rm e}\pi R_tC\tau_s}{2(I_b\tau_s - {\rm e}/2)} = \tau_s^2\ \frac{4}{\kappa\rho}\qquad .\end{aligned} \tag{1.3.16}$$

Note in particular that $\langle\delta\tau\rangle = \tau_s\sqrt{\pi/(\kappa\rho)} \ll t_\star$.

To obtain the period $\mathcal{T}$ of the SETOs one has to average the nonlinear expression (1.3.9): $\mathcal{T} = \langle\mathfrak{F}\rangle$. For small fluctuations $\langle\delta\tau\rangle$ we have :

$$\mathfrak{F}(\delta\tau) = \lim_{\delta\tau\to 0}\left[\delta\tau - \tau_s\ln\left(\frac{\kappa}{2+\kappa e^{-\delta\tau/\tau_s}}\right)\right] = t_\star + \frac{2\ \delta\tau}{2+\kappa} + \frac{\kappa\ \delta\tau^2}{\tau_s(2+\kappa)^2} + \mathcal{O}(\delta\tau^3)\,, \tag{1.3.17}$$

and

$$\mathcal{T} = t_\star + \frac{2\ \langle\delta\tau\rangle}{2+\kappa} + \frac{\kappa\ \left\langle\delta\tau^2\right\rangle}{\tau_s(2+\kappa)^2} + \mathcal{O}\left(\left\langle\delta\tau^3\right\rangle\right)\,. \tag{1.3.18}$$

In the SETOs region we can thus simplify to

$$\mathcal{T} = t_\star + 2\,\frac{\langle\delta\tau\rangle}{(2+\kappa)}\,. \tag{1.3.19}$$

Let us now come back to the probability. Conservation of the probability gives that $P_{n+1}(t) = 1 - P_n(t)$. Since in this approximation the behavior is quasiperiodic, the charge on the capacitor for the $(n+1)$th electron is *on average* $Q_f({\rm e}/2, \langle t - t_{n+1}\rangle) = Q_f({\rm e}/2, t - t_n - \mathcal{T})$. (A discussion on the precise validity of this last average can be found in appendix 1.A, where the problem is analyzed more rigorously.) The average charge can then be computed by averaging over a period as follows:

$$\langle Q\rangle = \int_{t_n}^{t_n+\mathcal{T}}\frac{dt}{\mathcal{T}}\left[Q_f\left(\frac{\rm e}{2}, t - t_n\right)P_n(t) + \ Q_f\left(\frac{\rm e}{2}, t - t_n - \mathcal{T}\right)P_{n+1}(t)\right]. \tag{1.3.20}$$

In the limit of $\rho \gg 1$ only the Gaussian part of the probability is relevant, and the integral gives:

$$\langle Q\rangle = Q_{\rm s} - \left(Q_{\rm s} - \frac{\rm e}{2}\right)\left(e^{\frac{\mathcal{T}}{\tau_s}} - 1\right)\frac{\tau_s}{\mathcal{T}}\left[1 - \sqrt{\frac{\pi}{\kappa\rho}}\, e^{\frac{1}{\kappa\rho}}\,{\rm Erfc}\left(\frac{1}{\sqrt{\kappa\rho}}\right)\right]. \tag{1.3.21}$$

We report for completeness the details of the calculation:

$$\begin{aligned}
\langle Q\rangle &= \int_{t_n}^{t_n+\mathcal{T}} \frac{dt}{\mathcal{T}}\left[Q_f\left(\frac{\rm e}{2}, t-t_n\right)P_n(t) + \; Q_f\left(\frac{\rm e}{2}, t-t_n-\mathcal{T}\right)P_{n+1}(t)\right] \simeq \\
&\simeq \int_{t_n}^{t_n+\mathcal{T}} \frac{dt}{\mathcal{T}}\left[Q_f\left(\frac{\rm e}{2}, t-t_n\right)P_n(t) + \; Q_f\left(\frac{\rm e}{2}, t-t_n-\mathcal{T}\right)(1-P_n(t))\right] = \\
&= \int_{t_n}^{t_n+\mathcal{T}} \frac{dt}{\mathcal{T}}\, Q_f\left(\frac{\rm e}{2}, t-t_n-\mathcal{T}\right) + \\
&\quad + \int_{t_n}^{t_n+\mathcal{T}} \frac{dt}{\mathcal{T}}\left[Q_f\left(\frac{\rm e}{2}, t-t_n\right) - Q_f\left(\frac{\rm e}{2}, t-t_n-\mathcal{T}\right)\right]P_n(t) = \\
&= Q_{\rm s} - \frac{\tau_s}{\mathcal{T}}\left(\frac{\rm e}{2} - Q_{\rm s}\right)\left(1 - e^{\mathcal{T}}\tau_s\right) + \\
&\quad + \frac{1}{\mathcal{T}}\left(\frac{\rm e}{2} - Q_{\rm s}\right)\left(1 - e^{\mathcal{T}}\tau_s\right)\int_{t_n}^{t_n+\mathcal{T}} dt \exp\left\{-\frac{t-t_n}{\tau_s}\right\}\exp\left\{-\frac{Q_{\rm s} - {\rm e}/2}{2{\rm e}R_t C\tau_s}(t-t_n)^2\right\} \simeq \\
&\simeq Q_{\rm s} - \frac{\tau_s}{\mathcal{T}}\left(\frac{\rm e}{2} - Q_{\rm s}\right)\left(1 - e^{\mathcal{T}}\tau_s\right) + \\
&\quad + \frac{\tau_s}{\mathcal{T}}\left(\frac{\rm e}{2} - Q_{\rm s}\right)\left(1 - e^{\mathcal{T}}\tau_s\right) e^{\frac{1}{\kappa\rho}}\sqrt{\frac{\pi}{\kappa\rho}}{\rm Erfc}\left(\frac{1}{\sqrt{\kappa\rho}}\right) \quad .
\end{aligned} \tag{1.3.22}$$

With little loss in the accuracy Eq. (1.3.21) can be simplified [using ${\rm Erfc}\left(1/\sqrt{\kappa\rho}\right) \simeq 1$, $\mathcal{T} \simeq t_\star$, and $e^{\frac{1}{\kappa\rho}} \simeq 1$] to the form

$$\langle Q\rangle \approx \frac{\rm e}{2}\left[\kappa + 1 - 2\left(1 - \sqrt{\frac{\pi}{\kappa\rho}}\right)/\ln\left(\frac{2+\kappa}{\kappa}\right)\right]. \tag{1.3.23}$$

The analytical expressions (1.3.21), (1.3.23), and (1.A.12) obtained in the appendix, are compared to the Monte Carlo results in Fig. (1.3.4).

These expressions describe the current with good accuracy, and in particular they all capture the presence of a minimum in the voltage V_J. This minimum signals the crossover region between two different kinds of SETOs. We indicated them in Fig. (1.3.1) as III.1 and III.2. The latter one appears for $1 \ll \kappa \ll \rho$. In this case, and in the extreme limit $\rho \to \infty$ the SETOs period becomes $\mathcal{T} = {\rm e}/I_b$, i.e. corresponds exactly to the time needed to the ideal current source to furnish a charge e. The saturation value for the charge (Q_s) in this regime is much larger than e/2, implying that only the linear part of the exponential in Eq. (1.2.3)

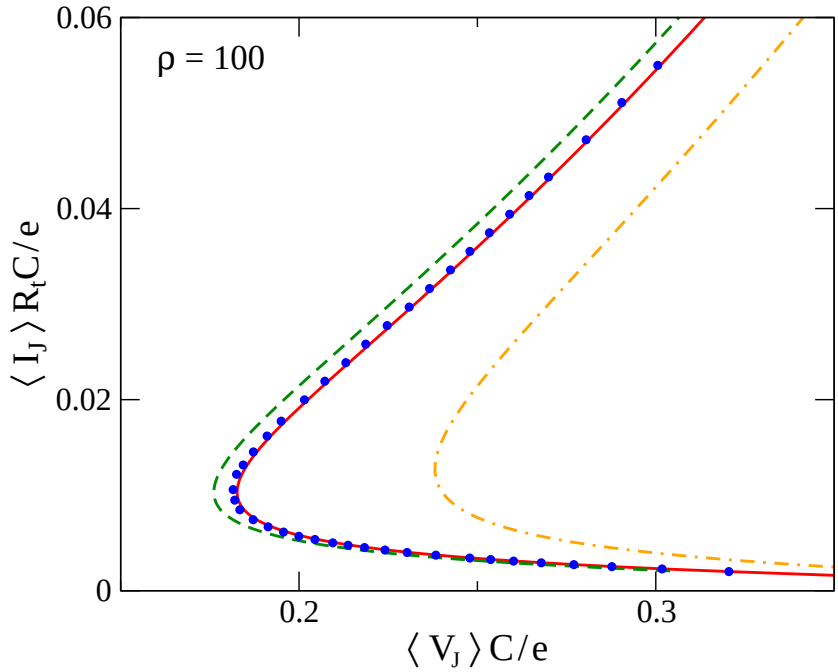

Figure 1.3.4: Comparison between the different approximations for the SETOs back-bending (or 'nose') of the current-voltage characteristics: Monte Carlo data (circles) are shown against analytical calculations from Eq. (1.A.12) (solid), Eq. (1.3.21) (dashed) and Eq. (1.3.23) (dot-dashed).

is explored. This is important since the small fluctuations in the hopping times do not affect the evolution equation for the next electron. One can readily verify that in the limit of an ideal current source the charge time dependence around each t_n is $Q(t) = I_b(t - ne/I_b)$. The nonlinear corrections instead add a stochastic dependence on the time evolution of the charge. The period, for instance, does not depend on $\langle \delta\tau \rangle$ anymore for $\kappa \to \infty$, as is clear from Eq. (1.3.19). This extreme limit is not realistic and thus the correction given in (1.3.19) are normally important.

Reducing the current bias, the saturation charge becomes of the order of e/2 ($\kappa = 2Q_s/\mathrm{e} - 1 < 1$) and the nonlinear behavior of $Q(t)$ begins to correlate different hopping events. The charge time evolution in this regime is characteristic and resembles a shark fin, as shown in Fig. (1.3.2). It is also clear from (1.3.19) that in this regime the stochastic fluctuations have the greatest impact on the average SETOs period.

These two regimes can be identified on the current plot Fig. (1.3.4) and in the analytical expression (1.3.23) by the two branches joined by a minimum of the voltage (the SETOs 'nose'). The large-bias behavior ($\kappa \gg 1$) of Eq. (1.3.23) gives $\mathrm{e}/(2C)\sqrt{\pi\kappa/\rho}$, which is the Averin-Likharev expression for the current of Eq. (1.2.6) ($\langle I_J \rangle \sim I_b$ in this limit), while in the opposite limit the long exponential charging time is dominating: $\langle V_J \rangle \approx (\mathrm{e}/C)\sqrt{\pi}/(\sqrt{\kappa\rho}\ln(2/\kappa))$.

The overall situation is summarized in Fig. (1.3.5). Since it is very difficult in practice

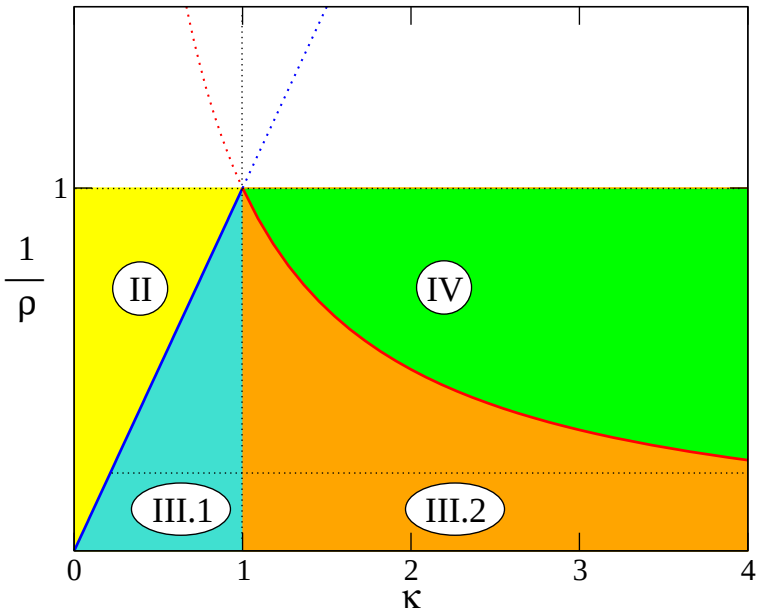

Figure 1.3.5: Scheme of transport regimes boundaries as a function of the relevant parameters: the tunneling/shunt resistances ratio $\rho^{-1} = R_t/R_s$ and the relative distance of the current bias from the threshold $\kappa = (I_b - I_{\rm th})/I_{\rm th}$. The SETOs regime exists only in the limit $\rho \gg 1$.

to experimentally reach large values of ρ, the plot in Fig. (1.3.5) suggests that a good experimental choice can be $\kappa = 1$, for which the SETOs appear for the lowest values of ρ. We will discuss in the following the correlation function of the charge in order to analyze quantitatively the evolution of the accuracy of the SETOs.

1.4 Charge-fluctuation spectrum

A quantitative measure of the accuracy of the SETOs is given by the time correlation of the charge. This can be defined as

$$S(\tau) = \langle Q(t+\tau)Q(t)\rangle - \langle Q(t+\tau)\rangle \langle Q(t)\rangle \ , \tag{1.4.1}$$

where the average is performed over a statistical ensemble and the result does not depend on t, since the stochastic process is stationary. Note also that this quantity is proportional to the spectrum of current fluctuations through the shunt resistance R_s: $S_{R_s}(\tau) = S(\tau)/\tau_s^2$ (see also appendix 1.B). In the case of voltage-biased junctions [see. Fig. (1.2.1)], $S(\tau)/\tau_s^2$ gives the current fluctuations that can be directly measured through the load resistance R.

For perfectly periodic charge oscillations the Fourier transform of (1.4.1) is given by a sum of Dirac delta functions at $\omega = 2\pi n/\mathcal{T}$, with n integer. The nonperiodic fluctuations introduce a finite width of these peaks. The form of $S(\omega)$ measures thus directly the accuracy

of the periodic charge transfer. In this section we derive with a simple procedure an analytical expression for $S(\omega)$ that allows us to better understand the origin of the fluctuations. In the next section we will compare these results to those obtained numerically by Monte Carlo simulations.

In order to calculate the Fourier transform of $S(\tau)$ for this stationary process it is convenient to define the charge $Q(t)$ over a time $0 < t < \Lambda$, with $\Lambda \gg \mathcal{T}$ so that many oscillations are present in a single sample of $Q(t)$. One can then calculate the Fourier series

$$Q_p = \int_0^\Lambda \frac{dt}{\Lambda} Q(t) e^{ip\frac{2\pi}{\Lambda}t} \quad , \quad Q(t) = \sum_p e^{-ip\frac{2\pi}{\Lambda}t} Q_p \,. \tag{1.4.2}$$

Substituting Eq. (1.4.2) into Eq. (1.4.1) and averaging over t one obtains:

$$S(\tau) = \sum_p \left\langle |Q_p|^2 \right\rangle e^{-ip\frac{2\pi}{\Lambda}\tau} - Q_0^2 \,, \tag{1.4.3}$$

which can be used numerically to compute the correlation function from the Monte Carlo data (see next section), or analytically, by performing the limit $\Lambda \to \infty$. In particular the Fourier transform can be defined as

$$S(\omega) = \int_{-\Lambda/2}^{+\Lambda/2} d\tau e^{i\omega\tau - 0^+|\tau|} S(\tau) \,, \tag{1.4.4}$$

which gives

$$S(\omega) = \sum_p \left(\left\langle |Q_p|^2 \right\rangle - \delta_{p,0} Q_0^2 \right) 2\pi\, \delta(\omega - \omega_p) \,, \tag{1.4.5}$$

with $\omega_p = 2\pi p/\Lambda$. The presence of the Dirac delta functions is an artifact consequent to the periodic extension induced by the Fourier transform. In practice, since the frequency scale $1/\Lambda$ is infinitesimal one can obtain the smooth function $S(\omega)$ by averaging the expression (1.4.5) for each value of ω over a small interval $2\pi/\Lambda$. This simply gives that

$$S(\omega_p) = \Lambda \left\langle |Q_p|^2 \right\rangle \tag{1.4.6}$$

for $p \neq 0$ (Wiener-Khinchin theorem).

The problem is now reduced to the calculation of the Fourier series of the charge. Using the definitions of t_n and τ_n given before [Eq. (1.3.7)] and assuming that the extrema of the time evolution of $Q(t)$ coincide with the two hopping events at times τ_0 and τ_N we can write:

$$Q_p = \sum_{n=0}^{N-1} \int_{\tau_n}^{\tau_{n+1}} \frac{dt}{\Lambda} Q(t)\, e^{i\omega_p t} = \sum_{n=0}^{N-1} e^{i\omega_p \tau_n} \int_0^{\tau_{n+1}-\tau_n} \frac{dt}{\Lambda}\, Q_f(\mathrm{e}/2, t - t_{n+1} + \tau_n)\, e^{i\omega_p t} \,. \tag{1.4.7}$$

In the limit of well-established SETOs the integral gives a contribution that fluctuates very little. On the contrary the exponentials are much more sensible to even small fluctuations of

the tunneling times, since the phase results from the accumulation of many different hopping events. For this reason we expect that the upper integration limit can be substituted with the period of the SETOs $\tau_{n+1} - \tau_n \approx \mathcal{T}$ and we use $Q_f\big(\mathrm{e}/2, t - (\mathcal{T} - \langle\delta\tau\rangle)\big)$ as the average charge dependence. The Fourier transform then takes the form

$$S(\omega) = N\mathcal{T}\left\langle |F(\omega)|^2 \right\rangle \mathcal{A}(\omega)\,, \tag{1.4.8}$$

where

$$F(\omega) = \frac{1}{N}\sum_{n=0}^{N-1} e^{i\omega t_n} \tag{1.4.9}$$

and

$$\mathcal{A}(\omega) = \left| e^{i\omega\langle\delta\tau\rangle}\int_0^{\mathcal{T}} \frac{dt}{\mathcal{T}}\, Q_f(e/2, t - \mathcal{T} + \langle\delta\tau\rangle) e^{i\omega t} \right|^2 . \tag{1.4.10}$$

Explicitly:

$$\begin{aligned}
\langle |Q_p|^2\rangle &= \left\langle \left| \sum_{n=0}^{N-1} \int_{\tau_n}^{\tau_{n+1}} \frac{dt}{\Lambda}\, Q(t)\, e^{i\omega_p t} \right|^2 \right\rangle = \\
&= \left\langle \left| \sum_{n=0}^{N-1} e^{i\omega_p t_n} \right|^2 \right\rangle \left\langle \left| e^{i\omega_p \delta\tau_n} \int_0^{\mathfrak{F}(\delta\tau_n)+\delta\tau_{n+1}-\delta\tau_n} \frac{dt'}{\mathcal{T}}\, Q_f(\mathrm{e}/2, t' + t_n + \delta\tau_n - t_{n+1})\, e^{i\omega_p t'} \right|^2 \right\rangle \simeq \\
&\simeq \left\langle \left| \sum_{n=0}^{N-1} e^{i\omega_p t_n} \right|^2 \right\rangle \left| \left\langle e^{i\omega_p \delta\tau_n} \int_0^{\mathfrak{F}(\delta\tau_n)+\delta\tau_{n+1}-\delta\tau_n} \frac{dt'}{\mathcal{T}}\, Q_f(\mathrm{e}/2, t' + t_n + \delta\tau_n - t_{n+1})\, e^{i\omega_p t'} \right\rangle \right|^2 \simeq \\
&\simeq \left\langle \left| \sum_{n=0}^{N-1} e^{i\omega_p t_n} \right|^2 \right\rangle \left| e^{i\omega_p\langle\delta\tau\rangle} \int_0^{\mathcal{T}} \frac{dt'}{\mathcal{T}}\, Q_f(\mathrm{e}/2, t' - \mathcal{T} + \langle\delta\tau\rangle)\, e^{i\omega_p t'} \right|^2 = \\
&= \left\langle |F(\omega_p)|^2 \right\rangle \mathcal{A}(\omega_p)\,.
\end{aligned} \tag{1.4.11}$$

The quantity $\mathcal{A}$ can be readily evaluated:

$$\mathcal{A}(\omega) = \left(\frac{\mathrm{e}\tau_s}{2\mathcal{T}}\right)^2 \left| \frac{\kappa+1}{\omega\tau_s}\left(e^{i\omega\mathcal{T}} - 1\right) - \frac{\kappa e^{-\langle\delta\tau\rangle/\tau_s}}{\omega\tau_s + i}\left(e^{i\omega\mathcal{T}} - e^{\mathcal{T}/\tau_s}\right) \right|^2 . \tag{1.4.12}$$

In order to proceed we have to evaluate also the average of $F(\omega)$. It is convenient to express the time at which one event happens as a sum over the delay between previous events using Eq. (1.3.8):

$$F(\omega) = \frac{e^{i\omega t_0}}{N}\left(1 + \sum_{n=1}^{N-1} \exp\left\{ i\omega \sum_{k=0}^{n-1} \mathfrak{F}(\delta\tau_k) \right\}\right) . \tag{1.4.13}$$

Now the average of $|F(\omega)|^2$ can be performed using the distribution function $\mathcal{P}(\delta\tau)$:

$$\left\langle |F(\omega)|^2 \right\rangle = \frac{1}{N}\left(1 + 2\,\mathfrak{Re}\left\{\frac{g(\omega)}{1-g(\omega)}\right\}\right) + \frac{\delta F}{N^2} \tag{1.4.14}$$

where we introduced the quantities:

$$g(\omega) = \left\langle e^{i\omega\mathfrak{F}(\delta\tau)} \right\rangle = \int_0^\infty d(\delta\tau)\mathcal{P}(\delta\tau)e^{i\omega\mathfrak{F}(\delta\tau)} \tag{1.4.15}$$

and $\delta F = 2\mathfrak{Re}\left\{g(g^N-1)/(1-g)^2\right\}$, whose contribution to $S(\omega)$ vanishes in the limit $N \to \infty$. The details of the calculation leading from Eq. (1.4.13) to Eq. (1.4.14) are as follows:

$$\begin{aligned}
\left\langle |F(\omega)|^2 \right\rangle =& \left\langle \left| \sum_{n=0}^{N-1} e^{i\omega t_n} \right|^2 \right\rangle = \\
=& \left\langle \left(1 + \sum_{n=1}^{N-1} \exp\left\{ i\omega \sum_{k=0}^{n-1} \mathfrak{F}(\delta\tau_k) \right\}\right)\left(1 + \sum_{m=1}^{N-1} \exp\left\{ -i\omega \sum_{k=0}^{m-1} \mathfrak{F}(\delta\tau_k) \right\}\right) \right\rangle = \\
=& 1 + \left\langle \sum_{n=1}^{N-1}\prod_{k=0}^{n-1} e^{i\omega\mathfrak{F}(\delta\tau_k)} \right\rangle + \left\langle \sum_{m=1}^{N-1}\prod_{k=0}^{m-1} e^{-i\omega\mathfrak{F}(\delta\tau_k)} \right\rangle + N - 1 \\
&+ \left\langle \sum_{n=1}^{N-1}\sum_{m=1}^{n-1} e^{i\omega\sum_{k=m}^{n-1}\mathfrak{F}(\delta\tau_k)} \right\rangle + \left\langle \sum_{n=1}^{N-1}\sum_{m=n+1}^{N-1} e^{-i\omega\sum_{k=n}^{m-1}\mathfrak{F}(\delta\tau_k)} \right\rangle = \\
=& N + \sum_{n=1}^{N-1}\prod_{k=0}^{n-1} \left\langle e^{i\omega\mathfrak{F}(\delta\tau_k)} \right\rangle + \sum_{m=1}^{N-1}\prod_{k=0}^{m-1} \left\langle e^{-i\omega\mathfrak{F}(\delta\tau_k)} \right\rangle + \\
&+ \sum_{n=1}^{N-1}\sum_{m=1}^{n-1}\prod_{k=m}^{n-1} \left\langle e^{i\omega\mathfrak{F}(\delta\tau_k)} \right\rangle + \sum_{n=1}^{N-1}\sum_{m=n+1}^{N-1}\prod_{k=n}^{m-1} \left\langle e^{-i\omega\mathfrak{F}(\delta\tau_k)} \right\rangle = \\
=& N + \sum_{n=1}^{N-1} g^n + \sum_{m=1}^{N-1} g^{*m} + \sum_{n=1}^{N-1}\sum_{m=1}^{n-1} g^{n-m} + \sum_{n=1}^{N-1}\sum_{m=n+1}^{N-1} g^{*m-n} = \\
=& N + g\frac{1-g^{N-1}}{1-g} + g^*\frac{1-g^{*N-1}}{1-g^*} + \sum_{n=1}^{N-1} g\frac{1-g^{n-1}}{1-g} + \sum_{n=1}^{N-1} g^*\frac{1-g^{*N-n-1}}{1-g^*} = \\
=& N + 2\mathfrak{Re}\left\{ g\frac{1-g^{N-1}}{1-g} \right\} + 2(N-1)\mathfrak{Re}\left\{\frac{g}{1-g}\right\} - 2\mathfrak{Re}\left\{ g\frac{1-g^{N-1}}{(1-g)^2} \right\} = \\
=& N + 2\mathfrak{Re}\left\{ \frac{(N-1)g - Ng^2 + g^{N+1}}{(1-g)^2} \right\} = \\
=& N + 2N\mathfrak{Re}\left\{\frac{g}{1-g}\right\} + 2\mathfrak{Re}\left\{\frac{g(g^N-1)}{(1-g)^2}\right\}.
\end{aligned} \tag{1.4.16}$$

In conclusion we find

$$S(\omega) = \left(1 + 2\,\mathfrak{Re}\left\{\frac{g(\omega)}{1-g(\omega)}\right\}\right)\mathcal{TA}(\omega) \tag{1.4.17}$$

that constitutes the central result of this section.

We are now in the position to study the spectrum of the charge fluctuations for the system at hand. As it can be seen from the form of (1.4.14) the function has a singularity for $g \to 1$. Since

$$|g(\omega)|^2 = \int_0^\infty dt \int_0^t dt' \; \mathcal{P}(t)\mathcal{P}(t') 2\cos(\omega t) \leq 1 \,, \tag{1.4.18}$$

a singularity is here present for $\omega \to 0$ or when the fluctuations are negligible so that $g \approx e^{i\omega\langle \mathfrak{F}(\delta\tau)\rangle}$. This picture predicts a series of peaks for the frequencies $\Omega_n = 2\pi n/\mathcal{T}$ with n integer. Small fluctuations introduce a finite width, regularizing the correlation function. The numerical integration in the expression of $g(\omega)$ is straightforward, but it is also possible to obtain an analytical expression. Deep in the SETOs regime $\mathcal{P}(\delta\tau)$ has a Gaussian behavior and provides a short cutoff time, so that we can expand the exponential in (1.4.15) to second order in $\delta\tau$. This gives

$$g(\omega) = e^{i\omega t_\star} \left(1 + \frac{2i\omega}{2+\kappa} \langle \delta\tau \rangle - \frac{\kappa^2 i\omega + 4\omega^2 \tau_s}{2(2+\kappa)^2} \frac{\langle \delta\tau^2 \rangle}{\tau_s} + \dots \right) . \tag{1.4.19}$$

The maximum of $\mathfrak{Re}\{g/(1-g)\}$ takes place for $\mathrm{Arg}[g(\omega)] = 0$, which at lowest order in $\langle \delta\tau \rangle$ gives for the position of the poles

$$\Omega_n = \frac{2\pi n}{t_\star} \left(1 - \frac{2\langle \delta\tau \rangle}{(2+\kappa)\, t_\star} \right) , \tag{1.4.20}$$

coinciding at linear order in $\langle \delta\tau \rangle / \tau_s$ with $2\pi n/\mathcal{T}$. The phase of g ($g = |g| e^{i\phi}$) thus vanishes at the minimum of $\mathfrak{Re}\{g/(1-g)\}$, so that near this point one can write at lowest order $\phi \approx \mathcal{T}(\omega - \Omega_n)$. The relevant part of (1.4.14) then reads

$$\mathfrak{Re} \left\{ \frac{g}{1-g} \right\} \approx \frac{(1-|g|)}{(1-|g|)^2 + \phi^2} \,, \tag{1.4.21}$$

and Eq. (1.4.8) takes the simple Lorentzian form

$$S(\omega) \simeq \mathcal{A}(\Omega_n) \, \frac{\Gamma_n/2}{\Gamma_n^2/4 + (\omega - \Omega_n)^2} \,, \tag{1.4.22}$$

with the full width at half maximum Γ_n defined by

$$\Gamma_n = 2\, \frac{1-|g|}{\mathcal{T}} = \frac{4\Omega_n^2}{\mathcal{T}(2+\kappa)^2} \left(\langle \delta\tau^2 \rangle - \langle \delta\tau \rangle^2 \right) . \tag{1.4.23}$$

The presence in this formula of the mean squared variance of delay in the tunneling time, i.e. $\left\langle \, (\delta\tau - \langle \delta\tau \rangle)^2 \right\rangle$, clearly indicates that the spread in the hopping event controls the width of the peak, as is physically expected. One also sees that the width of the poles increases with n. Performing the average with the Gaussian distribution we find $\left\langle \, (\delta\tau - \langle \delta\tau \rangle)^2 \right\rangle / \tau_s^2 = 4(1-\pi/4)/(\kappa\rho)$, hence

$$\Gamma_n = 4\, \frac{\Omega_n^2}{\mathcal{T}(2+\kappa)^2} \, \frac{\tau_s^2}{\kappa\rho} \, 4 \left(1 - \frac{\pi}{4} \right) , \tag{1.4.24}$$

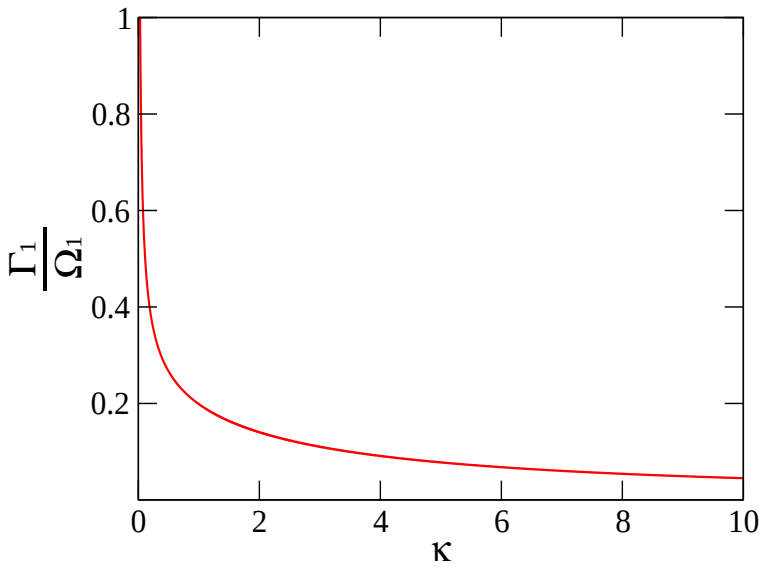

Figure 1.4.1: The relative width at half height of the first noise peak as a function of κ, given by Eq. (1.4.27), for $\rho = 10$.

and at first order we can approximate

$$\Omega_n \simeq \frac{2\pi n}{t_\star} = \frac{2\pi n}{R_s C \ln\left(\frac{2+k}{k}\right)} = \frac{2\pi n}{R_s C \ln\left(\frac{CV+\mathrm{e}/2}{CV-\mathrm{e}/2}\right)}\,, \tag{1.4.25}$$

Subsituting back in (1.4.24) and taking the limits $\rho \to \infty$ and $\kappa \to \infty$ we obtain [1]

$$\Gamma_n = \frac{2n^2\pi^2(4-\pi)}{R_s C}\frac{R_t}{R_s}\,. \tag{1.4.26}$$

For the relative width Γ_n/Ω_n we have the explicit expression

$$\frac{\Gamma_n}{\Omega_n} = \frac{32\pi\, n\,(1-\pi/4)}{\rho\,\kappa\,(2+\kappa)^2\,\ln^2(\kappa/(2+\kappa))}\,. \tag{1.4.27}$$

Eq. (1.4.27) allows us to study the width of the peak in the charge-correlation spectrum, and thus, the accuracy of the SETOs. It correctly gives that $\Gamma_1/(2\pi/\mathcal{T}) \ll 1$ in the SETOs regime ($1/\rho \ll \kappa \ll \rho$). It also shows [see. Fig. (1.4.1)] that the *relative* width Γ_1/Ω_1 is a monotonic decreasing function of the bias current (κ) for a given value of the resistance (ρ).

From the form of (1.4.22) it is clear that within this approximation the weight of the Lorentzian peak is controlled only by the form factor $\mathcal{A}(\Omega_n)$. Using its explicit expression one finds that it induces a relatively weak dependence on κ and ρ: we can approximate $\mathcal{A}(\Omega_1) \simeq \mathrm{e}^2/\left(4\pi^2 + \ln^2\left[\frac{2+\kappa}{\kappa}\right]\right)$, which saturates to a constant for $\kappa \to \infty$. The full variation

1. This expression does not agree with the expression (57) of Ref. [76], specifically we find a different functional dependence on R_s: $\Gamma \sim 1/R_s^2$ instead of $1/R_s$.

takes place in the $\kappa < 1$ region, where the shape of $Q(t)$ evolves from the shark-fin to the sawtooth form. From the form of Eq. (1.4.27) one can also see that for small κ the peak broadens and the SETOs are washed out when $\Gamma_1 \sim \Omega_1$ (for $\kappa \sim 1/\rho$). For large κ instead the theory predicts that the relative width decreases monotonically:

$$\frac{\Gamma_n}{\Omega_n} = \frac{8\pi n(1-\pi/4)}{\rho\kappa} \,. \tag{1.4.28}$$

In this limit the SETOs disappear by a decrease of the weight of the peak, but within our approximation this is not seen. Actually for sufficiently large current bias ($\kappa \sim \rho$) there is a finite probability that a single tunnel event is no more sufficient to bring the charge back in the Coulomb blockade region. This is quantified by the value of $P_n(t_n) < 1$, which, contrary to our hypothesis, becomes smaller than 1. One can expect that the theory roughly remains valid for the fraction of tunneling events that leaves $Q(t_n) < \mathrm{e}/2$, i.e. the fraction $P_n(t_n) < 1$. This would describe a peak that remains sharp, but that vanishes in weight as $P_n(t_n)$.

Another interesting and relevant limit is the low-frequency behavior of $S(\omega)$. Expanding Eq. (1.4.15) in ω

$$g(\omega) \simeq e^{\langle i\omega\mathfrak{F}\rangle} \simeq 1 + i\omega\,\langle\mathfrak{F}\rangle - \frac{\omega^2}{2!}\,\langle\mathfrak{F}^2\rangle - i\frac{\omega^3}{3!}\,\langle\mathfrak{F}^3\rangle + \mathcal{O}(\omega^4) \tag{1.4.29}$$

one can show that

$$N\,\big\langle|F(\omega)|^2\big\rangle = \frac{F_2 - F_1^2}{F_1^2} + \omega^2\,\frac{4F_1F_2F_3 - F_1^2F_4 - 3F_2^3}{12F_1^4} + \dots \tag{1.4.30}$$

where $F_n = \langle\mathfrak{F}^n\rangle$. If the fluctuations are negligible then $F_n = F_1^n$ and the noise at low frequency vanishes. In particular in our case the average (1.4.30) takes a simple form if the explicit expression of $\mathfrak{F}$ is used. We have in fact:

$$\begin{aligned}\langle\mathfrak{F}(\delta\tau)^n\rangle &\simeq \left\langle\left[\lim_{\delta\tau\to 0}\left(\delta\tau - \tau_s\ln\left(\frac{\kappa}{2+\kappa e^{-\delta\tau/\tau_s}}\right)\right)\right]^n\right\rangle = \\ &= \left\langle\left(t_\star + \frac{2\,\delta\tau}{2+\kappa} + \frac{\kappa\,\delta\tau^2}{(2+\kappa)^2\tau_s} + \mathcal{O}(\delta\tau^3)\right)^n\right\rangle .\end{aligned} \tag{1.4.31}$$

Up to $\mathcal{O}(\delta\tau^2)$ we can write then:

$$\begin{aligned}F_1 &\simeq t_\star + \frac{2\langle\delta\tau\rangle}{2+\kappa} + \frac{\kappa\langle\delta\tau^2\rangle}{(2+\kappa)^2\tau_s} \\ F_2 &\simeq t_\star^2 + \frac{4\,t_\star\langle\delta\tau\rangle}{2+\kappa} + \frac{4\,\langle\delta\tau^2\rangle}{(2+\kappa)^2} + \frac{2\,t_\star\kappa\langle\delta\tau^2\rangle}{(2+\kappa)^2\tau_s} \\ F_3 &\simeq t_\star^3 + \frac{6\,t_\star^2\langle\delta\tau\rangle}{2+\kappa} + \frac{12\,t_\star\langle\delta\tau^2\rangle}{(2+\kappa)^2} + \frac{3\,t_\star^2\kappa\langle\delta\tau^2\rangle}{(2+\kappa)^2\tau_s} \\ F_4 &\simeq t_\star^4 + \frac{8\,t_\star^3\langle\delta\tau\rangle}{2+\kappa} + \frac{24\,t_\star^2\langle\delta\tau^2\rangle}{(2+\kappa)^2} + \frac{4\,t_\star^3\kappa\langle\delta\tau^2\rangle}{(2+\kappa)^2\tau_s} ,\end{aligned} \tag{1.4.32}$$

and we rewrite (1.4.30) as

$$N\,\big\langle|F(\omega)|^2\big\rangle = \frac{F_2 - F_1^2}{F_1^2}\left(1 + \omega^2\,\frac{4F_1F_2F_3 - F_1^2F_4 - 3F_2^3}{12F_1^2(F_2 - F_1^2)}\right) , \tag{1.4.33}$$

with now

$$\begin{aligned}\frac{F_2 - F_1^2}{F_1^2} =& \frac{4\left(\langle\delta\tau^2\rangle - \langle\delta\tau\rangle^2\right)}{t_\star^2\,(2+\kappa)^2} + \mathcal{O}(\delta\tau^3)\\ 4F_1F_2F_3 - F_1^2F_4 - 3F_2^3 =& \frac{4\,t_\star^4\left(\langle\delta\tau^2\rangle - \langle\delta\tau\rangle^2\right)}{t_\star^2\,(2+\kappa)^2} + \mathcal{O}(\delta\tau^3)\\ 12F_1^2(F_2 - F_1^2) =& \frac{48\,t_\star^2\left(\langle\delta\tau^2\rangle - \langle\delta\tau\rangle^2\right)}{t_\star^2\,(2+\kappa)^2} + \mathcal{O}(\delta\tau^3)\,,\end{aligned} \tag{1.4.34}$$

leading finally to

$$N\left\langle|F(\omega)|^2\right\rangle = 4\,\frac{\langle\delta\tau^2\rangle - \langle\delta\tau\rangle^2}{t_\star^2\,(2+\kappa)^2}\left(1 + \frac{\omega^2 t_\star^2}{12} + \dots\right). \tag{1.4.35}$$

We find thus that in the SETOs regime the low-frequency noise is suppressed.

Eq. (1.4.35) together with the expansion of Eq. (1.4.12) for $\omega \to 0$ allows us to evaluate the zero-frequency Fano factor:

$$\mathbb{F} \equiv \frac{S_J(0)}{\mathrm{e}\,\langle I_J\rangle} = \frac{S(0)}{\tau_s^2 \mathrm{e}\,\langle I_J\rangle}\,, \tag{1.4.36}$$

where $S_J(\omega)$ is the noise spectrum of the current through the junction and the relation $S(\omega) = S_J(\omega)\tau_s^2/(1+\omega^2\tau_s^2)$ holds exactly, see appendix 1.B for more details. The reduction of the current fluctuations in the large ρ limit naturally leads to sub-Poissonian noise ($\mathbb{F} < 1$) vanishing for $\rho \to \infty$:

$$\mathbb{F} \simeq \frac{(4-\pi)(-2+(\kappa+1)t_\star/\tau_s)^2}{\rho\,\kappa\,(2+\kappa)^2(t_\star/\tau_s)^2}\,. \tag{1.4.37}$$

Nevertheless this expression is only qualitatively correct, since the analytical theory has been designed to describe accurately the noise for frequencies around the peak of the SETOs. This will be shown in the next section, where we present numerical simulations.

1.5 Numerical simulations

In this section we show numerical results obtained by Monte Carlo simulations for the charge-fluctuation spectrum. The purpose is to compare them with the analytical calculations of the preceding sections, valid for $\rho \gg 1$ and $1/\rho \ll \kappa \ll \rho$, and to explore the crossover region where the SETOs disappear.

The Monte Carlo simulations are performed by generating different realization of the stochastic time evolution of the charge $Q(t)$ over a time much longer than the SETOs period. The time evolution of the charge is obtained by discretizing the time on a nonuniform grid, such that in the time interval Δt the charge varies by a small quantity and the tunneling probability $P = \Gamma(Q(t))\Delta t$ is $< \mathcal{N} \ll 1$. The tunneling event is accepted or refused by

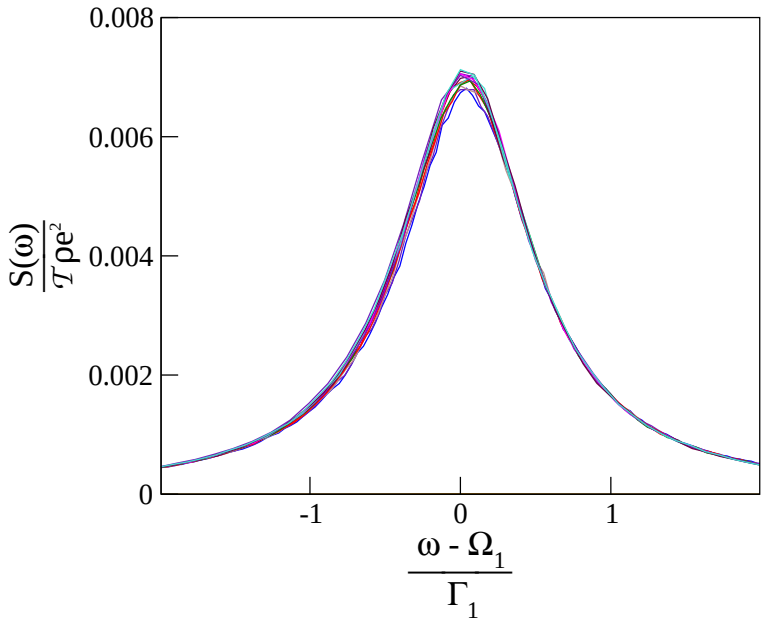

Figure 1.5.1: The noise peak at $\omega = \Omega_1$ obtained from Monte Carlo numerical simulations for values of ρ ranging from 80 to 200 in steps of 10. On the x-axis the frequency is shifted by Ω_1, so that the peak is at zero, and scaled by the width Γ_1 calculated in Eq. (1.4.23); on the y-axis the noise is scaled by $\mathcal{T}\rho\,\mathrm{e}^2$.

generating a random number between 0 and 1 and by comparing it to P. The deterministic evolution of $Q(t)$ between two events is simply given by Eq. (1.2.3). The sequence of time intervals of deterministic evolution interspersed by tunneling times so constructed gives the full knowledge of $Q(t)$ and constitutes the stochastic run. The square modulus of the Fourier transform of the charge is then easily analytically calculated piecewise, interval by interval. To obtain the noise as from (1.4.6), just a further average over several runs is needed. Typically $\mathcal{N} = .01$, each run counts 10^3 tunneling events, and an average over 10^4 realizations is performed.

Let us now discuss the numerical results. We begin by comparing the form of the first peak in the noise spectrum. It is shown scaled by the analytically calculated width Γ_1 in Fig. (1.5.1) for different values of ρ and given κ. The agreement is excellent. We then compare the full ω dependence of $S(\omega)$ obtained from Eq. (1.4.17) with the one calculated numerically. We show the comparison in Fig. (1.5.2) for the relevant case $\kappa = 1$ (which corresponds to the widest extension in ρ of the SETOs region) and for ρ ranging from 200 to 10. As expected, the agreement is very good deep in the SETOs regime, for $\rho \gg 1$, and at $\rho = 10$ all the essential features of the peak at $\omega = \Omega_1$ are still fairly well represented by the theory.

Let us now investigate how the SETOs disappear. From the experimental point of view a simple parameter that can be varied continuously is $\kappa \sim I_b$. We thus plot in Fig. (1.5.3)

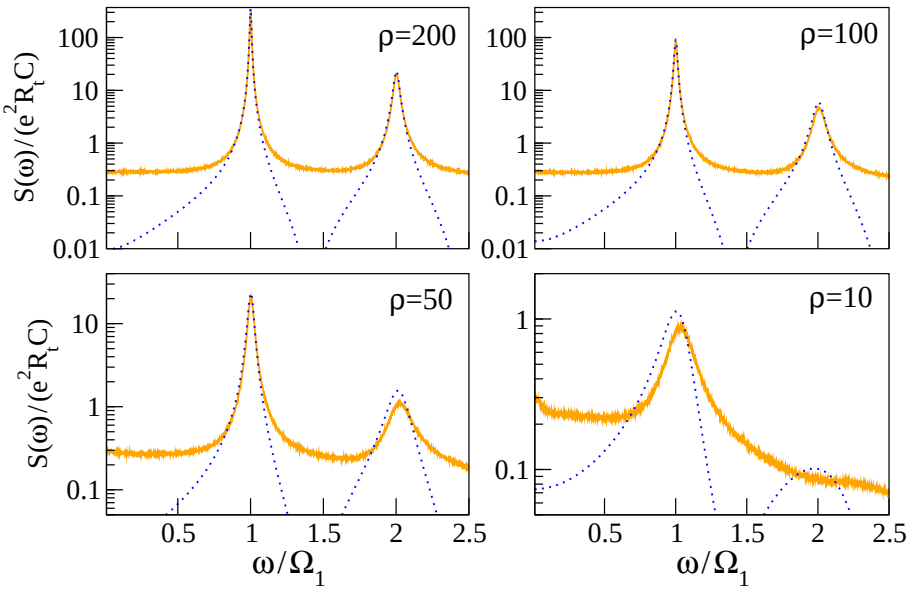

Figure 1.5.2: Comparison between Monte Carlo data for the charge-fluctuation spectrum and the analytical results obtained from Eq. (1.4.17) for different values of ρ, at fixed bias condition $\kappa = 1$. Logarithmic scale on the vertical axis.

the evolution of $S(\omega)$ for given $\rho = 10$ and 100 as a function of κ. These two plots show several interesting features. The first striking one is the reduction of the relative widths of the peaks by increasing κ. This is predicted by the analytical expression (1.4.27) and the numerical calculations assess its validity even outside the region of applicability of the analytical theory. Note that in Fig. (1.5.3) the frequency axis is scaled with Ω_1; thus the apparent weight of the peaks is reduced by the scaling, but it saturates in the region $\kappa \ll \rho$ as predicted by the analytical theory, and then starts to really decrease in the crossover region. The second visible feature is the appearance of a wide Lorentzian zero-frequency peak that remains the only structure for $\kappa \gg \rho$. This structure is due to the charge noise induced at the capacitance by the Poissonian current fluctuations generated by the tunnel junction. By solving the electromagnetic problem one finds $S(\omega) = C^2|Z(\omega)|^2 \mathrm{e}\,\langle I_J\rangle$, where $\mathrm{e}\,\langle I_J\rangle$ is the standard tunnel junction Poissonian white noise and $Z(\omega) = R_{\|}/(1 + i\omega R_{\|}C)$, with $R_{\|} = R_s R_t/(R_s + R_t)$, the impedance between the current source and the voltage at the capacitance. This gives:

$$S(\omega) = \frac{\mathrm{e}\langle I_J\rangle C^2 R_s^2}{1 + 2\rho + \rho^2(1 + \omega^2 R_t^2 C^2)}\,, \tag{1.5.1}$$

which fits our data very well (see appendix 1.B for more details).

Finally we show in Fig. (1.5.4) the evolution of $S(\omega)$ for $\kappa = 1$ and for ρ evolving from 1 to 100. This figure gives an idea of the expected spectrum at the optimal value $\kappa = 1$ as a function of ρ. It turns out that already at $\rho = 3$, $S(\omega)$ presents a very broad maximum and $\rho = 5$ is probably sufficient to observe a clear structure in $S(\omega)$.

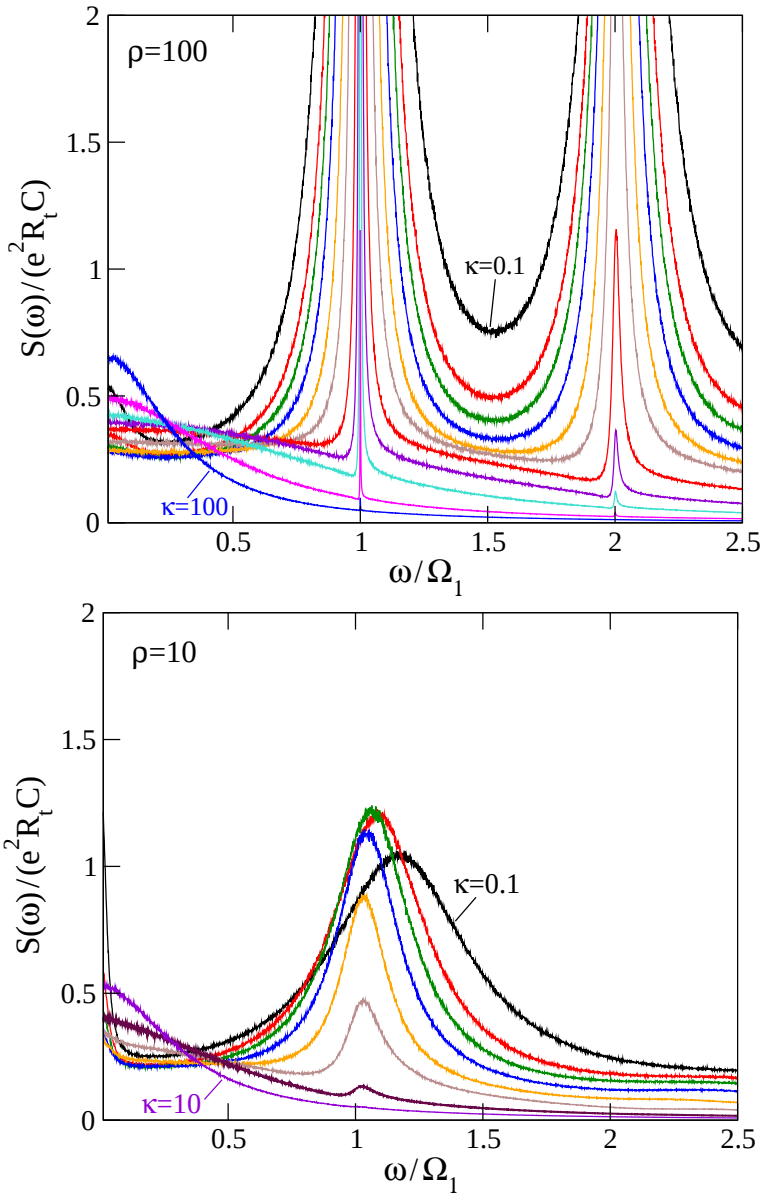

Figure 1.5.3: Monte Carlo spectra for different bias conditions κ at fixed junction environment ($\rho = 100/\rho = 10$ in the upper/lower panel). Increasing κ means here moving along a horizontal line in Fig. (1.3.5) toward the high-bias boundary of the SETOs region and it allows us to see how SETOs disappear.

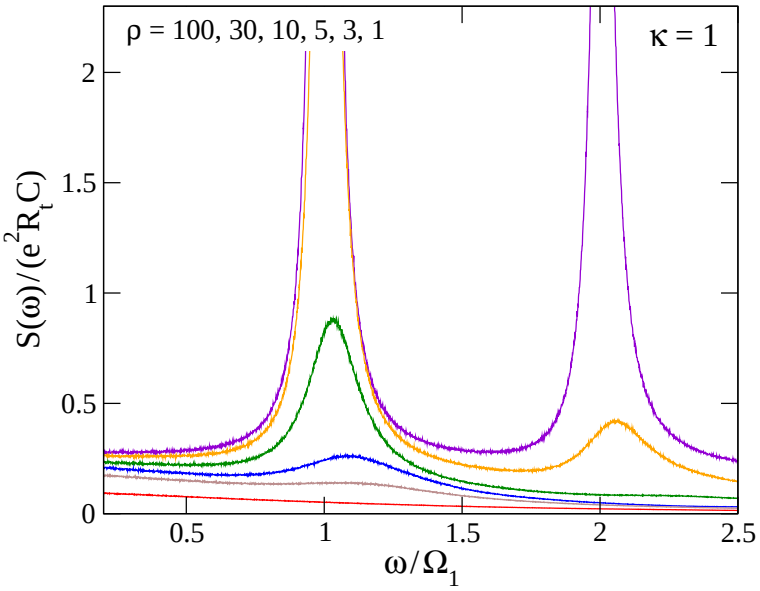

Figure 1.5.4: Monte Carlo spectra for fixed bias conditions $\kappa = 1$ and different values of ρ: the crossover from the SETOs regime to the $\rho \lesssim 1$ region is shown.

1.6 Summary and conclusions

In this chapter we have studied theoretically the electronic transport in a tunnel junction in the presence of a strongly resistive environment. The phenomenon of SETOs has been predicted to appear in this system for essentially infinite value of the external resistance, so that the junction can be seen as current biased. We investigated under which conditions the SETOs appear for a realistic finite value of the environment resistance. We found analytical expressions for the current [Eq. (1.3.21)] and for the charge-fluctuation spectrum [Eq. (1.4.8) with Eq. (1.4.23)]. Our analytical results describe very well the form of the peak in the charge noise, which can be regarded as the hallmark of the SETOs, since it quantifies the accuracy of the periodicity in the charge time dependence. We find that a ratio of R_s/R_t of the order of 5 can be sufficient to observe a clear structure in $S(\omega)$ if the bias current is chosen such that $I_b \approx 2I_{\rm th} = {\rm e}/R_sC$ (this can be converted on a condition on the voltage bias $V_b \approx {\rm e}/C$). This ratio should be obtainable experimentally. It has to be noticed however that the theory presented in this chapter is limited to the zero temperature case $k_BT \ll {\rm e}^2/2C$ and holds for a highly resistive environment where quantum fluctuations are negligible. A more realistic modeling of the resistance, say a RC-line, needs to account for both thermal and quantum effects, which will smear the Coulomb blockade gap and introduce spurious tunneling events for $|Q(t)| < {\rm e}/2$. We leave the discussion for the next two chapters, but we can anticipate that a comparison with the results here presented will show the presence of a maximum of the noise function at the optimal values $\kappa = 1$ surviving for accessible values of the environment resistance even at finite temperature and in the presence of quantum fluctuations.

Appendix

1.A Calculation of the I-V characteristics in the SETOs regime with a Master Equation approach

In this appendix we find expressions for the I-V characteristics taking into account the spread in the distribution probability of the charge. A full statistical description of the behavior of the system can be given in terms of the probability density $\sigma_n(Q,t)$ that at time t the charge in the capacitance is Q and n charges have crossed the junction. Conservation of the probability and the Master Equation describing electron tunneling (which we will be largely using and explaining later on) lead to the following set of coupled partial differential equations:

$$\frac{\partial \sigma_n(Q,t)}{\partial t} = \frac{\partial}{\partial Q}\left[\frac{(Q-Q_s)}{\tau_s}\sigma_n(Q,t)\right] - \Gamma\left(\frac{Q}{C}\right)\sigma_n(Q,t) + \Gamma\left(\frac{Q+\mathrm{e}}{C}\right)\sigma_{n-1}(Q+\mathrm{e},t)\,. \quad (1.A.1)$$

Eq. (1.A.1) is a generalization of the equations given in Ref. [76] to include the information on the number of electrons which have tunneled. The general solution of this equation is difficult in the presence of a finite resistance. But in the SETOs regime we can find an explicit solution by exploiting the fact that at every cycle the charge passes through the blocked range ($-\mathrm{e}/2 < Q < \mathrm{e}/2$). Let us assume that at $t = 0$ the distribution function is:

$$\sigma_n(Q,0) = \delta(Q-\mathrm{e}/2)\delta_{n,n_0}\,. \quad (1.A.2)$$

The differential equation (1.A.1) for $\sigma_{n_0}(Q,t)$ can be easily solved, since it decouples from the others ($\sigma_{n_0-1} = 0$):

$$\sigma_{n_0}(Q,t) = P(t)\delta\left(Q - Q_f\left(\frac{\mathrm{e}}{2},t\right)\right)\,, \quad (1.A.3)$$

where $P(t) = P_n(t)$ as given by Eq. (1.3.12) with $t_n = 0$ and Q_f is defined in Eq. (1.2.3). Once we know the solution for σ_{n_0} we can substitute it into Eq. (1.A.1) and find the solution for σ_{n_0+1}:

$$\frac{\partial \sigma_{n_0+1}(Q,t)}{\partial t} = \frac{\partial}{\partial Q}\left[\frac{(Q-Q_s)}{\tau_s}\sigma_{n_0+1}(Q,t)\right] + \Gamma\left(\frac{Q+\mathrm{e}}{C}\right)\sigma_{n_0}(Q+\mathrm{e},t)\,. \quad (1.A.4)$$

This can be done by using the ansatz

$$\begin{aligned}\sigma_{n_0+1}(Q,t) =& \int dQ' \delta\left(Q - Q_f\left(Q',t\right)\right) f(Q',t) = \\ =& \int dQ' \delta\left(Q - \left[(Q'-Q_s)e^{-t/\tau_s} + Q_s\right]\right) f(Q',t) = \\ =& f\left((Q-Q_s)e^{t/\tau_s} + Q_s, t\right) e^{t/\tau_s} ,\end{aligned} \tag{1.A.5}$$

which gives

$$\sigma_{n_0+1}(Q,t) = f(z(Q),t) e^{\frac{t}{\tau_s}} , \tag{1.A.6}$$

with $z(Q) = (Q-Q_s)e^{\frac{t}{\tau_s}} + Q_s$, and $f(z(Q),t) = 0$ for $z(Q) < \mathrm{e}/2$ and $t > \tau_s \ln\left(\frac{1}{2} - \frac{z(Q)}{\mathrm{e}}\right)$. The resulting differential equation for f reads

$$\begin{aligned}\frac{\partial f(z(Q),t)}{\partial t} =& e^{-\frac{t}{\tau_s}} \Gamma\left(\frac{Q+\mathrm{e}}{C}\right) \sigma_{n_0}(Q+\mathrm{e},t) = \\ =& e^{-\frac{t}{\tau_s}} \frac{Q+\mathrm{e}/2}{\mathrm{e}R_tC} P(t) \delta\left(Q + \mathrm{e} - \left(\frac{\mathrm{e}}{2} - Q_s\right) e^{-\frac{t}{\tau_s}} - Q_s\right) = \\ =& e^{-\frac{t}{\tau_s}} \left(Q_s + \frac{\mathrm{e}}{2} + (z(Q)-Q_s)e^{-\frac{t}{\tau_s}}\right) \frac{P(t)}{\mathrm{e}R_tC} \delta\left(\mathrm{e} + \left(z(Q) - \frac{\mathrm{e}}{2}\right) e^{-\frac{t}{\tau_s}}\right) .\end{aligned} \tag{1.A.7}$$

The equation can be integrated

$$\begin{aligned}f(z(Q),t) =& \int dt\, e^{-\frac{t}{\tau_s}} \left(Q_s + \frac{\mathrm{e}}{2} + (z(Q)-Q_s)e^{-\frac{t}{\tau_s}}\right) \frac{P(t)}{\mathrm{e}R_tC} \delta\left(\mathrm{e} + \left(z(Q) - \frac{\mathrm{e}}{2}\right) e^{-\frac{t}{\tau_s}}\right) = \\ =& \int dt\, e^{-\frac{t}{\tau_s}} \left(Q_s + \frac{\mathrm{e}}{2} + (z(Q)-Q_s)e^{-\frac{t}{\tau_s}}\right) \frac{P(t)}{\mathrm{e}R_tC} \frac{\delta(t-t_0)}{\left|-\frac{1}{\tau_s}\left(z(Q) - \frac{\mathrm{e}}{2}\right) e^{-\frac{t_0}{\tau_s}}\right|} = \\ =& e^{-\frac{t_0}{\tau_s}} \left(Q_s + \frac{\mathrm{e}}{2} + (z(Q)-Q_s)e^{-\frac{t_0}{\tau_s}}\right) \frac{P(t_0)}{\mathrm{e}R_tC} \frac{1}{\left|-\frac{1}{\tau_s}\left(z(Q) - \frac{\mathrm{e}}{2}\right) e^{-\frac{t_0}{\tau_s}}\right|} \quad ,\end{aligned} \tag{1.A.8}$$

for $t > t_0$ and $z(Q) < -\mathrm{e}/2$, with $t_0 = \tau_s \ln(1/2 - z(Q)/\mathrm{e})$, giving:

$$f(z(Q),t) = P\left(\tau_s \ln\left(\frac{1}{2} - \frac{z(Q)}{\mathrm{e}}\right)\right) \frac{\tau_s}{\mathrm{e}R_tC} \frac{\left(\frac{\mathrm{e}}{2} - Q_s\right)\left(z(Q) + \frac{\mathrm{e}}{2}\right)}{\left(z(Q) - \frac{\mathrm{e}}{2}\right)^2} \quad , \tag{1.A.9}$$

nonvanishing only for $t > \tau_s \ln(1/2 - z(Q)/\mathrm{e})$ and $z(Q) < -\mathrm{e}/2$, which equivalently results in the condition $Q_1(t) < Q < Q_2(t)$, with

$$\begin{aligned}Q_1(t) =& Q_s - \mathrm{e} - (Q_s - \mathrm{e}/2)e^{-t/\tau_s} \\ Q_2(t) =& Q_s - (Q_s + \mathrm{e}/2)e^{-t/\tau_s} \quad ,\end{aligned} \tag{1.A.10}$$

see Fig. 1.A.1. So we finally get for $\sigma_{n_0+1}(Q,t)$:

$$\sigma_{n_0+1}(Q,t) = \begin{cases} 0 & Q < Q_1(t) \\ e^{\frac{t}{\tau_s}} f(z(Q),t) & Q_1(t) < Q < Q_2(t) \\ 0 & Q > Q_2(t) \end{cases} . \tag{1.A.11}$$

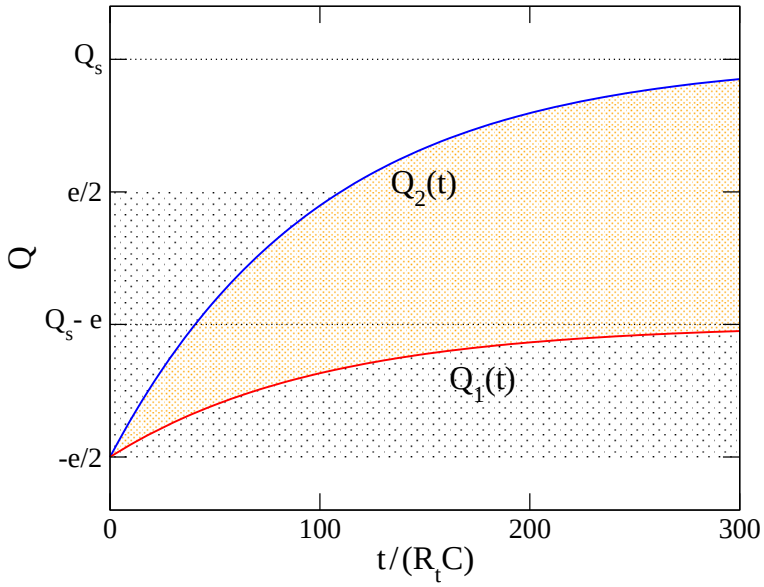

Figure 1.A.1: The functions $Q_1(t)$ and $Q_2(t)$ as in Eq.(1.A.10).

It is interesting to note that the distribution has now a finite spread in Q induced by the combined action of the stochastic fluctuations and of the finite value of the resistance. This is in contrast with the simpler approximation used in Sec. 1.3.2 to evaluate the average in Eq. (1.3.21), where we assumed that the spread was negligible, and that a delta function could be used to describe the distribution σ_{n_0+1}.

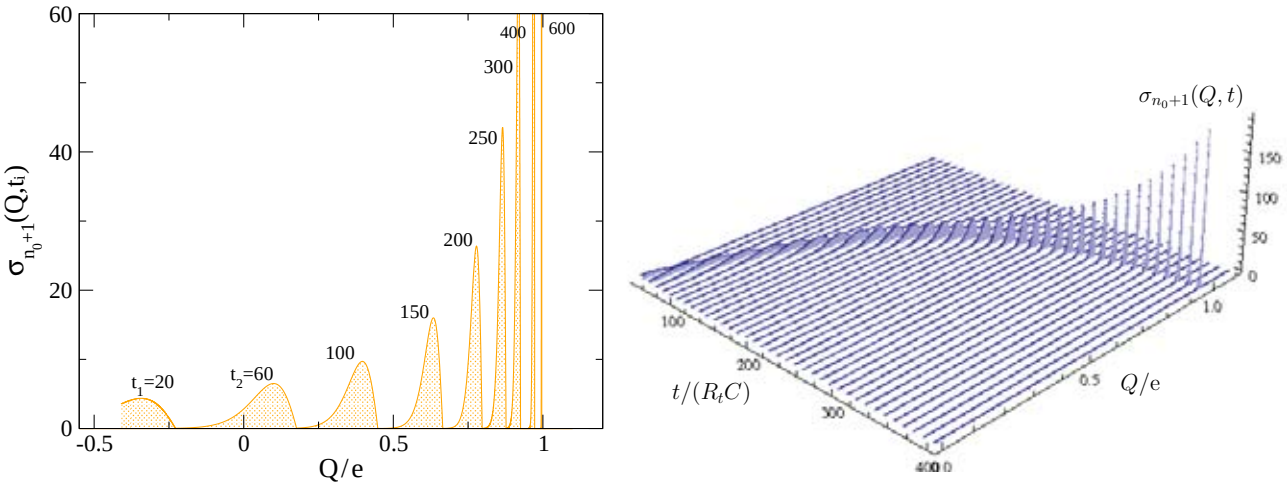

Figure 1.A.2: On the left, snapshots of the distribution $\sigma_{n_0+1}(Q,t)$ as a function of the charge for fixed times show that it shifts and shrinks as time goes by, tending towards a delta at the saturation value $Q_s/\mathrm{e} = 1$ ($\kappa = 1$ here). On the right, a 3D plot of the snapshots at large times in the $\{Q,t\}$ plane.

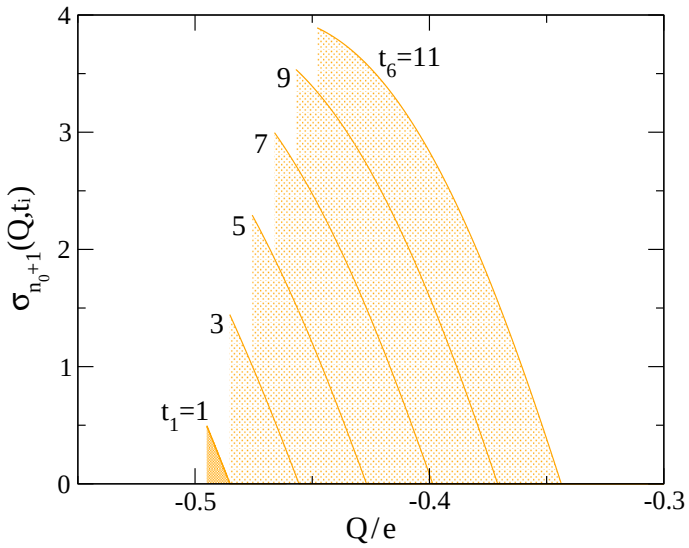

Figure 1.A.3: Snapshots of the distribution $\sigma_{n_0+1}(Q,t)$ in Eq. (1.A.11) as a function of the charge for fixed small times.

In Figs. 1.A.2 and 1.A.3 we show snapshots at different times of $\sigma_{n_0+1}(Q,t)$ as a function of Q. At long times it tends unsurprisingly to a delta at the saturation value Q_s (= e in the figures), which is where the natural time-evolution of the circuit pushes the charge (Fig. 1.A.2). At small times its behavior can be understood as follows. As it can be seen in Fig. 1.A.1, at very small times the distribution is nonvanishing only in a small interval close to $-\mathrm{e}/2$, which goes to zero for $t \to 0$ while enlarges and drifts away from $-\mathrm{e}/2$ at larger times (this explains why the curves for $t \leq 20$ appear to be truncated). We recall that $\sigma_{n_0+1}(Q,t)$ is the charge density distribution of the (n_0+1)th tunneled electron and its shape depends basically on how often do electrons tunnel with respect to the the 'velocity' of the recharge after tunneling. At small times the charge grows linearly in time and faster at $-\mathrm{e}/2$ than at e/2: $dQ/dt|_{-\mathrm{e}/2} > dQ/dt|_{\mathrm{e}/2}$. The tunneling rate grows also linearly in time at small times. In the charge distribution this results in an higher accumulation at the left border of the interval $Q_1 < Q < Q_2$ with respect to the right one with a linear triangular profile, as shown in Fig. 1.A.3. For larger times the linearity of the charge behavior no longer holds and the curvature influences the recharge process and the tunneling rate. As a result the shape of distribution starts to deform end evolves as in Fig. 1.A.2.

We can now calculate the average charge on the junction during a single oscillation:

$$\langle Q \rangle = \int_0^{\mathcal{T}} \frac{dt}{\mathcal{T}} \left(Q_f\left(\frac{\mathrm{e}}{2}, t\right) P(t) + \int_{Q_1(t)}^{Q_2(t)} dQ\; Q\; \sigma_{n_0+1}(Q,t) \right) . \tag{1.A.12}$$

The numerical integration of this expression leads to the result shown in Fig. (1.3.4).

1.B More details about current fluctuations

We want here to consider in more details the sources of fluctuations and noise in the circuit at hand, explaining the relation between charge noise and current noise introduced in the Fano factor discussion of Sec. 1.4 and motivating the high-bias formula for the charge noise (1.5.1). Let us start by separating the different current contributions in our circuit.

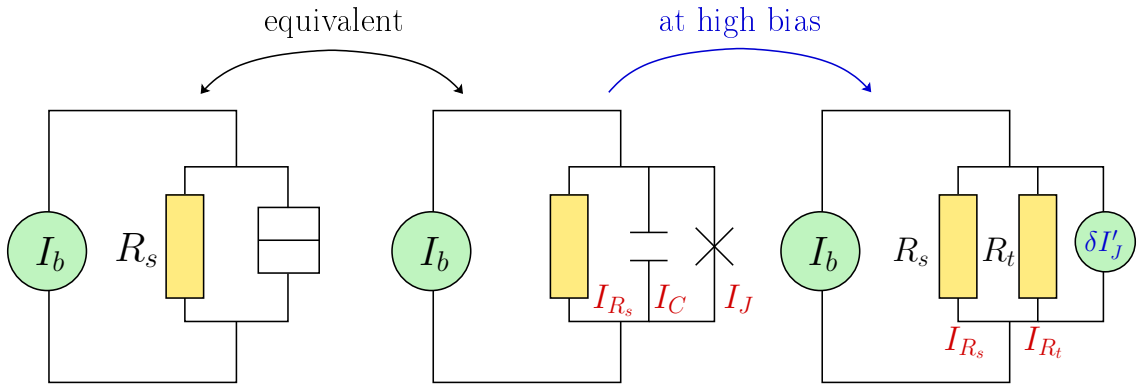

Figure 1.B.1: The tunnel junction circuit of Fig.1.2.1 (left) showed in an equivalent way (middle), separating the tunnel junction explicitly in the contributions from the capacitor and tunneling. I_{R_s}, I_C, and I_J are the current through the resistor R_s, the current at the capacitor and the pure tunneling term respectively. On the right the high-bias limit is also shown: the junction behaves as a resistor R_t plus a source of Poissonian fluctuations $\delta I'_J$.

In Fig. 1.B.1 (middle scheme) we call I_{R_s} the current through the resistance R_s and we separate the current through the junction in $I_C = \dot{Q}$ and I_J, associated to the charging of the capacitor in time and the tunneling of electrons respectively. The different currents are related by the following relation:

$$I_b = I_{R_s} + I_J + I_C = \frac{Q}{R_s} + I_J + \dot{Q}\,. \tag{1.B.1}$$

We can now express the fluctuation of I_J in terms of the fluctuations of I_{R_s} and I_C:

$$\delta I_J(t) = -\frac{\delta Q(t)}{R_s C} - \delta\dot{Q}(t)\,, \tag{1.B.2}$$

where we have used the short notation $\delta A = A - \langle A \rangle$. Recalling the definitions of the charge noise in Eqs. (1.4.1) and (1.4.4), we introduce also the resistor noise and the current noise as:

$$S_{R_s}(\omega) = \int dt_1 \int_{-\Lambda/2}^{\Lambda/2} \frac{dt_2}{\Lambda} \left\langle \frac{\delta Q(t_1)}{R_s C} \frac{\delta Q(t_2)}{R_s C} \right\rangle e^{i\omega(t_1 - t_2)}$$

$$S_J(\omega) = \int dt_1 \int_{-\Lambda/2}^{\Lambda/2} \frac{dt_2}{\Lambda} \left\langle \delta I_J(t_1) \delta I_J(t_2) \right\rangle e^{i\omega(t_1 - t_2)} \,. \tag{1.B.3}$$

From the first line of the previous equation the relation between the charge noise and the noise at the resistor is immediately evident: $S_{R_s}(\omega) = S(\omega)/(R_s^2 C^2)$. By then substituting Eq. (1.B.2) in the second line we easily see that the relation between charge noise and current noise is as given in Sec. 1.4:

$$S_J(\omega) = \left(-\frac{1}{R_s C} + i\omega\right)\left(-\frac{1}{R_s C} - i\omega\right) S(\omega) = \frac{1 + R_s^2 C^2 \omega^2}{R_s^2 C^2} S(\omega) \,. \tag{1.B.4}$$

We also note that the zero-frequency spectrum of the fluctuations through the resistance and through the junction are the same $S(0) = R_s^2 C^2 S_J(0) = R_s^2 C^2 S_{R_s}(0)$.

Moreover, we can consider the high-bias limit for the circuit. In this case the junction behaves as a resistor R_t plus a source of Poissonian fluctuations which we indicate in Fig. 1.B.1 (rightmost scheme) as $\delta I'_J$. The spectrum of these high-bias fluctuations is the bare shot noise through the junction $S'_J(\omega) \sim \mathrm{e}\langle I_J \rangle$. They contribute together with the fluctuations across the resistance R_t to the total fluctuations of the current at the junction:

$$\delta I_J = \delta I'_J + \delta I_{R_t} \,. \tag{1.B.5}$$

The last equality allows us to explicitly find out the relation between the charge noise S_J and this shot noise term S'_J, as we now show. Eq. (1.B.2) becomes here

$$\frac{\delta Q(t)}{R_\parallel} + \delta \dot{Q}(t) + \delta I'_J(t) = 0 \,, \tag{1.B.6}$$

so that we dispose of the following relation between $\delta I'_J$ and the charge fluctuations

$$\delta Q(\omega) = \frac{-\delta I'_J(\omega)}{\frac{1}{R_\parallel C} + i\omega} \,, \tag{1.B.7}$$

leading to

$$\delta I_{R_t}(\omega) = \frac{\delta Q(\omega)}{R_t C} = \frac{-\delta I'_J(\omega)}{R_t C \left(\frac{1}{R_\parallel C} + i\omega\right)} \,. \tag{1.B.8}$$

Eq. (1.B.5) becomes then

$$\delta I_J(\omega) = \delta I'_J(\omega) \left(\frac{R_t C \left(\frac{1}{R_\parallel C} + i\omega\right) - 1}{R_t C \left(\frac{1}{R_\parallel C} + i\omega\right)} \right) \,, \tag{1.B.9}$$

leading finally to

$$S_J(\omega) = S'_J(\omega) \, \frac{\left(1 - \frac{R_t}{R_\parallel}\right)^2 + R_t^2 C^2 \omega^2}{R_t^2 C^2 \left(\frac{1}{R_\parallel^2 C^2} + \omega^2\right)} \,. \tag{1.B.10}$$

Using Eq. (1.B.4) we can thus conclude

$$S(\omega) = S'_J(\omega)\,\frac{R_s^2C^2}{(1+\rho)^2+R_s^2C^2\omega^2} = \frac{\mathrm{e}\langle I_J\rangle R_s^2C^2}{(1+\rho)^2+R_s^2C^2\omega^2}\,. \tag{1.B.11}$$

which is exactly Eq. (1.5.1). We show in Fig. 1.B.2 an example of the very good agreement of this formula with the numerical simulations in the high-bias limit.

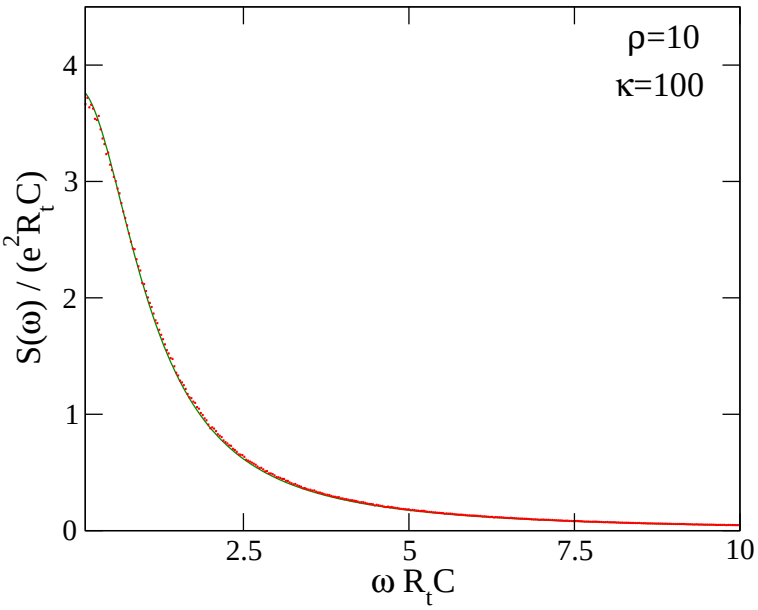

Figure 1.B.2: Very good agreement between the numerical simulations (dots) for the charge noise in the limit of very high bias ($\kappa = 100$) and the analytical estimation of Eq. (1.B.11) (solid line). Here $\rho = 10$.

Chapter 2

Thermal fluctuations

In chapter 1 we considered the vanishing-temperature case, which has allowed us to find the time dynamics of the electron tunneling through a simple analytical approach. We showed that the SETOs regime appears for $R_s > R_t \, (\gg R_Q)$. A question does now naturally arise: what happens to SETOs if we consider the effect of a finite temperature? Thermal effects are expected to act against the appearance of a clear noise peak in the charge/current-fluctuation spectrum. Would SETOs still be traceable at least in the Fano factor? When $T \neq 0$ the Coulomb gap is smeared and the electron-tunneling rate is given by the full expression (1.1.9). To model the junction transport in the presence of a finite temperature it is thus convenient to resort to a different technique, both analytically and numerically, with respect to the one used in chapter 1: we will tackle the problem by means of a Master Equation (ME) approach, as has been briefly introduced in appendix 1.A.

2.1 Finite temperature charge noise

We consider the system of chapter 1 at finite temperature, the 'orthodox' framework set by assumption $R_s \gg R_Q$ still holding. To implement numerical simulations and calculate the Fano factor we choose for convenience to resort to a ME technique instead of Monte Carlo: we find the stationary solution of the ME for the charge density distribution $\sigma(Q,t)$, and use it to calculate the zero-frequency and finite-frequency noise. We recall that $\sigma(Q,t)dQ$ is the probability that at time t the charge on the capacitance is between Q and $Q+dQ$ [cfr. with $\sigma_n(Q,t)$ in appendix 1.A, here we do not care about how many electrons have tunneled through the junction and we sum over the n index; see also Ref. [76] Eq. (31a)]. The full ME reads

$$\begin{aligned}\frac{\partial\sigma(Q,t)}{\partial t} = &-I_b\frac{\partial\sigma(Q,t)}{\partial Q} + \frac{1}{R_s}\frac{\partial}{\partial Q}\left(k_BT\frac{\partial\sigma(Q,t)}{\partial Q} + \frac{Q}{C}\sigma(Q,t)\right) + \\ &- \Big(\Gamma^+(Q)+\Gamma^-(Q)\Big)\sigma(Q,t) + \Gamma^-(Q+\mathrm{e})\sigma(Q+\mathrm{e},t) + \Gamma^+(Q-\mathrm{e})\sigma(Q-\mathrm{e},t)\,.\end{aligned} \tag{2.1.1}$$

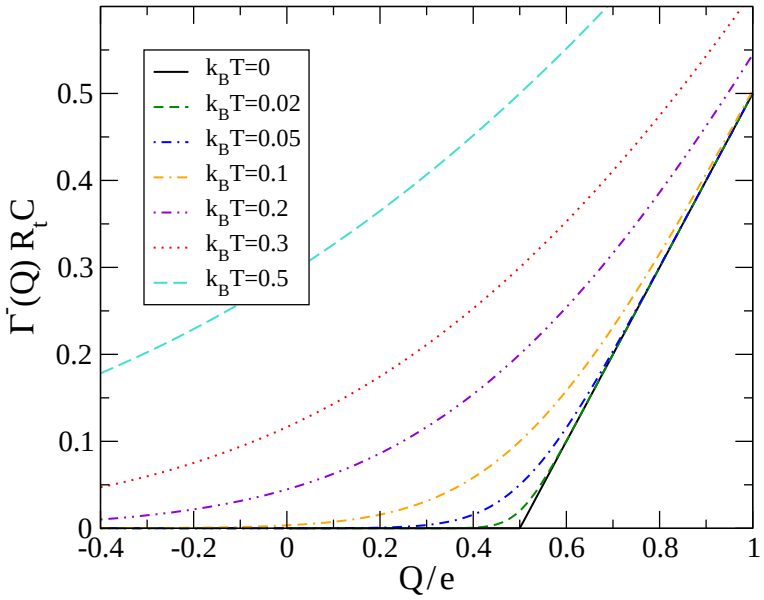

Figure 2.1.1: The $\Gamma^{-}(Q)$ tunneling rate for several temperatures as given by Eq. (2.1.2); $\Gamma^{+}(Q)$ is not plotted here, as is just given by $\Gamma^{-}(-Q)$. Temperature in units of e^2/C.

The electron-tunneling rate is now given by Eq. (1.1.9) instead of Eqs. (1.1.10) and (1.2.1). We distinguish between backward and forward rates:

$$\Gamma^{\pm}(Q) = \frac{\Delta E^{\pm}(Q)}{\mathrm{e}^2 R_t} \left(\exp\left\{ \frac{\Delta E^{\pm}(Q)}{k_B T} \right\} - 1 \right)^{-1} , \tag{2.1.2}$$

with $\Delta E^{\pm}(Q) = E(Q \pm \mathrm{e}) - E(Q)$, explicitly:

$$\begin{aligned} \Delta E^{+}(Q) &= \frac{\mathrm{e}}{C}\left(Q + \frac{\mathrm{e}}{2}\right) \\ \Delta E^{-}(Q) &= -\frac{\mathrm{e}}{C}\left(Q - \frac{\mathrm{e}}{2}\right) \\ \Delta E^{+}(Q - \mathrm{e}) &= \frac{\mathrm{e}}{C}\left(Q - \frac{\mathrm{e}}{2}\right) = -\Delta E^{-}(Q) \\ \Delta E^{-}(Q + \mathrm{e}) &= -\frac{\mathrm{e}}{C}\left(Q + \frac{\mathrm{e}}{2}\right) = -\Delta E^{+}(Q) \end{aligned} \tag{2.1.3}$$

We plot $\Gamma^{-}(Q)$ in Fig. 2.1.1. The charge noise reads ($\delta Q = Q - \langle Q \rangle$):

$$\begin{aligned} S(\tau) =& \langle Q(t+\tau)Q(t)\rangle - \langle Q(t+\tau)\rangle\langle Q(t)\rangle = \langle \delta Q(t+\tau)\delta Q(t)\rangle = \\ =& \int d(\delta Q_1) \int d(\delta Q_2)\ \delta Q_2\ \sigma(Q_2, t+\tau | Q_1, t)\ \delta Q_1\ \sigma(Q_1, t) = \\ =& \int d(\delta Q_1) \int d(\delta Q_2)\ \delta Q_2\ \sigma(Q_2, t+\tau | Q_1, t)\ \delta Q_1\ \sigma^{\mathrm{st}} , \end{aligned} \tag{2.1.4}$$

where $\sigma(\ |\ )$ is the conditional probability density [1], with $\sigma(Q_2, t | Q_1, t) = \delta(Q_2 - Q_1)$, and σ^{st} is the stationary charge distribution.

1. $\sigma(Q_2, t_2 | Q_1, t_1)$ is the conditional probability density that the charge on the capacitance is Q_2 at time t_2 if it was Q_1 at t_1.

We give in the following a few details of the numerical implementation. The first step is to discretize Eq. (2.1.1):

$$\begin{aligned} &Q \to \mathbf{q} = \{q_i\}_{i=1,N} \\ &\sigma \to \boldsymbol{\sigma} = \{\sigma_i\}_{i=1,N} \\ &\sigma(\ |\ ) \to \boldsymbol{\Sigma} = \{\sigma_{ij}\}_{i,j=1,N} \\ &q_{i+1} - q_i = \Delta\,. \end{aligned} \tag{2.1.5}$$

The discretized derivatives read

$$\frac{\partial \sigma_i}{\partial Q} \to \frac{\sigma_{i+1} - \sigma_i}{\Delta} \quad , \quad \frac{\partial^2 \sigma_i}{\partial Q^2} \to \frac{\sigma_{i+1} - 2\sigma_i + \sigma_{i-1}}{\Delta^2}\,. \tag{2.1.6}$$

The ME can be then be written in matrix form as $\frac{\partial \boldsymbol{\sigma}}{\partial t} = \mathbf{M}\boldsymbol{\sigma}$, or by components $\frac{\partial \sigma_i}{\partial t} = \sum_{ik} M_{i,k}\sigma_k$, with $\mathbf{M}$ a sparse matrix which has non-zero entries:

$$\begin{aligned} M_{i,i} &= \frac{I_b}{\Delta} - \frac{2k_BT}{R_s\Delta^2} + \frac{1}{\tau_s} - \frac{q_i}{\tau_s\Delta} - \Gamma^+(q_i) - \Gamma^-(q_i) \\ M_{i,i+1} &= -\frac{I_b}{\Delta} + \frac{k_BT}{R_s\Delta^2} + \frac{q_i}{\tau_s\Delta} \\ M_{i,i-1} &= \frac{k_BT}{R_s\Delta^2} \\ M_{i,i+N\Delta} &= \Gamma^-(q_{i+N\Delta}) \\ M_{i,i-N\Delta} &= \Gamma^+(q_{i-N\Delta})\,. \end{aligned} \tag{2.1.7}$$

The conditional probability density obeys the differential equation:

$$\begin{cases} \dot{\sigma}_{ij} = \sum_k M_{i,k}\sigma_{kj} \\ \sigma_{ij}(0) = \delta_{ij}/\Delta \end{cases} , \tag{2.1.8}$$

which passing to Laplace transform reads

$$z\sigma_{ij}(z) - \sigma_{ij}(0) = \sum_k M_{i,k}\sigma_{kj}(z)\,. \tag{2.1.9}$$

We thus look for the solution of

$$z\sigma_{ij}(z) - \sum_k M_{i,k}\sigma_{kj}(z) = \delta_{ij}/\Delta\,, \tag{2.1.10}$$

or, in matrix form, $(z - \mathbf{M})\boldsymbol{\Sigma}(z) = \mathbb{1}/\Delta$, thus

$$\boldsymbol{\Sigma}(z) = (z - \mathbf{M})^{-1}/\Delta\,. \tag{2.1.11}$$

Substituting in the Laplace transform of discretized (2.1.4) we get:

$$S(z) = \sum_i \sum_j \Delta^2\, \delta q_i\, \sigma_{ij}(z)\, \delta q_j\, \sigma_j^{\rm st} = \sum_i \sum_j \Delta\, \delta q_i\, (z - \mathbf{M})^{-1}_{ij}\, \delta q_j\, \sigma_j^{\rm st}\,. \tag{2.1.12}$$

We can now write the Fourier transform as

$$\begin{aligned} S(\omega) &= \int_{-\infty}^{+\infty} d\tau e^{i\omega\tau} S(\tau) = \int_{0}^{+\infty} d\tau e^{i\omega\tau} S(\tau) + \int_{0}^{+\infty} d\tau e^{-i\omega\tau} S(-\tau) = \\ &= \int_{0}^{+\infty} d\tau S(\tau) \left(e^{i\omega\tau} + e^{-i\omega\tau} \right) = S(z = -i\omega + \epsilon) + S(z = i\omega + \epsilon) \,, \end{aligned} \tag{2.1.13}$$

where we have used the fact that $S(\tau) = S(-\tau)$. The final expression for the charge noise reads

$$\begin{aligned} S(\omega) =& \sum_{ij} \Delta \delta q_i \left(\frac{1}{\mathbb{1}(\epsilon + i\omega) - \mathbf{M}} + \frac{1}{\mathbb{1}(\epsilon - i\omega) - \mathbf{M}} \right)_{ij} \delta q_j \sigma_j^{\mathrm{st}} = \\ =& \sum_{ij} \Delta \delta q_i \left(\frac{-2\mathbf{M}}{\mathbb{1}\omega^2 + \mathbf{M}^2} \right)_{ij} \delta q_j \sigma_j^{\mathrm{st}} \,. \end{aligned} \tag{2.1.14}$$

2.2 Finite temperature current noise

Here we introduce an alternative approach to directly calculate the current-noise. As we stated in the discussion about the Fano factor of section 1.4 and in appendix 1.B, the following relation between charge-noise and current-noise holds exactly at $T = 0$:

$$S(\omega) = \frac{\tau_s^2}{(1 + \omega^2 \tau_s^2)} \, S_J(\omega) \,. \tag{2.2.1}$$

At finite temperature however, the thermal fluctuations at the resistor need to be taken into account: the current at the junction fluctuates now also due to the thermal noise coming from the resistance R_s. This thermal contribution, say δI_{kT}, has classically the standard white noise spectrum (Johnson-Nyquist noise) $S_{kT} = 2k_B T/R_s$. The problem is that thermal fluctuations at the resistor and fluctuations of the charge at the junction are strongly correlated. To write the correct relation between charge-noise and current-noise at finite temperature, one would therefore need to know the mixed correlators of the type $\langle \delta Q(t_1) \delta I_{kT}(t_2) \rangle$. Extracting the current-noise from the charge-noise is thus delicate at finite temperature. The knowledge of the current-noise is on the other hand needed to have direct access to the Fano factor:

$$\mathbb{F} \equiv \frac{S_J(0)}{\mathrm{e} \, \langle I_J \rangle} \,. \tag{2.2.2}$$

Fortunately, we can resort to the possibility of directly computing the current-noise S_J given by the technique of Refs. [113–115].

We start again from the ME but keeping track of the number of electrons having tunneled through the junction, as it is done in appendix 1.A, see Eq. (1.A.1):

$$\begin{aligned} \frac{\partial \sigma_n(Q,t)}{\partial t} =& \mathcal{L}_0 \sigma_n(Q,t) - \left(\Gamma^+(Q) + \Gamma^-(Q) \right) \sigma_n(Q,t) + \\ &+ \Gamma^-(Q + \mathrm{e}) \sigma_{n-1}(Q + \mathrm{e}, t) + \Gamma^+(Q - \mathrm{e}) \sigma_{n+1}(Q - \mathrm{e}, t) \,, \end{aligned} \tag{2.2.3}$$

with

$$\mathcal{L}_0\sigma_n(Q,t) = -I_b\frac{\partial\sigma_n(Q,t)}{\partial Q} + \frac{1}{R_s}\frac{\partial}{\partial Q}\left(k_BT\frac{\partial\sigma_n(Q,t)}{\partial Q} + \frac{Q}{C}\sigma_n(Q,t)\right). \tag{2.2.4}$$

We then define the Fourier series:

$$\sigma_\chi(Q,t) = \sum_{n=-\infty}^{+\infty} e^{i\chi n}\sigma_n(Q,t)\,, \tag{2.2.5}$$

and the following relations hold:

$$\begin{aligned}\sum_{n=-\infty}^{+\infty} e^{i\chi n}\sigma_{n-1}(Q,t) =& e^{i\chi}\sigma_\chi(Q+\mathrm{e},t)\\ \sum_{n=-\infty}^{+\infty} e^{i\chi n}\sigma_{n+1}(Q,t) =& e^{-i\chi}\sigma_\chi(Q-\mathrm{e},t)\,.\end{aligned} \tag{2.2.6}$$

The Master Equation (2.2.3) in the χ-space reads:

$$\begin{aligned}\frac{\partial\sigma_\chi(Q,t)}{\partial t} =& \mathcal{L}_0\sigma_\chi(Q,t) - \left(\Gamma^+(Q)+\Gamma^-(Q)\right)\sigma_\chi(Q,t) +\\ &+\Gamma^-(Q+\mathrm{e})e^{i\chi}\sigma_\chi(Q+\mathrm{e},t) + \Gamma^+(Q-\mathrm{e})e^{-i\chi}\sigma_\chi(Q-\mathrm{e},t)\,.\end{aligned} \tag{2.2.7}$$

As in Sec. 2.1, we discretize Q and σ_χ for the numerical implementation: $\sigma_\chi \to \boldsymbol{\sigma}_\chi = \{\sigma^i_\chi\}_i$ and we write the ME in matrix form as $\frac{\partial\boldsymbol{\sigma}_\chi}{\partial t} = \boldsymbol{\mathcal{L}\sigma}_\chi$, or by components $\frac{\partial\sigma^i_\chi}{\partial t} = \sum_{ik}\mathcal{L}_{i,k}\sigma^k_\chi$ with $\mathcal{L}$ a sparse matrix which has non-zero entries:

$$\begin{aligned}\mathcal{L}_{i,i} &= \frac{I_b}{\Delta} - \frac{2k_BT}{R_s\Delta^2} + \frac{1}{\tau_s} - \frac{q_i}{\tau_s\Delta} - \Gamma^+(q_i) - \Gamma^-(q_i)\\ \mathcal{L}_{i,i+1} &= -\frac{I_b}{\Delta} + \frac{k_BT}{R_s\Delta^2} + \frac{q_i}{\tau_s\Delta}\\ \mathcal{L}_{i,i-1} &= \frac{k_BT}{R_s\Delta^2}\\ \mathcal{L}_{i,i+N\Delta} &= \Gamma^-(q_{i+N\Delta})e^{i\chi}\\ \mathcal{L}_{i,i-N\Delta} &= \Gamma^+(q_{i-N\Delta})e^{-i\chi}\,.\end{aligned} \tag{2.2.8}$$

As in Ref. [113], the current noise is then given by

$$S_J(t) = \delta(t)\mathbf{w}^t\boldsymbol{\mathcal{L}''\sigma} + \mathbf{w}^t\boldsymbol{\mathcal{L}'}e^{\boldsymbol{\mathcal{L}}t}\boldsymbol{\mathcal{L}'\sigma} - (\mathbf{w}^t\boldsymbol{\mathcal{L}'\sigma})^2\,, \tag{2.2.9}$$

where $\mathbf{w}^t = (1,1,1,....,1)/(\mathbf{w}^t\boldsymbol{\sigma})$, the matrix $\boldsymbol{\mathcal{L}'} = \frac{\partial\boldsymbol{\mathcal{L}}(\chi)}{\partial i\chi}\Big|_{\chi=0}$ has non-zero entries

$$\begin{aligned}\mathcal{L}'_{i,i+N\Delta} =& \Gamma^-(q_{i+N\Delta})e^{i\chi}\\ \mathcal{L}'_{i,i-N\Delta} =& -\Gamma^+(q_{i-N\Delta})e^{i\chi}\,,\end{aligned} \tag{2.2.10}$$

and the matrix $\boldsymbol{\mathcal{L}''} = \frac{\partial^2\boldsymbol{\mathcal{L}}(\chi)}{\partial(i\chi)^2}\Big|_{\chi=0}$ has non-zero entries

$$\begin{aligned}\mathcal{L}''_{i,i+N\Delta} =& \Gamma^-(q_{i+N\Delta})e^{i\chi}\\ \mathcal{L}''_{i,i-N\Delta} =& \Gamma^+(q_{i-N\Delta})e^{i\chi}\,.\end{aligned} \tag{2.2.11}$$

By introducing $\tilde{\boldsymbol{\mathcal{L}}}' = \boldsymbol{\mathcal{L}}' - \mathbf{w}^t \boldsymbol{\mathcal{L}}' \boldsymbol{\sigma}$, we can rewrite (2.2.9) as

$$S_J(t) = \delta(t) \mathbf{w}^t \boldsymbol{\mathcal{L}}'' \boldsymbol{\sigma} + \mathbf{w}^t \tilde{\boldsymbol{\mathcal{L}}}' e^{\boldsymbol{\mathcal{L}} t} \tilde{\boldsymbol{\mathcal{L}}}' \boldsymbol{\sigma} \,. \tag{2.2.12}$$

The Fourier transform reads then:

$$S_J(\omega) = \mathbf{w}^t \boldsymbol{\mathcal{L}}'' \boldsymbol{\sigma} - 2 \mathbf{w}^t \tilde{\boldsymbol{\mathcal{L}}}' \frac{\boldsymbol{\mathcal{L}}}{\mathbb{1}\omega^2 + \boldsymbol{\mathcal{L}}^2} \tilde{\boldsymbol{\mathcal{L}}}' \boldsymbol{\sigma} \,, \tag{2.2.13}$$

or

$$S_J(\omega) = \sum_{ijkl} w_i^t \mathcal{L}''_{ij} \sigma_j - 2 w_i^t \tilde{\mathcal{L}}'_{ij} \left(\frac{\boldsymbol{\mathcal{L}}}{\mathbb{1}\omega^2 + \boldsymbol{\mathcal{L}}^2} \right)_{jk} \tilde{\mathcal{L}}'_{kl} \sigma_l^{\mathrm{st}} \,, \tag{2.2.14}$$

where $\boldsymbol{\sigma}^{\mathrm{st}}$ is the stationary result of the ME as in (2.1.14).

2.3 Numerical results

We show here the results of numerical simulations for the charge-noise spectrum at finite temperature, to be compared to the zero-temperature results of section 1.5. We solve the ME for the stationary charge distribution $\boldsymbol{\sigma}^{\mathrm{st}}$, which we use to obtain the charge-noise via Eq. (2.1.14). Fig. 2.3.1 reports the I-V characteristics at different temperatures for $\rho = 100$ and $\rho = 10$. The zero-T case was also shown in Fig. 1.2.2. The back-bending, or 'nose', which was fully explained by our analytical model in section 1.3.2, already disappears at temperatures which are still relatively low with respect to the Coulomb energy scale ($k_B T \sim 0.05\, \mathrm{e}^2/C$). As is to be expected, SETOs are being washed out by thermal effects. This appears even more clearly by inspecting the evolution of the SETOs peak in the charge-noise spectrum: we plot it in Fig. 2.3.2 for the case $\kappa = 1$, i.e. optimum bias condition, $\rho = 100$ and $\rho = 10$, which in particularly represents an experimentally reasonable resistive environment that is sufficiently large for the spectrum to display a clear peak (see Fig. 1.5.2). The peak is no more visible already at $k_B T \sim 0.05\, \mathrm{e}^2/C$. We note that the disappearance of the back-bending in the I-V curves at fixed ρ is quicker than the disappearance of the charge-noise peak for rising temperature.

We can try to clarify here the interpretation of these results. Thermal effects participate with two contributions to the ME. We have seen first of all that the temperature smoothens the tunneling rates with respect to the $T = 0$ case [cfr. Eqs. (1.2.1) and (1.1.9)]: electrons can now tunnel even before the charge has reached the value of e/2, the sooner the higher is the temperature, and a sharp threshold does not exist anymore. This damages already the periodicity of the SETOs. Secondly, the temperature enters directly in the ME itself with a diffusive term, introducing fluctuations of the charge at the junction which are a source of thermal noise affecting the charge-noise spectrum. In order to evaluate the respective importance of these two contributions with the numerical calculations we have tried to implement the ME (2.1.1) switching off the temperature *only* in the tunneling rates and we found the results very little differing to the full-temperature ones. This clearly indicates that the most

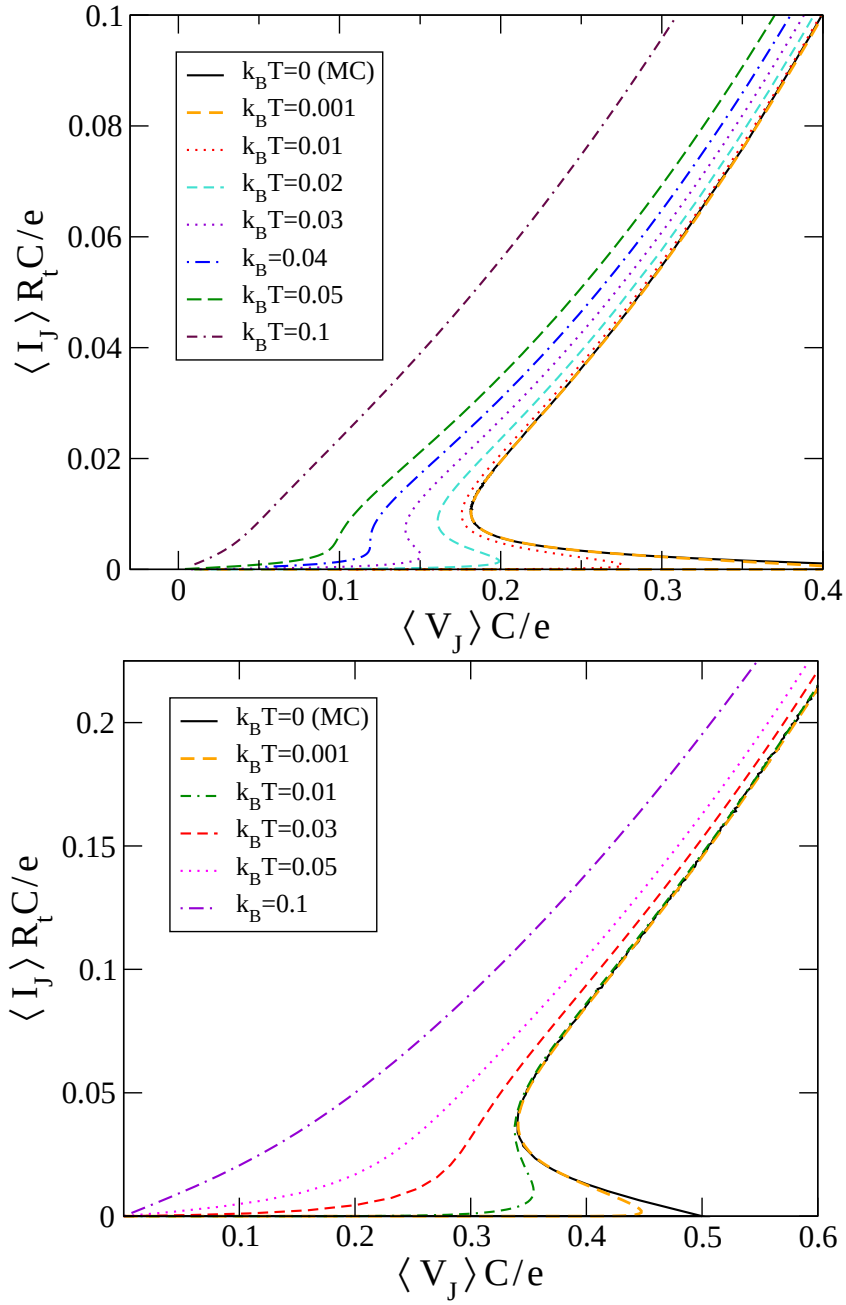

Figure 2.3.1: *I-V* characteristics for different values of the temperature (units of e^2/C), with $\rho = 100$ (top) and $\rho = 10$ (bottom): the zero-T curves (solid black) are the one obtained with Monte Carlo simulations already shown in Fig. 1.2.2.

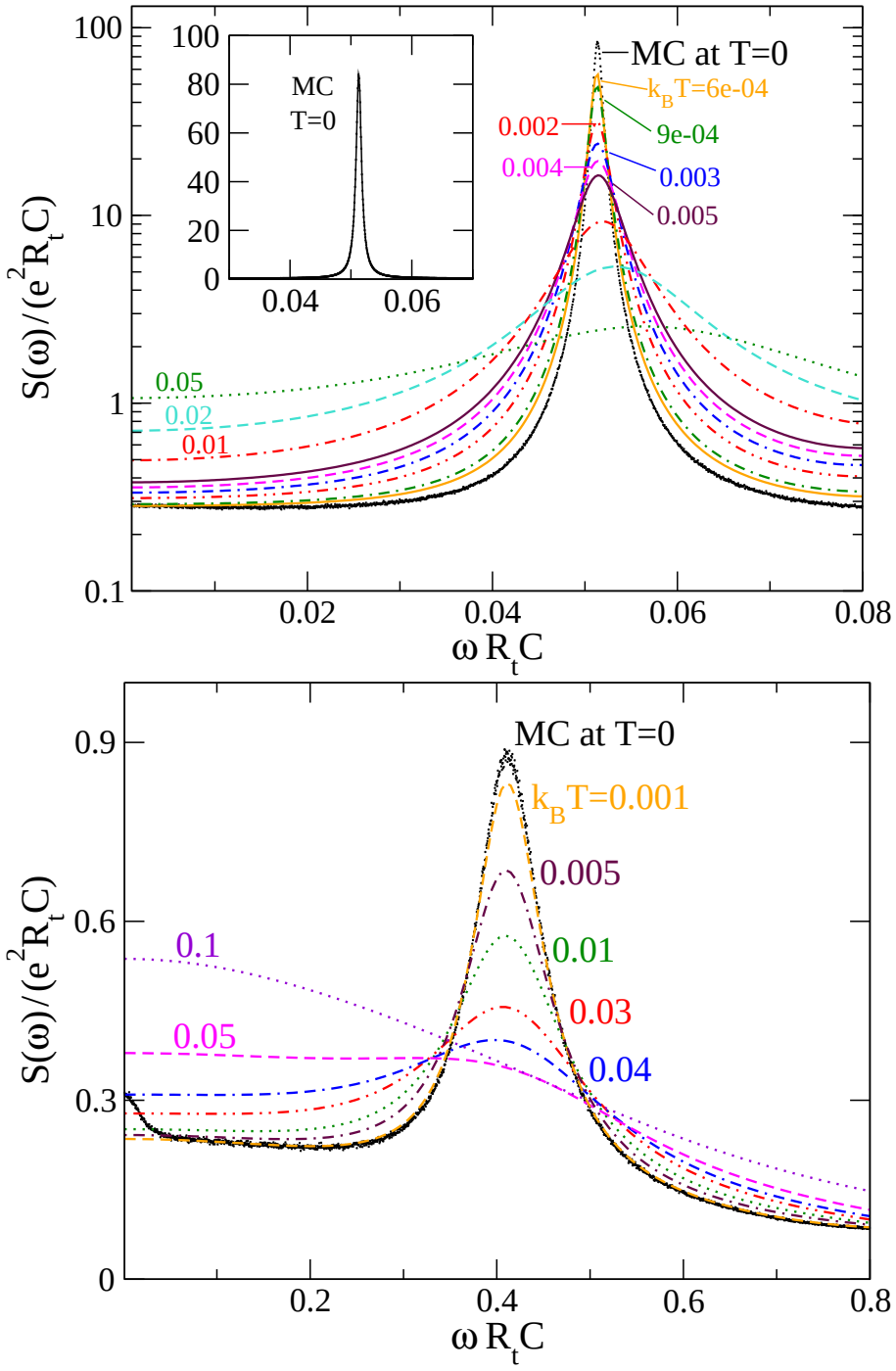

Figure 2.3.2: The charge noise $S(\omega)$ computed at different temperatures by numerically solving the ME and using Eq. (2.1.14), compared to the zero-temperature result obtained in chapter 1 by Monte Carlo simulations (black dots). Here $\kappa = 1$ and $\rho = 100$ in the upper panel (y axis in logscale), while $\rho = 10$ in the lower panel. The SETOs peak is severely smeared by thermal effects already for $k_B T$ as small as $0.01\,\mathrm{e}^2/C$.

important thermal effects are the ones associated with charge fluctuations. From the numerical results we can conclude that not only temperature acts against SETOs, as is obvious, but they appear to be extremely delicate and sensitive to thermal effects, which represents a serious warning for all possible experimental observations/applications attempts. In the next section we provide a quantitative analytical estimation of the effect of thermal charge fluctuations on the SETOs peak, to clarify the scale of temperature (energy) involved.

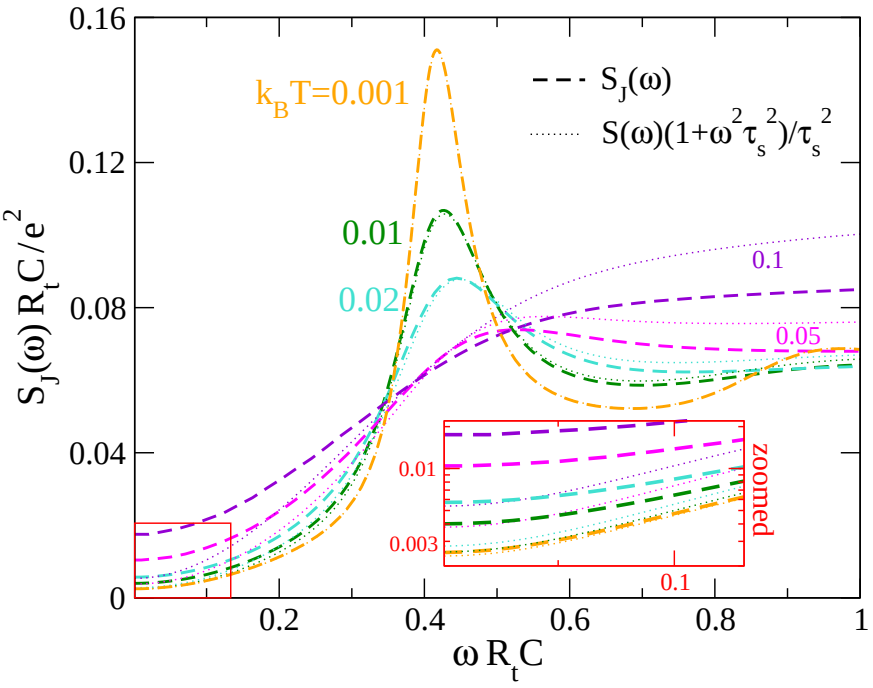

Figure 2.3.3: The current noise $S_J(\omega)$ (thick dashed) computed at different temperatures by numerically solving the ME and using Eq. (2.2.13), compared to the charge noise $S(\omega)$ (thin dotted) times the factor $(1+\omega^2\tau_s^2)/\tau_s^2$ given by Eq. (2.2.1), which establishes the exact relation between the two at zero temperature. Here $\kappa = 1$ and $\rho = 10$, as in the lower panel of Fig. 2.3.2. In the inset a zoom of the low-frequency region, with logarithmic vertical scale.

To complete the overview on the numerical results we shall also show computations of the current noise obtained via Eq. (2.2.13). As explained at the beginning of Sec. 2.2, we will need the zero-frequency current noise $S_J(0)$ to numerically compute the Fano factor and compare it with analytical results (see Sec. 2.5). It is then useful first to compare here the full-frequency spectrum $S_J(\omega)$ with the charge noise $S(\omega)$ to see how Eq. (2.2.1) fails at finite temperature. We thus report in Fig. 2.3.3 the current noise for different temperatures compared to the charge noise scaled by the factor $(1+\omega^2\tau_s^2)/\tau_s^2$: the agreement at the peak remains good even at temperatures which already significantly influence the SETOs ($k_BT \sim 0.1\,e^2/C$, as we have seen before) but the low-frequency spectrum is instead more

importantly affected. Eq. (2.2.1) is thus a good approximation for frequencies close to the peak up to $k_BT \sim 0.1\,\mathrm{e}^2/C$ but does not hold at low frequency: this confirms that we cannot obtain the Fano factor from the charge noise and we need instead directly the current noise.

2.4 Analytical estimation of the effect of thermal charge fluctuations on the SETOs peak

How exactly thermal charge fluctuations act against SETOs? In section 1.3.2 we have seen that at $T = 0$ SETOs are controlled by the delay time in tunneling of electrons after the threshold, and we found that the width of the charge-noise peak depends on the spread of this tunneling time $\langle\,\delta\tau^2\rangle - \langle\delta\tau\rangle^2$ [see Eq. (1.4.23)]. We now add to the picture a thermal source of charge fluctuations [see also appendix 1.B and the beginning of Sec. 2.2], with the standard thermal noise spectrum $S_{kT}(\omega) = \hbar\omega/R_s\coth(2k_BT/(\hbar\omega))$, and investigate how it competes with the zero-temperature mechanism. We can see the effect of the thermal charge fluctuations as a delay in the time required to reach the threshold. This delay, call it Δt_{kT}, has then a spread

$$\langle\Delta t_{kT}^2\rangle = \langle\Delta Q_{kT}^2\rangle \Big/ \left[\frac{d}{dt}Q_f\left(-\mathrm{e}/2,t\right)\right]\Big|_{Q_f=\mathrm{e}/2} = \frac{\langle\Delta Q_{kT}^2\rangle}{\kappa\mathrm{e}/(2R_sC)}\,, \tag{2.4.1}$$

where the spread of the charge $\langle\Delta Q_{kT}^2\rangle$ can be readily calculated knowing $S_{kT}(\omega)$ as

$$\langle\Delta Q_{kT}^2\rangle = \int_0^t dt_1\int_0^t dt_2\int_{-\infty}^{+\infty}\frac{d\omega}{2\pi}S_{kT}(\omega)e^{i\omega(t_1-t_2)}\,. \tag{2.4.2}$$

The relevant time scale t is here exactly the time $t_\star$ needed to recharge from $-\mathrm{e}/2$ to $\mathrm{e}/2$ without thermal fluctuations, given in Eq. 1.3.6. It corresponds to frequencies which are well above the thermal energy scale $t_\star \ll \hbar/k_BT$, so that we can carry out explicitly the integrations in Eq. (2.4.2):

$$\begin{aligned}\langle\Delta Q_{kT}^2\rangle &= \int_0^{t_\star}dt_1\int_0^{t_\star}dt_2\int_{-\infty}^{+\infty}\frac{d\omega}{2\pi}\,S_{kT}(\omega)\,e^{i\omega(t_1-t_2)} = \int_{-\infty}^{+\infty}\frac{d\omega}{2\pi}\,S_{kT}(\omega)\,\frac{4\sin^2(\omega t_\star/2)}{\omega^2} = \\ &= t_\star\int_{-\infty}^{+\infty}\frac{dx}{2\pi}\,S_{kT}(x/t_\star)\,\frac{4\sin^2(x/2)}{x^2} \simeq t_\star\int_{-\infty}^{+\infty}\frac{dx}{2\pi}\,\frac{2k_BT}{R_s}\,\frac{4\sin^2(x/2)}{x^2} = \\ &= t_\star\frac{4}{\pi}\frac{2k_BT}{R_s}\int_0^{+\infty}dx\,\frac{\sin^2(x/2)}{x^2} = t_\star\frac{2k_BT}{R_s}\,.\end{aligned} \tag{2.4.3}$$

This gives

$$\langle\Delta t_{kT}^2\rangle = 8\,\tau_s^2\ln\left(\frac{2+\kappa}{\kappa}\right)\frac{\tilde{T}}{\kappa^2}\,, \tag{2.4.4}$$

where we have defined the dimensionless temperature $\tilde{T} \equiv k_B T/(\mathrm{e}^2/C)$. This time spread acts against the periodicity of SETOs and gives a contribution analogous to the zero-temperature spread $\langle\, \delta\tau^2\rangle - \langle\delta\tau\rangle^2$ in Eq. (1.4.23). We can now quantify the importance of the thermal effect by comparing the two terms:

$$\frac{\langle\, \delta\tau^2\rangle - \langle\delta\tau\rangle^2}{\langle \Delta t_{kT}^2\rangle} = \frac{1}{4}\left(1-\frac{\pi}{4}\right)\frac{\kappa}{\rho}\left[\ln\left(\frac{2+\kappa}{\kappa}\right)\right]^{-1}\tilde{T}^{-1}\,. \tag{2.4.5}$$

From the previous equation we can estimate the two contributions to have the same order for

$$\tilde{T} \sim \frac{1}{4}\left(1-\frac{\pi}{4}\right)\frac{\kappa}{\rho}\left[\ln\left(\frac{2+\kappa}{\kappa}\right)\right]^{-1}\,. \tag{2.4.6}$$

For $\kappa = 1$ and $\rho = 10$ or $\rho = 100$, this corresponds to $\tilde{T} \sim 0.015$ and $\tilde{T} \sim 0.0015$ respectively, which is consistent with what Fig. 2.3.2 displays. This thus explains why thermal effects become important even for $k_B T \ll \mathrm{e}^2/C$.

2.5 The high-voltage limit

It is now also very interesting to explore analytically the high-voltage limit with the ME approach. For convenience we will here neglect the temperature dependence in the tunneling rate, but keep the temperature-dependent term in the ME, which gives the main contribution as we said in Sec. 2.3. Only $\Gamma^-(Q)$ and $\Gamma^-(Q+\mathrm{e})$ are thus nonvanishing, and Eq. (2.2.7) reads:

$$\begin{aligned}\frac{\partial\sigma_\chi(Q,t)}{\partial t} =& -I_b\frac{\partial\sigma_\chi(Q,t)}{\partial Q} + \frac{1}{R_s}\frac{\partial}{\partial Q}\left(k_B T\frac{\partial\sigma_\chi(Q,t)}{\partial Q} + \frac{Q}{C}\sigma_\chi(Q,t)\right) + \\ &- \Gamma^-(Q)\sigma_\chi(Q,t) + \Gamma^-(Q+\mathrm{e})e^{i\chi}\sigma_\chi(Q+\mathrm{e},t)\,.\end{aligned} \tag{2.5.1}$$

We define $\Gamma_0 \equiv (R_t C)^{-1}$ and rewrite the rate as

$$\Gamma^-(Q) = \frac{1}{\mathrm{e}R_t C}\left(Q-\frac{\mathrm{e}}{2}\right) = \frac{\Gamma_0}{\mathrm{e}}\left(Q-\frac{\mathrm{e}}{2}\right)\,. \tag{2.5.2}$$

We also introduce the moments of the σ-distribution, defined as

$$S_\chi^{(k)}(t) \equiv \int_{-\infty}^{+\infty} dQ\; Q^k\;\sigma_\chi(Q,t)\,. \tag{2.5.3}$$

The knowledge of these moments gives access to the relevant quantities of the system, such as average charge and average current at the junction and also the zero-frequency noise from which we can obtain the Fano factor. We have in fact:

$$\begin{aligned} S_0^{(0)} &= \int_{-\infty}^{+\infty} dQ\;\sigma(Q) = 1 \\ S_0^{(1)} &= \int_{-\infty}^{+\infty} dQ\; Q\;\sigma(Q) = \langle Q\rangle \\ S_0^{(2)} &= \int_{-\infty}^{+\infty} dQ\; Q^2\;\sigma(Q) = \langle Q^2\rangle\,, \end{aligned} \tag{2.5.4}$$

where the absence of time dependence means we are dealing with the stationary quantities, and

$$\begin{aligned}
&\partial_{i\chi}\big|_{\chi=0}\partial_t S_\chi^{(0)} = \partial_t\langle N(t)\rangle = \frac{\langle I_J\rangle}{\mathrm{e}}\\
&\partial^2_{i\chi}\big|_{\chi=0}\partial_t S_\chi^{(0)} = \partial_t\langle N^2(t)\rangle\\
&\langle N(t)\rangle = \partial_{i\chi}\big|_{\chi=0} S_\chi^{(0)} = \frac{\langle I_J\rangle t}{\mathrm{e}}\\
&\langle N^2(t)\rangle = \partial^2_{i\chi}\big|_{\chi=0} S_\chi^{(0)}\,.
\end{aligned} \tag{2.5.5}$$

The zero-frequency noise $S_J(0) = \mathrm{e}^2\partial_t\left(\langle N^2(t)\rangle - \langle N(t)\rangle^2\right)$ is then given by

$$\frac{S_J(0)}{\mathrm{e}^2} = \partial_t\left[\partial^2_{i\chi}\big|_{\chi=0} S_\chi^{(0)} - \left(\partial_{i\chi}\big|_{\chi=0} S_\chi^{(0)}\right)^2\right] = \partial^2_{i\chi}\big|_{\chi=0}\partial_t S_\chi^{(0)} - 2\frac{\langle I_J\rangle^2}{\mathrm{e}^2}t\,. \tag{2.5.6}$$

To lighten the notation we define

$$\partial^n_{i\chi}\big|_{\chi=0} S_\chi^{(k)} \equiv \partial^n_\chi S_0^{(k)}\,. \tag{2.5.7}$$

We thus need to calculate $\partial^2_\chi\partial_t S_0^{(0)}$. We start by calculating $\partial_t S_\chi^{(0)}$, using Eq. 2.5.1:

$$\partial_t S_\chi^{(0)}(t) = \int_{-\infty}^{+\infty} dQ\;\partial_t\sigma_\chi(Q,t) = \frac{\Gamma_0}{2}\left(1-e^{i\chi}\right)S_\chi^{(0)}(t) - \frac{\Gamma_0}{\mathrm{e}}\left(1-e^{i\chi}\right)S_\chi^{(1)}(t)\,, \tag{2.5.8}$$

and analogously

$$\begin{aligned}
\partial_t S_\chi^{(1)}(t) = \int_{-\infty}^{+\infty} dQ\;Q\;\partial_t\sigma_\chi(Q,t) &= \left(I_b + \frac{\Gamma_0\mathrm{e}}{2}e^{i\chi}\right)S_\chi^{(0)}(t) +\\
&+\left(\frac{\Gamma_0}{2}(1-3e^{i\chi}) - \frac{1}{R_sC}\right)S_\chi^{(1)}(t) + \frac{\Gamma_0}{\mathrm{e}}\left(e^{i\chi}-1\right)S_\chi^{(2)}(t)\,.
\end{aligned} \tag{2.5.9}$$

By taking the stationary solution of (2.5.9) at $\chi = 0$ we can already extract the stationary average value of the charge:

$$0 = \left(I_b + \frac{\Gamma_0\mathrm{e}}{2}\right)S_0^{(0)} - \left(\Gamma_0 + \frac{1}{R_sC}\right)S_0^{(1)} = I_b + \frac{\Gamma_0\mathrm{e}}{2} - \left(\Gamma_0 + \frac{1}{R_sC}\right)\langle Q\rangle\,, \tag{2.5.10}$$

which gives:

$$\langle Q\rangle = \frac{I_b + \frac{\Gamma_0\mathrm{e}}{2}}{\Gamma_0 + \frac{1}{R_tC}} = R_\parallel C\left(I_b + \frac{\mathrm{e}}{2R_tC}\right)\,, \tag{2.5.11}$$

with $1/R_\parallel = 1/R_s + 1/R_t$. By taking the first derivative of Eq. (2.5.8) with respect to $i\chi$ we also have

$$\partial_{i\chi}\partial_t S_\chi^{(0)} = -\frac{\Gamma_0}{2}e^{i\chi}S_\chi^{(0)} + \frac{\Gamma_0}{\mathrm{e}}e^{i\chi}S_\chi^{(1)} + \frac{\Gamma_0}{2}\left(1-e^{i\chi}\right)\partial_{i\chi}S_\chi^{(0)} - \frac{\Gamma_0}{\mathrm{e}}\left(1-e^{i\chi}\right)\partial_{i\chi}S_\chi^{(1)}\,, \tag{2.5.12}$$

which at $\chi = 0$ immediately gives the average value of the current at the junction:

$$\frac{\langle I_J\rangle}{\mathrm{e}} = \partial_\chi\partial_t S_0^{(0)} = -\frac{\Gamma_0}{2}S_0^{(0)} + \frac{\Gamma_0}{\mathrm{e}}S_0^{(1)} = -\frac{\Gamma_0}{2} + \frac{\Gamma_0}{\mathrm{e}}\langle Q\rangle = \frac{\Gamma_0 R_\parallel C}{\mathrm{e}}\left(I_b - \frac{\mathrm{e}}{2R_sC}\right)\,. \tag{2.5.13}$$

To calculate the noise we need the second derivative of Eq. (2.5.8) at $\chi = 0$ (see Eq. (2.5.6):

$$\begin{aligned}\partial_\chi^2 \partial_t S_0^{(0)} &= -\frac{\Gamma_0}{2} S_0^{(0)} + \frac{\Gamma_0}{\mathrm{e}} S_0^{(1)} - \Gamma_0\, \partial_\chi \partial_t S_0^{(0)} + \frac{2\Gamma_0}{\mathrm{e}}\, \partial_\chi \partial_t S_0^{(1)} = \\ &= \frac{\Gamma_0}{\mathrm{e}} \left(\langle Q \rangle - \frac{\mathrm{e}}{2} \right) - \Gamma_0\, \partial_\chi \partial_t S_0^{(0)} + \frac{2\Gamma_0}{\mathrm{e}}\, \partial_\chi \partial_t S_0^{(1)}\,,\end{aligned} \tag{2.5.14}$$

where $\partial_\chi \partial_t S_0^{(0)}$ is known [see Eq. (2.5.5)], and we thus further need to calculate only $\partial_\chi \partial_t S_0^{(1)}$. This is done by taking the first derivative with respect to $i\chi$ of Eq. (2.5.9):

$$\begin{aligned}\partial_{i\chi} \partial_t S_\chi^{(1)} =& I_b \partial_{i\chi} S_\chi^{(0)} + \frac{\Gamma_0 \mathrm{e}}{2} \partial_{i\chi} S_\chi^{(0)} + \frac{\Gamma_0 \mathrm{e}}{2} S_\chi^{(0)} + \\ &- \frac{3\Gamma_0}{2} S_\chi^{(1)} - \Gamma_0 \partial_{i\chi} S_\chi^{(1)} - \frac{1}{R_s C} \partial_{i\chi} S_\chi^{(1)} + \frac{\Gamma_0}{\mathrm{e}} S_\chi^{(2)}\,,\end{aligned} \tag{2.5.15}$$

giving at $\chi = 0$

$$\begin{aligned}\partial_\chi \partial_t S_0^{(1)} =& \frac{\Gamma_0 \mathrm{e}}{2} S_0^{(0)} - \frac{3\Gamma_0}{2} S_0^{(1)} + \frac{\Gamma_0}{\mathrm{e}} S_0^{(2)} + \\ &+ \left(I_b + \frac{\Gamma_0 \mathrm{e}}{2} \right) \partial_\chi S_0^{(0)} - \left(\frac{1}{R_s C} + \Gamma_0 \right) \partial_\chi S_0^{(1)} = \\ =& \frac{\Gamma_0 \mathrm{e}}{2} - \frac{3\Gamma_0}{2} \langle Q \rangle + \frac{\Gamma_0}{\mathrm{e}} \langle Q^2 \rangle + \\ &+ \left(I_b + \frac{\Gamma_0 \mathrm{e}}{2} \right) \frac{\langle I_J \rangle t}{\mathrm{e}} - \left(\frac{1}{R_s C} + \Gamma_0 \right) \partial_\chi S_0^{(1)}\,.\end{aligned} \tag{2.5.16}$$

We see that in order to be able to solve this differential equation for $\partial_\chi S_0^{(1)}$ we still need to calculate the second moment $S_0^{(2)} = \langle Q^2 \rangle$. As in Eqs. (2.5.8) and (2.5.9) we have

$$\begin{aligned}\partial_t S_\chi^{(2)}(t) = \int_{-\infty}^{+\infty} dQ\; Q^2\; \partial_t \sigma_\chi(Q,t) =& \left(\frac{2 k_B T}{R_s} - \frac{\Gamma_0 \mathrm{e}^2}{2} e^{i\chi} \right) S_\chi^{(0)} + 2 \left(I_b + \Gamma_0 \mathrm{e}\, e^{i\chi} \right) S_\chi^{(1)} + \\ &+ \left(-\frac{2}{R_s C} + \frac{\Gamma_0}{2} - 2\Gamma_0 e^{i\chi} - \frac{\Gamma_0}{2} e^{i\chi} \right) S_\chi^{(2)} + \frac{\Gamma_0}{\mathrm{e}} \left(e^{i\chi} - 1 \right) S_\chi^{(3)}\,.\end{aligned} \tag{2.5.17}$$

and the stationary solution at $\chi = 0$ gives

$$0 = \frac{2 k_B T}{R_s} - \frac{\Gamma_0 \mathrm{e}^2}{2} + 2 \left(I_b + \Gamma_0 \mathrm{e} \right) \langle Q \rangle - 2 \left(\frac{1}{R_s C} + \Gamma_0 \right) \langle Q^2 \rangle\,, \tag{2.5.18}$$

thus

$$\langle Q^2 \rangle = R_\parallel C \left(I_b + \Gamma_0 \mathrm{e} \right) \langle Q \rangle - R_\parallel C\, \Gamma_0 \frac{\mathrm{e}^2}{4} + R_\parallel C \frac{k_B T}{R_s}\,. \tag{2.5.19}$$

The differential equation (2.5.16) contains now known functions and we write it in the form

$$\partial_\chi \partial_t S_0^{(1)} = -\eta\, \partial_\chi S_0^{(1)} + a t + b\,, \tag{2.5.20}$$

with

$$\begin{aligned}\eta &= \left(R_{\|}C\right)^{-1}\\ a &= \left(I_b + \frac{\Gamma_0 \mathrm{e}}{2}\right)\frac{\langle I_J\rangle}{\mathrm{e}} = \frac{\langle Q\rangle}{R_{\|}C}\frac{\langle I_J\rangle}{\mathrm{e}}\\ b &= \frac{\Gamma_0\mathrm{e}}{2} - \frac{3\Gamma_0}{2}\langle Q\rangle + \frac{\Gamma_0}{\mathrm{e}}\langle Q^2\rangle\,.\end{aligned} \tag{2.5.21}$$

The solution for $t \to \infty$ is easily found as

$$\partial_\chi S_0^{(1)} \simeq \frac{a}{\eta}\,t + \frac{b - a/\eta}{\eta}\,. \tag{2.5.22}$$

By plugging it in Eq. (2.5.14), we can now calculate the zero-frequency noise (2.5.6):

$$\begin{aligned}\frac{S_J(0)}{\mathrm{e}^2} &= \partial_\chi^2\partial_t S_0^{(0)} - 2\frac{\langle I_J\rangle^2}{\mathrm{e}^2}t =\\ &= \frac{\Gamma_0}{\mathrm{e}}\left(\langle Q\rangle - \frac{\mathrm{e}}{2}\right) + \frac{2\Gamma_0}{\mathrm{e}}\left(\frac{a}{\eta}\,t + \frac{b-a/\eta}{\eta}\right) - \Gamma_0\frac{\langle I_J\rangle t}{\mathrm{e}} - 2\frac{\langle I_J\rangle^2}{\mathrm{e}^2}t =\\ &= \frac{\Gamma_0}{\mathrm{e}}\left(\langle Q\rangle - \frac{\mathrm{e}}{2}\right) + \frac{2\Gamma_0}{\mathrm{e}}\,\frac{b-a/\eta}{\eta}\,,\end{aligned} \tag{2.5.23}$$

where we see that the linear terms in t cancel out exactly, leaving the result time-independent as it has to be. We can now easily obtain an explicit analytic expression for the Fano factor, defined in Eq. (2.2.2), to be compared with the numerical results obtained via the implementation described in Sec. 2.2:

$$\mathbb{F} = \frac{R_t^2}{(R_s+R_t)^2} + 4\,\frac{k_BT}{\mathrm{e}^2/C}\,\frac{R_s}{R_s+R_t}\,\frac{\mathrm{e}/(2R_sC)}{I_b - \frac{\mathrm{e}}{2R_sC}} = \frac{1}{(1+\rho)^2} + 4\,\frac{k_BT}{\mathrm{e}^2/C}\,\frac{\rho}{1+\rho}\,\frac{1}{\kappa}\,. \tag{2.5.24}$$

A few interesting comments arise from this result. Eq. (2.5.24) contains both the contribution of the shot noise and the contribution of the noise due to fluctuations of the charge. The pure shot noise of a tunnel junction due to random uncorrelated tunneling events would lead to a Fano factor identically equal to one, and this Poissonian limit is correctly retrieved by taking $\rho \to 0$ in Eq. (2.5.24). In the presence of an even slightly resistive environment $R_s \neq 0$, and therefore particularly in the case of the SETOs regime, a correlation between tunneling events is established and the Fano factor becomes sub-Poissonian. What Eq. (2.5.24) tells us, is that it actually remains sub-Poissonian also at high bias, well beyond the border of the standard SETOs region [established by the condition (1.3.5)]: we see that at zero temperature the high-bias Fano factor is a constant < 1 depending only on the ratio R_s/R_t. This means that tunneling events remain correlated even if we are biasing far away from the blockade region and SETOs are washed out. In Fig. 2.5.1 we reproduce the results of numerical simulations for the Fano factor as a function of the average voltage across the junction: the high-bias saturation value is exactly the theoretical one $1/(1+\rho)^2$.

The correction at finite temperature goes to zero as $I_b \to \infty$, so it is practically negligible at sufficiently high bias. For fixed bias however the temperature acts against the correlation

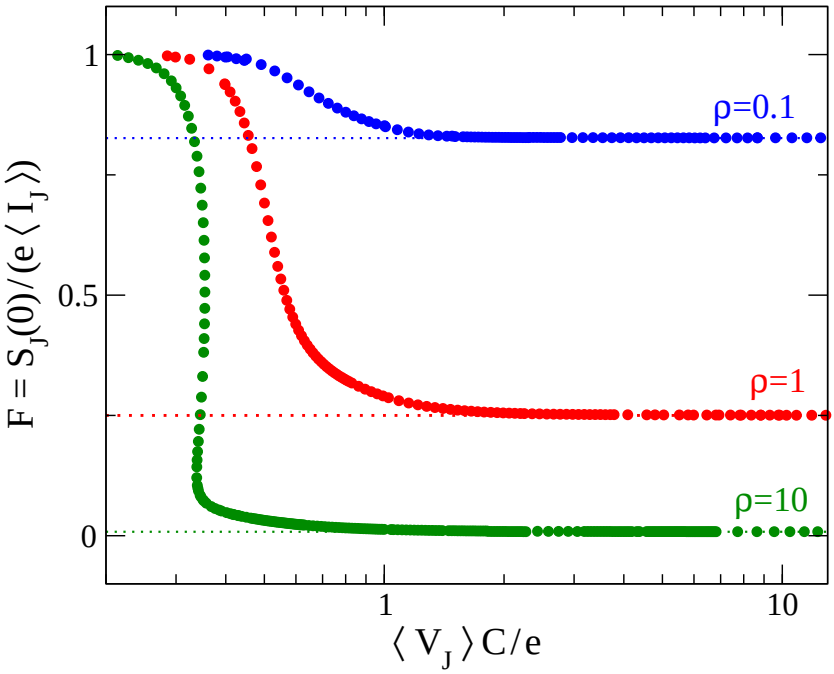

Figure 2.5.1: Fano factor as a function of the average voltage across the junction $\langle V_J \rangle$ for $\rho = 0.1, 1, 10$. The results of numerical simulations for high enough bias (equivalently, high enough average voltage) reproduce exactly the analytical value given by Eq. (2.5.24) (dotted lines). The temperature here is low enough ($k_B T = 0.01\,\mathrm{e}^2/C$) for its correction to Eq. (2.5.24) to be negligible. Logarithmic scale on x-axis.

of tunneling events, resulting in a higher Fano factor, as it can be seen from Fig. 2.5.2, where we show the analytical temperature dependence of $\mathbb{F}$. At fixed bias and in the limit of very large resistance R_s the junction noise is in practice just the thermal classical Johnson-Nyquist noise of the resistor, $S \sim 2k_B T/R_s$, leading to a Fano factor $\mathbb{F} \sim 2k_B T/(\mathrm{e} R_s I_b)$, which is exactly the limit of Eq. (2.5.24) for $\rho \to \infty$. Fig. 2.5.3 shows that numerical results for the Fano factor as a function of ρ at fixed bias perfectly match the analytical results.

The link between the Fano factor behavior and the correlations appears very clearly from our analytical analysis. Note that $\partial_\chi S_0^{(1)} \equiv \langle QN \rangle$ and using $\langle N \rangle = \langle I_J \rangle t/\mathrm{e}$ [see (2.5.5)] together with Eq. (2.5.22) we have thus

$$\langle QN \rangle = \langle Q \rangle \langle N \rangle + \frac{b - a/\eta}{\eta}\,, \tag{2.5.25}$$

from which it follows

$$\langle\langle QN \rangle\rangle = \langle QN \rangle - \langle Q \rangle \langle N \rangle = \frac{b - a/\eta}{\eta} \neq 0\,, \tag{2.5.26}$$

and also $S_J(0)/\mathrm{e}^2 = \Gamma_0/\mathrm{e}\,(\langle Q \rangle - \mathrm{e}/2) + 2\Gamma_0/\mathrm{e}\,\langle\langle QN \rangle\rangle$. If we impose $\langle\langle QN \rangle\rangle = 0$ we find $\mathbb{F} = 1$ identically, which is the standard shot-noise result. We therefore see that the sub-Poissonian behavior of the Fano factor comes exactly from the fact that the charge at the

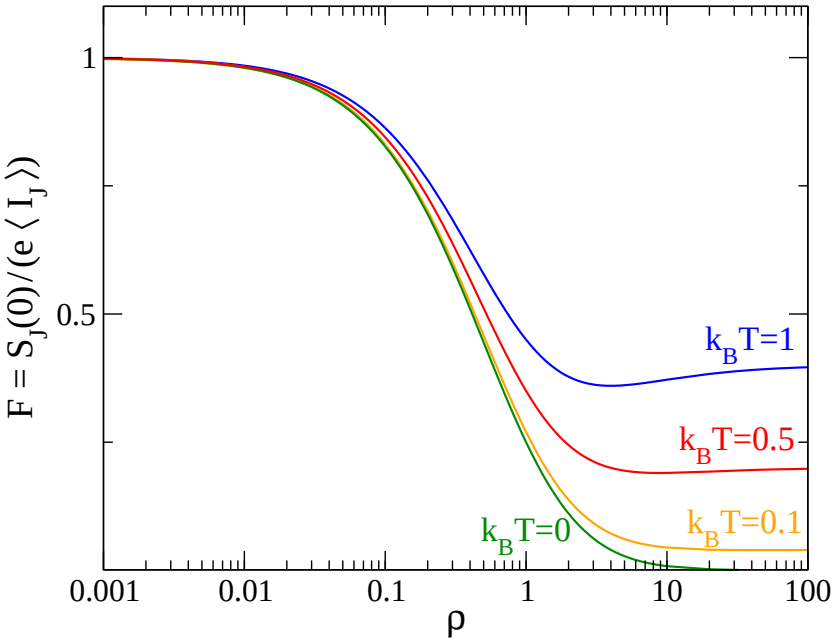

Figure 2.5.2: Theoretical high-bias ($\kappa = 10$) Fano factor as a function of ρ for different temperatures (in units of e^2/C). Logarithmic scale on x-axis.

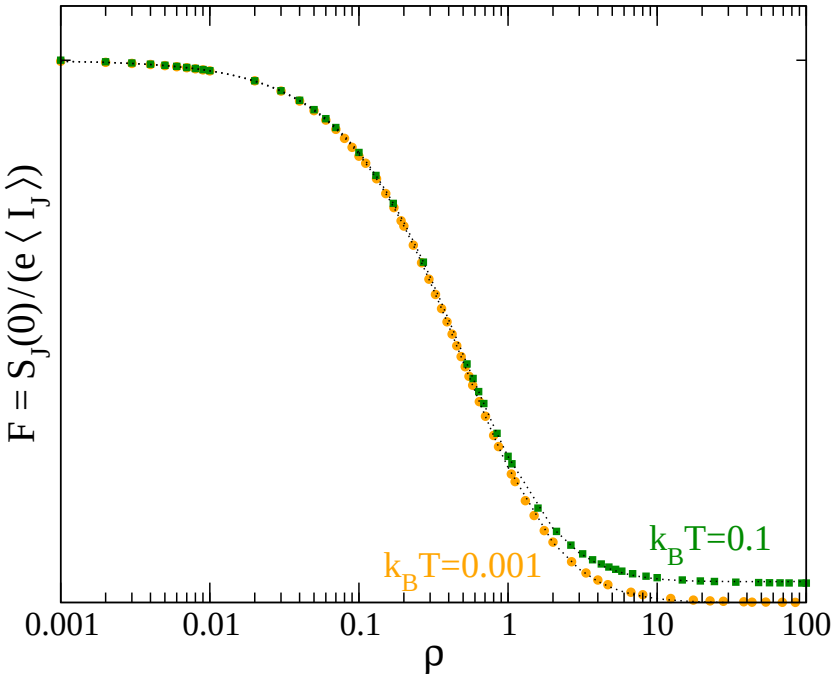

Figure 2.5.3: The Fano factor at high bias ($\kappa = 10$) numerically calculated by solving the ME for two different temperatures (circles $k_BT = 10^{-3}\,e^2/C$ and squares $k_BT = 0.1\,e^2/C$) compared to the analytical result given by Eq. (2.5.24) (dotted lines). Logarithmic scale on x-axis.

junction and the number of tunneled electrons are correlated quantities, i.e. the cumulant $\langle\langle QN\rangle\rangle$ is nonvanishing.

2.6 Conclusions

We have presented the generalization to the case of nonvanishing temperature of the analysis of the single-electron transport through the tunnel junction introduced in chapter 1. Discussions about thermal effects were already present in the early literature, see for example Ref. [80], but only in the strict $R_s = \infty$ limit. A complete and rigorous treatment of thermal effects in the presence of environments with large but finite resistance $R_s \gg R_Q$ was lacking, in particular focused on the influence on the SETOs regime. Via numerical simulations we have shown that SETOs are rather sensitive to thermally induced charge fluctuations, which seem to be destructive even at temperatures corresponding to energies still low compared to the Coulomb energy. We provided an analytical estimation which explains the temperature/energy scale involved by thermal effects. The adopted Master Equation technique has also allowed us to analyze analytically the high-bias limit and clarify some features of the Fano factor.

Chapter 3

Effects of the electromagnetic environment

The aim of this chapter is to drop the assumption $R_s \gg R_Q$ and investigate the possibility that $R_s \lesssim R_Q$. In particular we shall follow the behavior of the system from a high-impedance environment to a low-impedance one, discussing the crossover from the purely classical case ($R_s \gg R_Q$) to the quantum fluctuations dominated regime ($R_s \ll R_Q$). How SETOs are influenced by quantum fluctuations of the environment?

The concern about going beyond the ideal high-impedance, current-biased point of view and treat the environment in a more realistic way is well-motivated. The problem of modeling the electromagnetic environment of real circuits has been considered both theoretically and experimentally since the 1990s, see for example Refs. [82, 89, 116–118]. It is clear that the ideal picture of a pure resistive environment which can be tuned at will to switch from the voltage-bias scheme to the current-bias scheme is hardly realizable experimentally. Let us represent the environment as a generic impedance $Z(\omega)$. As very clearly explained in Ref. [116], up to moderately high frequencies the value of the impedance can be made large by a clever choice of the leads shape and material; but no matter how careful the design of the junction, at frequencies of the order $\sim 10^{14} - 10^{15}$ Hz radiation phenomena dominate and the impedance becomes of the order of the vacuum impedance $Z_{\text{vacuum}} \simeq 377\ \Omega$. In other words, in practice even the best Ohmic environment will start to behave as a RC transmission line at high frequencies. In Fig. 3.0.1 (taken from Ref. [116]) we show the behavior of the modulus $|Z(\omega)|$: the environmental impedance is modeled as a transmission line with total capacitance C_ℓ and total resistance R_ℓ and with characteristic impedance $Z_\ell < Z_{\text{vacuum}}$. With standard leads typical values of R_ℓ are in the range $100\ \Omega - 1\ \text{k}\Omega$, which is comparable with Z_ℓ, and the environment behaves in practice as a resistor Z_ℓ (solid blue line); if on the other hand special effort is made in obtaining high-resistance leads, with $R_\ell \sim 100\ \text{k}\Omega$ much higher than Z_ℓ, then the environment behaves as a resistor R_ℓ but only until frequency of the order of $(R_\ell C_\ell)^{-1}$, when it unavoidably enters a RC-line regime with a $\omega^{-1/2}$ fall-off until a saturation value is

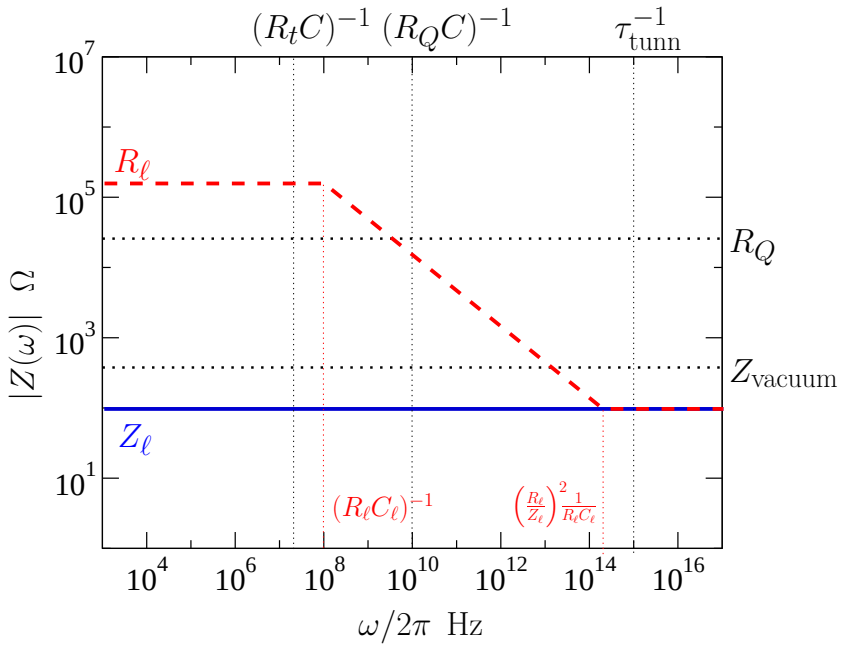

Figure 3.0.1: Scheme of the behavior of the modulus of a realistic environmental impedance as a function of the frequency, reproduced from Ref. [116]. The impedance is modeled as a RC-line with parameters R_ℓ, C_ℓ and Z_ℓ. Solid blue line: standard case where the leads resistance is comparable to Z_ℓ and the impedance behaves as a resistor Z_ℓ; dashed red line: with high-resistance leads ($R_\ell \gg Z_\ell$) the impedance behaves as a resistor R_ℓ up to frequencies $\sim (R_\ell C_\ell)^{-1}$, when it starts to decrease as $\omega^{-1/2}$ and then reaches the value Z_ℓ of the standard case. The frequencies corresponding to three characteristic time scales of the system are represented (dotted black vertical lines): $(R_tC)^{-1}$ is the tunneling rate, R_QC is the uncertainty time associated to the Coulomb energy and $\tau_{\rm tunn}$ is the (very short) tunneling time.

reached and the frequency-independent behavior of the standard case is retrieved (dashed red line). The perfect current-bias scheme with $|Z(\omega)| \gg R_Q$ cannot thus exist, at least not at all frequencies, since when the impedance behaves as Z_ℓ the inequality $Z_\ell < Z_{\rm vacuum} \ll R_Q$ holds [1]. The question whether the environment of a realistic tunnel junction circuit is or not appropriate to make single-charge effects visible is therefore delicate. From the experimental point of view special efforts are thus required to improve (at the relevant frequencies) from the standard, easily set up working regime $R_s \lesssim R_Q$ to the less straightforward $R_s \gtrsim R_Q$. On the theoretical side, investigating how precisely single-charge effects arise in a real environment stands as a key issue and implies in principle being able to describe all the regimes swept by a change of the resistance R_s from the ideal SETOs value $R_s \gg R_t \gg R_Q$ to an opposite

1. the ratio between the vacuum impedance and the quantum resistance is equal to twice the fine structure constant $e^2/(4\pi\varepsilon_0\hbar c) \sim 1/137$.

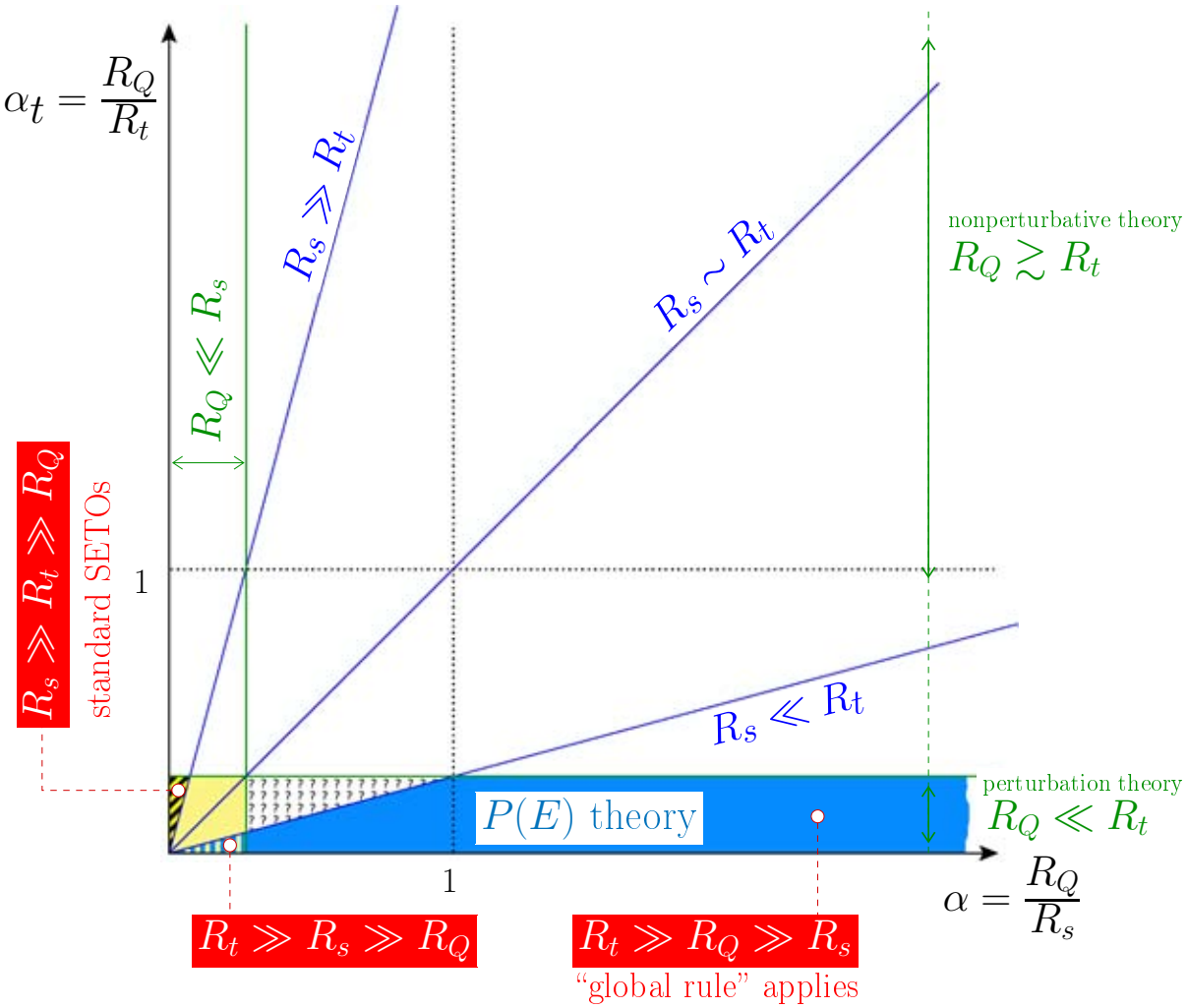

Figure 3.0.2: Phase-diagram-like overview of the possible transport regimes as a function of the relevant ratios $\alpha = R_Q/R_s$ and $\alpha_t = R_Q/R_t$. The perturbation theory which underlines the orthodox and $P(E)$ theories applies for $R_t \gg R_Q$, i.e. in the horizontal stripe at the bottom of the graph. The ideal SETOs studied in chapter 1 appear in a small triangle on the left side close to the origin. The $P(E)$ theory holds in the blue slice going from $R_t \gg R_s > R_Q$ to the limit $R_t \gg R_Q \gg R_s$.

(closer to reality) one $R_t \gtrsim R_Q \gtrsim R_s$.

In order to better clarify the different possible regimes we show in Fig. 3.0.2 a phase-diagram scheme of the plane of the parameters $\alpha \equiv R_Q/R_s$ and $\alpha_t \equiv R_Q/R_t$. For $\alpha \ll 1$ quantum fluctuations are not important: a description with a classical Master Equation works just fine and we have applied the orthodox theory of chapter 1 in the square $\{\alpha \ll 1, \alpha_t \ll 1\}$ at the bottom-left of the chart. SETOs live in a very small triangle at the extreme left, where the condition $R_s \gg R_t \gg R_Q$ is satisfied. The standard theory which on the other hand

provides a description of the crossover from high to low-impedance environment for a tunnel junction system goes under the name of '$P(E)$ theory' and has been reviewed by Ingold and Nazarov in Ref. [110]: it holds in the blue slice of Fig. 3.0.2 going from $R_t \gg R_s > R_Q$ to the limit $R_t \gg R_Q \gg R_s$. Quantum fluctuations of the environment are completely accounted for by the $P(E)$ theory, which provides suitable expressions for the tunneling rates. These tunneling rates, as we will see in Sec. 3.1, reduce to the orthodox theory ones in the limit $\alpha \ll 1$.

We point out that both orthodox and $P(E)$ theories are based on a perturbation-theory treatment of the tunneling, and this implies that the condition $R_t \gg R_Q$ must always be satisfied. This selects the bottom rectangle $\alpha_t \ll 1$ in Fig. 3.0.2. Here the extreme limits of *ideal* SETOs and *strong* quantum fluctuation effects lay on opposite sides.

To explore a region where possibly strong single-electron time-correlation effects manifest and quantum fluctuations are also important would require to leave the framework of the perturbation theory and enter the domain $R_Q \gtrsim R_t$. This has been investigated both with analytical nonperturbative approaches [119–127] and by numerical Monte Carlo simulations [120, 122, 128]. It has been demonstrated [119, 120, 129] that at sufficiently low temperatures, even for large values of the ratio $R_Q/R_t \equiv \alpha_t$ strong quantum fluctuations do not destroy Coulomb blockade but have a renormalization effect on the junction capacitance, so that the Coulomb gap is also renormalized $E_c^* \propto E_c \exp(-2\alpha_t)$. The price to pay is then a much lower temperature ($k_B T \ll E_c^*$) for single-charge effects to be visible, making them very difficult to observe. The $\alpha_t \gg 1$ regime seems therefore unattractive from the experimental point of view for probing SETOs. A theoretical study of nonperturbative SETOs (which in Fig. 3.0.2 would show up in the $\alpha \ll 1$, $\alpha_t \gg 1$ region) can be found in Ref. [119], where a formula for the I-V characteristics is given, and in Ref. [130]. To our knowledge these are the only works in the literature done in this regime, of very difficult experimental access.

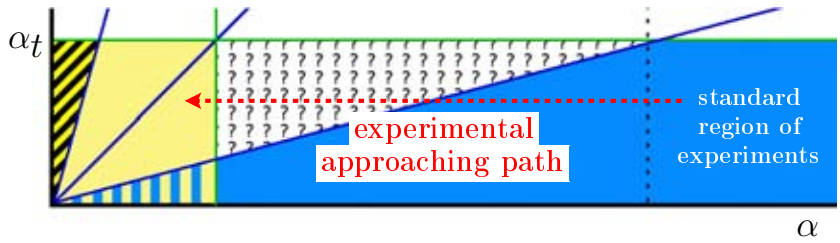

Figure 3.0.3: Zoom on the relevant area of Fig. 3.0.2: possible experimental improvements in making high-resistive environments push exactly in the direction of the still unexplored crossover area between $P(E)$ and orthodox theories.

We shall then purposefully focus on the tunneling regime represented by the area $\alpha_t \ll 1$ and ask ourselves how to describe the crossover from the left border where quantum fluctuations are irrelevant to the right one where they control transport, accounting throughout for the charge non-equilibrium effects which are responsible for the SETOs. In particular, we will

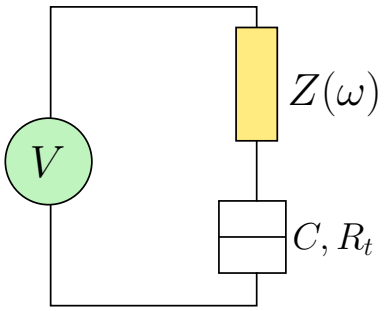

Figure 3.1.1: Generic circuit scheme considered within the $P(E)$-theory framework. The environment is modeled by a generic impedance $Z(\omega)$. With $Z(\omega) = R_s$ and $V = V_b$ the circuit is equivalent to the one introduced in chapter 1.

discuss on how to deal with the unexplored region (question-marks patterned in Fig. 3.0.2) $R_s > R_t \gg R_Q$ where SETOs are weak but still surviving and quantum fluctuations are expected to have a small but not-negligible effect. We note that the direction of possible experimental improvement in constructing high-resistive environments pushes exactly through this intermediate region (see Fig. 3.0.3), which thus deserves more theoretical interest. As we will illustrate in Sec. 3.3, the key point will be to exploit both the classical Master Equation of chapters 1, 2 and the $P(E)$ theory. The bases of the $P(E)$ and ME approaches are hence recalled in Secs. 3.1 and 3.2 respectively, to establish the needed theoretical context.

3.1 The $P(E)$ theory and the calculation of the tunneling rates

In this section we briefly illustrate the main steps for the derivation of the $P(E)$ theory. The $P(E)$ theory is the standard way to describe electron tunneling in the presence of dissipation, i.e. accounting for quantum fluctuations induced by coupling with an environment. We consider a circuit with a tunnel junction in series with a voltage source and a dissipative element represented by a generic impedance $Z(\omega)$, see Fig. 3.1.1.

As explained in Sec. 1.2, with $Z(\omega) = R_s$ this circuit is exactly equivalent to the one studied so far (with a current bias and a parallel resistance). The effects of dissipation manifest as oscillations of the voltage $V_J(t)$ across the junction induced by the environment. These voltage oscillations are equivalently oscillations of the phase at the junction ϕ, which is directly related to the voltage by the relation

$$\phi(t) = \frac{\mathrm{e}}{\hbar} \int_{-\infty}^{t} dt' \, V_J(t') \,. \tag{3.1.1}$$

We can thus model the dissipative element of the circuit as a set of harmonic LC-oscillators coupled to the phase. In the presence of the external voltage source V, the average phase evolves as $(\mathrm{e}/\hbar)Vt$ and the average charge on the junction capacitor is given by CV, it is

thus convenient for the following to introduce the shifted charge and phase $\tilde{Q} = Q - CV$ and $\tilde{\phi}(t) = \phi(t) - \frac{\mathrm{e}}{\hbar}Vt$, which conserve the same commutation relations as the unshifted variables, i.e. $[\tilde{\phi}, \tilde{Q}] = i\mathrm{e}$. The Hamiltonian of the environment reads then

$$H_{\mathrm{env}} = \frac{\tilde{Q}^2}{2C} + \sum_{n=1}^{N} \left(\frac{q_n^2}{2C_n} + \left(\frac{\hbar}{\mathrm{e}}\right)^2 \frac{1}{2L_n} (\tilde{\phi} - \phi_n)^2 \right) , \tag{3.1.2}$$

where the first term describes the charging energy of the junction capacitor and the second term is the sum over the environmental degrees of freedom represented by harmonic oscillators of frequency $\omega_n = 1/\sqrt{L_n C_n}$ bilinearly coupled to the phase $\tilde{\phi}$. We note that this is the exact electromagnetic equivalent of the quantum description of a brownian particle in a bath of harmonic oscillators, see for example [131]. For the details of the microscopic foundation of such a model of the dissipation see Ref. [110]. We will just comment here that Eq. (3.1.2) describes correctly the classical charge relaxation of the circuit and is thus an equivalent description which allows us to treat the environment quantum mechanically. The link between the model parameters L_n, C_n and the macroscopic impedance can be retrieved by writing the Heisenberg equations of motions corresponding to the Hamiltonian (3.1.2) and solving for the charge $\tilde{Q}(t)$:

$$\dot{\tilde{Q}}(t) + \frac{1}{C} \int_0^t ds\, Y(t-s)\, \tilde{Q}(s) = I_N(t) \,, \tag{3.1.3}$$

where $Y(t) = \sum_{n=1}^{N} \cos(\omega_n t)/L_n$: the Fourier transform of this function is the admittance and is exactly the inverse macroscopic impedance $Y(\omega) = 1/Z(\omega)$. Including the tunneling part in the description of the circuit, we finally get the total Hamiltonian $H_{\mathrm{tot}} = H_{\mathrm{qp}} + H_T + H_{\mathrm{env}}$, where

$$H_{\mathrm{qp}} = \sum_{\kappa\sigma} (\epsilon_\kappa + \mathrm{e}V) c^\dagger_{\kappa\sigma} c_{\kappa\sigma} + \sum_{p\sigma} \epsilon_q c^\dagger_{q\sigma} c_{q\sigma} \tag{3.1.4}$$

is the contribution due to the quasiparticles in the two electrodes and

$$H_T = \sum_{\kappa q\sigma} T_{\kappa q} c^\dagger_{q\sigma} c_{\kappa\sigma} e^{-i\tilde{\phi}} + \text{ h.c.} \tag{3.1.5}$$

the proper tunneling term which couples H_{qp} and H_{env}. Starting from H_{tot} the tunneling rates are calculated after introducing two important assumptions: i) the tunneling resistance R_t, which is inversely proportional to the square of the tunneling matrix element, is large compared to the resistance quantum R_Q:

$$R_t \gg R_Q \,. \tag{3.1.6}$$

This allows us to treat the tunneling Hamiltonian H_T as a perturbation and justifies resorting to the Fermi golden rule; ii) between tunneling events the environment has always the time to thermalize, i.e. thermal equilibrium of the modes distribution is always achieved before a new tunneling event, and the quasiparticle states are always equilibrium states described by Fermi functions. This requires in practice the time between two tunneling events to be large compared to the charge relaxation time. The rate of tunneling is proportional to the

square of the tunneling matrix element and so inversely proportional to R_t. More precisely if we call $\Delta\tau$ the average time between tunneling events we have $\Delta\tau \sim \mathrm{e}R_t/V$. The charge relaxation time for example in the case $Z(\omega) = R_s$ is instead $\sim R_s C$. Since $V \sim \mathrm{e}/(2C)$, this corresponds to the requirement

$$R_t \gg R_s \,. \tag{3.1.7}$$

These assumptions lead to the following final expression for the (backward and forward) tunneling rates $\overrightarrow{\Gamma}(V)$ and $\overleftarrow{\Gamma}(V) = \overrightarrow{\Gamma}(-V)$ [2]:

$$\overrightarrow{\Gamma}(V) = \frac{1}{\mathrm{e}^2 R_t} \int_{-\infty}^{+\infty} dE \; \frac{E}{1 - e^{-\beta E}} \; P(\mathrm{e}V - E) \,. \tag{3.1.8}$$

The key ingredient of Eq. (3.1.8) is the $P(E)$ density probability function which describes the exchange of energy between tunneling electrons and environmental modes. It quantifies in practice the probability that an electron exchanges an energy E with the environment and it is defined as the Fourier transform of the phase-phase correlation function $\mathcal{J}(t) \equiv \langle[\tilde{\phi}(t) - \tilde{\phi}(0)]\tilde{\phi}(0)\rangle$:

$$P(E) = \frac{1}{2\pi\hbar} \int_{-\infty}^{+\infty} dt \; \exp\left(\mathcal{J}(t) + \frac{i}{\hbar} E t\right) . \tag{3.1.9}$$

Eq.(3.1.8) can be read as the convolution product of the probability per unit time that a tunneling event converts an energy E into quasiparticle excitations in the electrodes, i.e. $(R_t \mathrm{e}^2)^{-1} E/(1 - e^{-\beta E})$, and the probability $P(E)$ that the electromagnetic environment absorbs an energy E during the tunneling process. The fluctuation-dissipation theorem relates the Fourier transform of the equilibrium phase-phase correlation function to a dynamical susceptibility which describes the charge relaxation [110], leading to the equality

$$\int_{-\infty}^{+\infty} dt \, e^{-i\omega t} \, \langle \tilde{\phi}(0)\tilde{\phi}(t)\rangle = \frac{2\hbar}{1 - e^{-\beta\hbar\omega}} \left(\frac{\mathrm{e}}{\hbar}\right)^2 \frac{\mathfrak{Re}\{Z_t(\omega)\}}{\omega} \,, \tag{3.1.10}$$

where Z_t is the total impedance of the circuit consisting of the capacitance of the junction C in parallel with the external impedance of the environment $Z(\omega)$:

$$Z_t(\omega) = \frac{1}{i\omega C + Z(\omega)^{-1}} \,. \tag{3.1.11}$$

The explicit expression for $\mathcal{J}(t)$ is then readily calculated as:

$$\mathcal{J}(t) = 2 \int_0^{\infty} \frac{d\omega}{\omega} \, \frac{\mathfrak{Re}\{Z_t(\omega)\}}{R_Q} \left[\coth\left(\frac{\beta\hbar\omega}{2}\right)\big(\cos(\omega t) - 1\big) - i\sin(\omega t)\right] . \tag{3.1.12}$$

The behavior of the $P(E)$ function is immediately obtained in simple limits: if the impedance of the environment is zero, i.e. we are in the pure voltage-biased case, then $P(E) = \delta(E)$ and

2. we follow here the notation of Ingold and Nazarov in Ref. [110], to distinguish the rates calculated via the $P(E)$ theory with the orthodox theory one: $\overrightarrow{\Gamma}(V)$ is the $P(E)$-theory version of $\Gamma^-(Q/C)$ in Eq. (2.1.2) and $\overleftarrow{\Gamma}(V)$ of $\Gamma^+(Q/C)$.

only 'elastic' tunneling is possible, in the sense that tunneling electrons cannot couple to the modes of the electromagnetic environment of the junction. As we said in Sec. 1.1, this prevents single-charge effects to arise in a single junction and there will exist no Coulomb blockade. If instead the impedance is low but finite, $P(E)$ peaks at low voltages and has a long tail at large voltages. At high impedance $P(E) = \delta(E - E_c)$ and we retrieve the ideal current-biased case: there is perfect overlap in this limit between the Averin & Likharev orthodox theory and Ingold & Nazarov theory for what concerns the expression of the tunneling rates.

Three important general properties are associated with the function $P(E)$ independently of temperature and environmental impedance:

- it is positive and normalized (as required by a probability function):

$$\int_{-\infty}^{+\infty} dE\ P(E) = e^{\mathcal{J}(0)} = 1\,, \tag{3.1.13}$$

- it satisfies the sum rule:

$$\int_{-\infty}^{+\infty} dE\ E\ P(E) = i\hbar \mathcal{J}'(0) = E_c\,, \tag{3.1.14}$$

- it satisfies the detailed balance symmetry:

$$P(-E) = e^{-\beta E} P(E)\,. \tag{3.1.15}$$

$P(E)$ cannot be evaluated analytically except for the aforementioned simple limits and numerical methods have to be used. One option is to use directly Eqs. (3.1.9), (3.1.12) and (3.1.11) [starting from $Z_t(\omega)$ to calculate $\partial\mathcal{J}/\partial t$ and then going back to the frequency domain to obtain $P(E)$], but involves two slowly-converging Fourier integrals and a standard integration. The other option is to evaluate $P(E)$ without going to the time domain, by means of an integral equation (see for example ref. [132]) whose derivation we sketch in the following. We start by writing

$$EP(E) = \int_{-\infty}^{+\infty} \frac{dt}{2\pi\hbar}\, E\, e^{\mathcal{J}(t)} e^{iEt/\hbar} = \int_{-\infty}^{+\infty} \frac{dt}{2\pi\hbar} e^{\mathcal{J}(t)}\, \frac{\hbar}{i}\, \frac{d}{dt} e^{iEt/\hbar} = \frac{i}{2\pi} \int_{-\infty}^{+\infty} dt\, e^{iEt/\hbar} e^{\mathcal{J}(t)} \mathcal{J}'(t)\,, \tag{3.1.16}$$

where

$$\begin{aligned} \mathcal{J}'(t) =& -2i \int_0^{\infty} d\omega\, \zeta(\omega) \left[\cos(\omega t) - i \sin(\omega t) \coth\left(\frac{\beta\hbar\omega}{2}\right)\right] = \\ =& -i \int_0^{\infty} d\omega\, \zeta(\omega) \left[e^{i\omega t} \left(1 - \coth\left(\frac{\beta\hbar\omega}{2}\right)\right) + e^{-i\omega t} \left(1 + \coth\left(\frac{\beta\hbar\omega}{2}\right)\right)\right], \end{aligned} \tag{3.1.17}$$

with $\zeta(\omega) \equiv \frac{\mathfrak{Re}\{Z_t(\omega)\}}{R_Q}$. By using (3.1.17) and the inverse Fourier transform

$$e^{\mathcal{J}(t)} = \int_{-\infty}^{+\infty} dE\, P(E)\, e^{-\frac{iEt}{\hbar}}\,, \tag{3.1.18}$$

and by defining $\tilde{\zeta}(\omega) = \theta(\omega)\zeta(\omega)$, we have thus:

$$\begin{aligned}
EP(E) =& \frac{1}{2\pi}\int_{-\infty}^{+\infty}d\omega\int_{-\infty}^{+\infty}dE'\int_{-\infty}^{+\infty}dt\ \tilde{\zeta}(\omega)\Bigg[e^{i\left(\frac{E}{\hbar}-\frac{E'}{\hbar}+\omega\right)t}\left(1-\coth\left(\frac{\beta\hbar\omega}{2}\right)\right)+\\
&+e^{i\left(\frac{E}{\hbar}-\frac{E'}{\hbar}-\omega\right)t}\left(1+\coth\left(\frac{\beta\hbar\omega}{2}\right)\right)\Bigg]P(E')=\\
=&\hbar\int_{-\infty}^{+\infty}d\omega\int_{-\infty}^{+\infty}dE'\int_{-\infty}^{+\infty}dt\ \tilde{\zeta}(\omega)\Bigg[\delta(E-E'+\hbar\omega)\left(1-\coth\left(\frac{\beta\hbar\omega}{2}\right)\right)+\\
&+\delta(E-E'-\hbar\omega)\left(1+\coth\left(\frac{\beta\hbar\omega}{2}\right)\right)\Bigg]P(E')=\\
=&\int_{-\infty}^{+\infty}d\omega\int_{-\infty}^{+\infty}dE'\int_{-\infty}^{+\infty}dt\ \tilde{\zeta}(\omega)\Bigg[\delta\left(\frac{E-E'}{\hbar}+\omega\right)\left(1-\coth\left(\frac{\beta\hbar\omega}{2}\right)\right)+\\
&+\delta\left(\frac{E-E'}{\hbar}-\omega\right)\left(1+\coth\left(\frac{\beta\hbar\omega}{2}\right)\right)\Bigg]P(E')=\\
=&\int_{-\infty}^{+\infty}dE'\left(1+\coth\left(\frac{\beta(E-E')}{2}\right)\right)\left[\tilde{\zeta}\left(\frac{E'-E}{\hbar}\right)+\tilde{\zeta}\left(\frac{E-E'}{\hbar}\right)\right]P(E')\,. \qquad (3.1.19)
\end{aligned}$$

After straightforward manipulation Eq. (3.1.19) can be rewritten as:

$$\begin{aligned}
EP(E) =& \int_0^{\infty}dx\ \zeta\left(\frac{x}{\hbar}\right)\Bigg[\left(1+\coth\left(\frac{\beta x}{2}\right)\right)P(E-x)+\\
&+\left(1+\coth\left(\frac{-\beta x}{2}\right)\right)P(E+x)\Bigg]=\\
=&\int_0^{\infty}dx\ \zeta\left(\frac{x}{\hbar}\right)\Bigg[P(E-x)+P(E+x)+\\
&+\coth\left(\frac{\beta x}{2}\right)\left(P(E-x)-P(E+x)\right)\Bigg]\,.
\end{aligned} \qquad (3.1.20)$$

At zero temperature [$\beta = +\infty$, $\coth(\beta\hbar\omega/2) = 1$] we have that the function $P(E)$ vanishes for negative energy, as it should [3], and we can simplify Eq. (3.1.19) obtaining

$$E\,P(E) = 2\int_0^{+\infty}dE'\,\zeta\left(\frac{E'-E}{\hbar}\right)P(E') = 2\int_0^{+\infty}dE'\ \frac{\mathfrak{Re}\left\{Z_t\left(\frac{E'-E}{\hbar}\right)\right\}}{R_Q}\,P(E')\,, \qquad (3.1.21)$$

which is formula (75) of Ref. [110].

Substituting $Z(\omega) = R_s$ in Eq. (3.1.11), and using $R_Q = h/\mathrm{e}^2$ we can write

$$\zeta\left(\frac{E-E'}{\hbar}\right) = \left(\alpha+\frac{1}{\alpha}\frac{(E-E')^2}{\hbar^2}R_Q^2C^2\right)^{-1} = \left(\alpha+\frac{(E-E')^2}{\alpha}\frac{\pi^2}{E_c^2}\right)^{-1}\,. \qquad (3.1.22)$$

3. $P(E)$ for negative energy is the probability density of a tunneling electron *absorbing* an energy E from the environment, so $P(E)$ for all $E < 0$ must vanish at zero temperature.

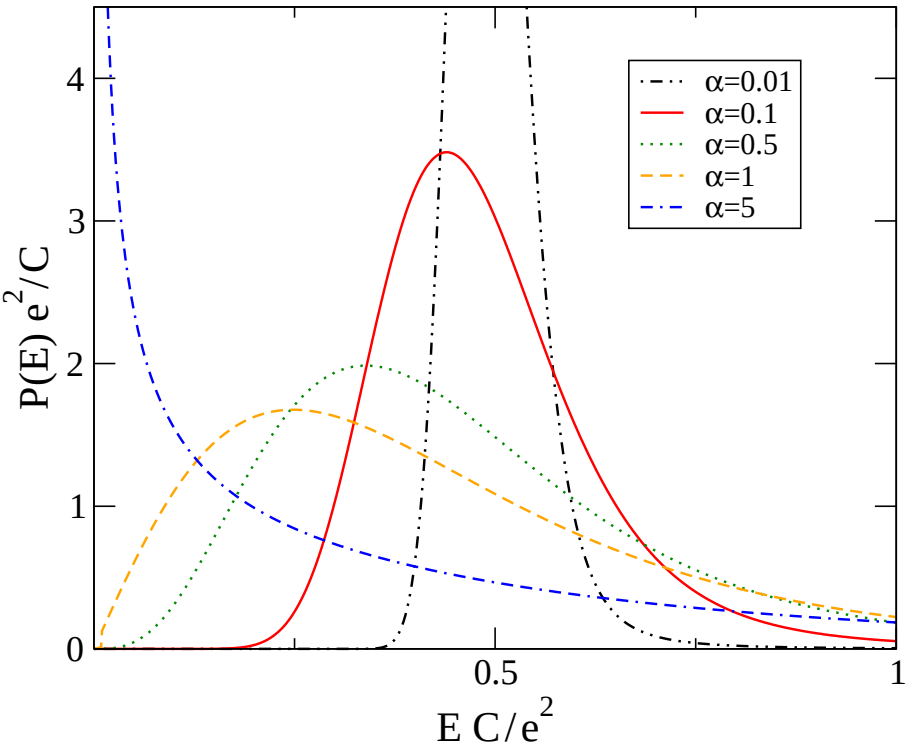

Figure 3.1.2: The function $P(E)$ at zero temperature as calculated from formula (3.1.21) displayed for different values of $\alpha = R_Q/R_s$.

Eq. (3.1.20) reads then explicitly:

$$EP(E) - \int_0^\infty dx \, \frac{P(E-x) + P(E+x) + \coth\left(\frac{\beta x}{2}\right)\left(P(E-x) - P(E+x)\right)}{\alpha + \frac{x^2}{\alpha}\frac{\pi^2}{E_c^2}} = 0\,. \quad (3.1.23)$$

The former expression is ready to be discretized and numerically implemented. We solve it by linear system solution technique (see appendix 3.A for technical details) and obtain the function $P(E)$ for different values of the temperature and of α. In Fig. 3.1.2 we show a plot of the zero-temperature $P(E)$ for varying α, while in Fig. 3.1.3 we vary the temperature for $\alpha = 0.1$.

Useful analytical results can be obtained in the high-impedance limit. In this case environmental modes concentrate at low frequency

$$\mathfrak{Re}\{Z_t(\omega)\} = \frac{R_s}{1+\omega^2(R_sC)^2} \to \frac{\pi}{C}\,\delta(\omega) \quad \text{for } R_s \to \infty \quad (3.1.24)$$

and the short-time expansion of Eq. (3.1.9)

$$P(E) \simeq \frac{1}{2\pi\hbar}\int_{-\infty}^{+\infty} dt \, \exp\left(\mathcal{J}(0) + \mathcal{J}'(0)t + \mathcal{J}''(0)t^2/2\right)\exp\left(\frac{i}{\hbar}Et\right) \quad (3.1.25)$$

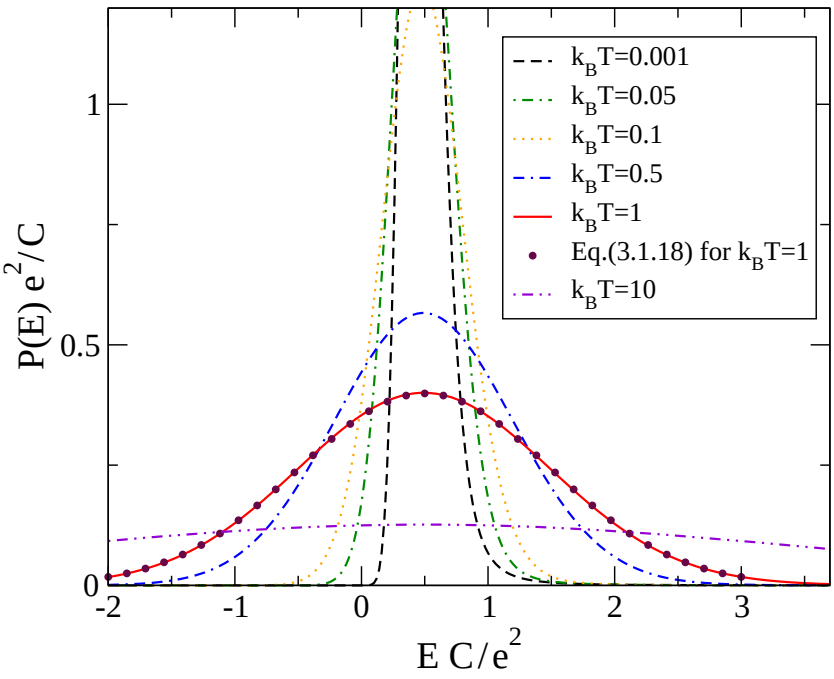

Figure 3.1.3: The function $P(E)$ for $\alpha = 0.1$ as calculated from formula (3.1.20) displayed for different temperatures. The circles correspond to the high-impedance analytical curve of Eq. (3.1.27). Temperatures are in units of e^2/C.

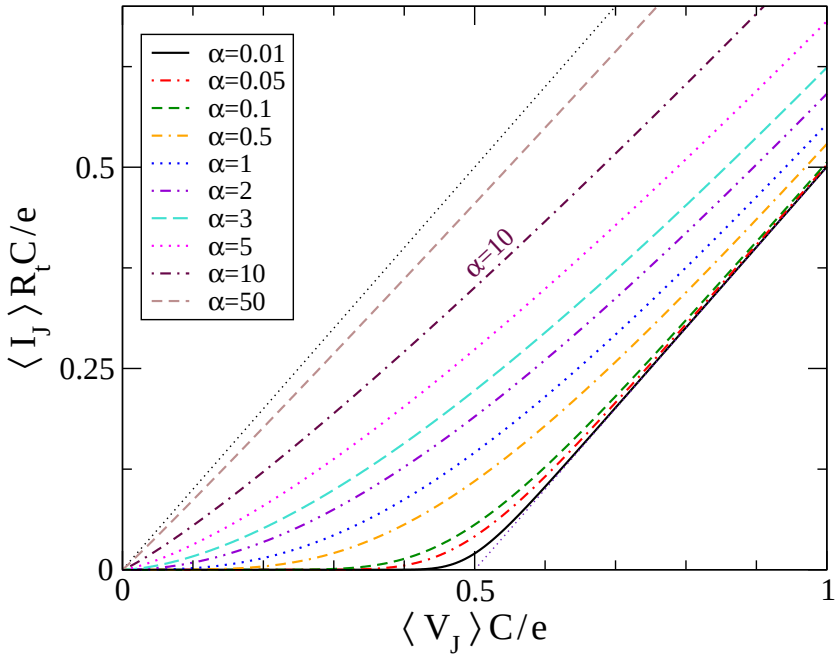

Figure 3.1.4: I-V characteristics at zero temperature from the $P(E)$ theory, as calculated by formula (3.1.28), displayed for different values of α.

always holds. With Eqs. (3.1.13), (3.1.14) and

$$\begin{aligned}\mathcal{J}''(0) &= -2\int_0^\infty \frac{d\omega}{\omega}\,\frac{\mathfrak{Re}\{Z_t(\omega)\}}{R_Q}\coth\left(\frac{\beta\hbar\omega}{2}\right)\omega^2 \simeq \\ &\simeq -2\int_0^\infty \frac{d\omega}{\omega}\,\frac{\mathfrak{Re}\{Z_t(\omega)\}}{R_Q}\frac{2k_BT}{\hbar\omega}\omega^2 = -2\,\frac{k_BTE_c}{\hbar^2}\,,\end{aligned} \tag{3.1.26}$$

we have then

$$P(E) \simeq \frac{1}{2}\sqrt{\frac{1}{\pi k_BTE_c}}\,\exp\left(-\frac{(E-E_c)^2}{4k_BTE_c}\right)\,, \tag{3.1.27}$$

holding for $\alpha \ll k_BT/E_c$ (which thus defines the boundary of the high-impedance limit). We reported the analytical curve for $k_BT = 2E_c$ in Fig. 3.1.3 to show the perfect match with the numerical result.

Once $P(E)$ and thus the tunneling rates (3.1.8) are known, also the I-V characteristics can be easily obtained as

$$I(V) = \mathrm{e}\left(\overrightarrow{\Gamma}(V) - \overleftarrow{\Gamma}(V)\right) = \frac{1}{\mathrm{e}R_t}\left(1-e^{-\beta\mathrm{e}V}\right)\int_{-\infty}^{+\infty}dE\,\frac{E}{1-e^{-\beta E}}\,P(\mathrm{e}V-E)\,. \tag{3.1.28}$$

Note that at $T = 0$ only the forward rate is nonvanishing and it coincides in practice with the I-V characteristic: $I(V) = \mathrm{e}\overrightarrow{\Gamma}(V)$, which we show in Fig. 3.1.4.

3.2 On the derivation of the classical ME

In this section we would like to briefly illustrate the derivation of the classic Master Equation in the form used in chapter 1 and chapter 2, see Eqs. (1.A.1), (2.1.1). This clarifies under which conditions a classical description of the charge fluctuations in a tunnel junction circuit is justified and moreover allows us to make an interesting bridge with the Master Equation analysis of the two-level system presented in part I: as it turns out in fact the same Born and Markov approximations introduced there to derive the ME (4.1.18) are also at the basis of the classic ME for the tunnel junction circuit. We follow mainly Ref. [131], focusing on the second and third terms of the right hand side of Eq. (2.1.1), neglecting the tunneling terms and leaving out of the picture the current source. For a complete, though somehow more involved derivation see directly Averin and Likharev in Ref. [76].

Let us consider the reduced dynamics described by the Hamiltonian (3.1.2). As we have seen, in the framework of the $P(E)$ theory the charge degree of freedom is considered as part of the environment, which always thermalizes between tunneling events, and the transient dynamics of the charge is not important in that context. Here we are interested instead exactly to this transient dynamics and the charge degrees of freedom requires a special treatment: it becomes the new 'system', while the bath of harmonic oscillators is the environment. We thus rename the Hamiltonian (3.1.2) as $\hat{H}_{\mathrm{ME}}$ and separate it in four contributions:

$\hat{H}_{\rm ME} = \hat{H}_S + \hat{V}_c + \hat{H}_B + \hat{H}_I$, where

$$\hat{H}_S = \frac{\hat{Q}^2}{2C} \tag{3.2.1}$$

$$\hat{V}_c = \hat{\phi}^2 \sum_{n=1}^{N} \frac{1}{2} \left(\frac{\hbar}{\mathrm{e}}\right)^2 \frac{1}{L_n} \tag{3.2.2}$$

$$\hat{H}_I = -\hat{\phi} \sum_{n=1}^{N} \left(\frac{\hbar}{\mathrm{e}}\right)^2 \frac{1}{L_n} \hat{\phi}_n \tag{3.2.3}$$

$$\hat{H}_B = \sum_{n=1}^{N} \left(\frac{\hat{q}_n^2}{2C_n} + \frac{1}{2} \left(\frac{\hbar}{\mathrm{e}}\right)^2 \frac{1}{L_n} \hat{\phi}_n^2 \right) . \tag{3.2.4}$$

We used the explicit hat notation for operators and will keep it for the rest of the section. $\hat{H}_{\rm ME}$ has the same form as Eq. (4.1.1) of part I: $\hat{H}_S$ represents the new reduced system (equivalent to a free brownian particle), $\hat{H}_B$ is the bath of harmonic oscillators, $\hat{H}_I$ the coupling between the two and $\hat{V}_c$ a 'counter-term' acting as an effective potential and separated out for convenience. Introducing the scaled phase variable $\hat{\varphi} = (\hbar/\mathrm{e})\hat{\phi}$, which satisfies the new commutation relation $\left[\hat{\varphi}, \hat{Q}\right] = i\hbar$, and with $\kappa_n \equiv 1/L_n$ and $\omega_n^2 = (L_n C_n)^{-1}$, Eq. (3.2.1) reads

$$\hat{H}_S = \frac{\hat{Q}^2}{2C} \tag{3.2.5}$$

$$\hat{V}_c = \hat{\varphi}^2 \sum_{n=1}^{N} \frac{\kappa_n^2}{2C_n \omega_n^2} \tag{3.2.6}$$

$$\hat{H}_I = -\hat{\varphi} \sum_{n=1}^{N} \kappa_n \hat{\varphi}_n \tag{3.2.7}$$

$$\hat{H}_B = \sum_{n=1}^{N} \left(\frac{\hat{q}_n^2}{2C_n} + \frac{1}{2} C_n \omega_n^2 \hat{\varphi}_n^2 \right) . \tag{3.2.8}$$

We are interested in a weak-coupling, high-temperature limit, which we will rigorously define in the following, where the bath relaxation times are faster than the relevant scale for the charge dynamics. We can then treat H_I as a perturbation and resort to the same exact approach of Sec. 4.1 of part I: starting from the Liouville-von Neumann equation for the total density matrix of the system described by $\hat{H}_{\rm ME}$, we trace out the bath degrees of freedom and apply the Born-Markov approximation obtaining the following ME for the reduced density matrix $\hat{\rho}_S$ in interaction representation:

$$\begin{aligned} \frac{d}{dt}\hat{\rho}_S(t) = &-\frac{i}{\hbar}\left[\frac{\hat{Q}^2}{2C} + \hat{V}_c(\hat{\varphi}), \hat{\rho}_S(t)\right] + \\ &+\frac{1}{\hbar^2}\int_0^\infty d\tau \Bigg(\frac{i}{2} D(\tau) \Big[\hat{\varphi}, \Big\{\hat{\varphi}(-\tau), \hat{\rho}_S(t)\Big\}\Big] + \\ &\qquad -\frac{1}{2} D_1(\tau) \Big[\hat{\varphi}, \Big[\hat{\varphi}(-\tau), \hat{\rho}_S(t)\Big]\Big] \Bigg) , \end{aligned} \tag{3.2.9}$$

where we have introduced the bath correlation functions:

$$\begin{aligned} D(\tau) &= i\langle\Big[\hat{B},\hat{B}(-\tau)\Big]\rangle \\ D_1(\tau) &= \langle\Big[\hat{B},\hat{B}(-\tau)\Big]\rangle\,. \end{aligned} \tag{3.2.10}$$

with $\hat{B}=\sum_n \hat{\varphi}_n/L_n$. These correspond in practice to the real and imaginary part of the function $\mathcal{C}(t)$ of part I chapter 4. Following here the same formalism and introducing the spectral density

$$J(\omega)=\sum_n \frac{k_n^2}{2C_n\omega_n}\delta(\omega-\omega_n)\,, \tag{3.2.11}$$

we can express them as

$$\begin{aligned} D(\tau) =& 2\hbar\int_0^\infty d\omega J(\omega)\sin(\omega\tau) \\ D_1(\tau) =& 2\hbar\int_0^\infty d\omega J(\omega)\coth\left(\frac{\hbar\omega}{2k_BT}\right)\cos(\omega\tau)\,, \end{aligned} \tag{3.2.12}$$

which is the analogous of Eq. (4.0.3) [part I]. By substituting the explicit time evolution of the phase operator

$$\hat{\varphi}(-\tau)=\exp\left(-\frac{i\hat{H}_S\tau}{\hbar}\right)\hat{\varphi}\,\exp\left(\frac{i\hat{H}_S\tau}{\hbar}\right)=\hat{\varphi}-\tau\frac{\hat{Q}}{C}\,, \tag{3.2.13}$$

Eq. (3.2.9) can be rewritten as

$$\begin{aligned} \frac{d}{dt}\hat{\rho}_S(t) =& -\frac{i}{\hbar}\left[\frac{\hat{Q}^2}{2C}+\hat{V}_c(x),\hat{\rho}_S(t)\right]+ \\ &+\frac{1}{\hbar^2}\int_0^\infty d\tau\Big(\frac{i}{2}D(\tau)\Big(\Big[\hat{\varphi},\Big\{\hat{\varphi},\hat{\rho}_S(t)\Big\}\Big]-\frac{\tau}{C}\Big[\hat{\varphi},\Big\{\hat{Q},\hat{\rho}_S(t)\Big\}\Big]\Big) \\ &\qquad -\frac{1}{2}D_1(\tau)\Big(\Big[\hat{\varphi},\Big[\hat{\varphi},\hat{\rho}_S(t)\Big]\Big]-\frac{\tau}{C}\Big[\hat{\varphi},\Big[\hat{Q},\hat{\rho}_S(t)\Big]\Big]\Big)\Big) = \\ &\qquad =-\frac{i}{\hbar}\left[\frac{\hat{Q}^2}{2C}+\hat{V}_c(x),\hat{\rho}_S(t)\right]+ \\ &+\frac{1}{\hbar^2}\Big(\underbrace{\frac{i}{2}\int_0^\infty d\tau D(\tau)\Big[\hat{\varphi},\Big\{\hat{\varphi},\hat{\rho}_S(t)\Big\}\Big]}_{(1)}-\underbrace{\frac{i}{2C}\int_0^\infty d\tau\tau D(\tau)\Big[\hat{\varphi},\Big\{\hat{Q},\hat{\rho}_S(t)\Big\}\Big]}_{(2)} \\ &\quad -\underbrace{\frac{1}{2}\int_0^\infty d\tau D_1(\tau)\Big[\hat{\varphi},\Big[\hat{\varphi},\hat{\rho}_S(t)\Big]\Big]}_{(3)}+\underbrace{\frac{1}{2C}\int_0^\infty d\tau\tau D_1(\tau)\Big[\hat{\varphi},\Big[\hat{Q},\hat{\rho}_S(t)\Big]\Big]}_{(4)}\Big)\,. \end{aligned} \tag{3.2.14}$$

With [4]:

$$\int_0^\infty d\tau D(\tau)=\;2\hbar\int_0^\infty d\omega J(\omega)\mathrm{PV}\left(\frac{1}{\omega}\right)=2\hbar\sum_n\frac{\kappa_n^2}{2C_n\omega_n^2} \tag{3.2.15}$$

4. we use $\int_0^\infty d\tau\sin(\omega\tau)=\mathrm{PV}(1/\omega)$. and $\int_0^\infty d\tau\tau\sin(\omega\tau)=-\partial_\omega\int_0^\infty d\tau\cos(\omega\tau)=-\delta'(0)$. PV stands for the Cauchy principal value.

$$\int_0^\infty d\tau\, \tau\, D(\tau) = -2\hbar \int_0^\infty d\omega J(\omega)\delta'(\omega) = \hbar J'(0) \tag{3.2.16}$$

$$\int_0^\infty d\tau D_1(\tau) = 2\hbar \int_0^\infty d\omega J(\omega) \coth\left(\frac{\hbar\omega}{2k_BT}\right)\delta(\omega) \tag{3.2.17}$$

$$\int_0^\infty d\tau\, \tau\, D_1(\tau) = 2\hbar \int_0^\infty d\omega J(\omega) \coth\left(\frac{\hbar\omega}{2k_BT}\right) \int_0^\infty d\tau\, \tau \cos(\omega\tau)\,, \tag{3.2.18}$$

we can simplify Eq. (3.2.14). Since $\left[\hat{\varphi}, \left\{\hat{\varphi}, \hat{\rho}_S(t)\right\}\right] = \left[\hat{\varphi}^2, \hat{\rho}_S(t)\right]$, we see that term (1) exactly compensates the counter-term $-\frac{i}{\hbar}\left[\hat{V}_c(\hat{\varphi}), \hat{\rho}_S(t)\right]$. We are then left with an equation in the form:

$$\begin{aligned}\frac{d}{dt}\hat{\rho}_S(t) = &-\frac{i}{\hbar}\left[\frac{\hat{Q}^2}{2C}, \hat{\rho}_S(t)\right] - A_1\left[\hat{\varphi}, \left\{\hat{Q}, \hat{\rho}_S(t)\right\}\right] + \\ &- A_2\left[\hat{\varphi}, \left[\hat{\varphi}, \hat{\rho}_S(t)\right]\right] + A_3\left[\hat{\varphi}, \left[\hat{Q}, \hat{\rho}_S(t)\right]\right],\end{aligned} \tag{3.2.19}$$

with

$$A_1 = \frac{i}{2\hbar C} J'(0) \tag{3.2.20}$$

$$A_2 = \frac{1}{\hbar}\int_0^\infty d\omega J(\omega) \coth\left(\frac{\hbar\omega}{2k_BT}\right)\delta(\omega) \tag{3.2.21}$$

$$A_3 = \frac{1}{\hbar C}\int_0^\infty d\omega J(\omega) \coth\left(\frac{\hbar\omega}{2k_BT}\right)\partial_\omega PV\left(\frac{1}{\omega}\right). \tag{3.2.22}$$

We need now to relate the spectral density $J(\omega)$ to the macroscopic impedance $Z(\omega) = R_s$ of our circuit. This is easily done by writing explicitly the Fourier transform of the $Y(t)$ function introduced in Eq. (3.1.3):

$$Y(\omega) = \int_{-\infty}^{+\infty} dt\, Y(t)\, e^{i\omega t} = \lim_{\epsilon\to 0}\sum_n \frac{1}{L_n}\, \frac{-i\omega}{\omega_n^2 - \omega^2 - i\,\epsilon\,\mathrm{sign}(\omega)}\,. \tag{3.2.23}$$

As we said this is the admittance and $Z(\omega) = 1/Y(\omega)$. By using Eq. (3.2.11) we can immediately rewrite

$$Y(\omega) = \lim_{\epsilon\to 0}\left(-2i\omega \int_{-\infty}^{+\infty} d\omega'\, \frac{J(\omega')}{\omega'}\, \frac{1}{\omega'^2 - \omega^2 - i\,\epsilon\,\mathrm{sign}(\omega)}\right). \tag{3.2.24}$$

Taking the real part

$$\mathfrak{Re}\{Y(\omega)\} = 2\omega \int_{-\infty}^{+\infty} d\omega'\, \frac{J(\omega')}{\omega'}\, \delta(\omega'^2 - \omega^2) = \frac{J(\omega)}{\omega}\,, \tag{3.2.25}$$

leads finally to

$$J(\omega) = \omega\, \mathfrak{Re}\left\{\frac{1}{Z(\omega)}\right\} = \frac{\omega}{R_s}\,. \tag{3.2.26}$$

We can thus calculate $A_1 = i/(2\hbar R_s C)$ and $A_2 = k_B T/(\hbar^2 R_s)$ in Eq. (3.2.20). In practice we know that the impedance spectrum cannot be flat up to arbitrarily high frequency, there will be thus exist a cutoff Ω_c ruling the behavior of $J(\omega)$ at high frequencies. This gives $A_3 \approx \frac{2k_B T}{\hbar^2 R_s C \Omega_c}$. Using $Q \sim C\dot{\varphi} \sim C(R_s C)^{-1}\varphi$ we see that the ratio between the third term and the second one in Eq. (3.2.19) is $\sim (R_s C\Omega_c)^{-1} \equiv \omega_{\rm RC}/\Omega_c \ll 1$, allowing us to neglect the former. Eq. (3.2.19) reduces then to the well-known Caldeira-Leggett form

$$\frac{d}{dt}\hat{\rho}_S(t) = -\frac{i}{\hbar}\left[\frac{\hat{Q}^2}{2C}, \hat{\rho}_S(t)\right] - \frac{i}{2\hbar R_s C}\Big[\hat{\varphi}, \Big\{\hat{Q}, \hat{\rho}_S(t)\Big\}\Big] - \frac{k_B T}{\hbar^2 R_s}\Big[\hat{\varphi}, \Big[\hat{\varphi}, \hat{\rho}_S(t)\Big]\Big]\,. \tag{3.2.27}$$

The first term describes the free coherent dynamics of the subsystem $H_{\rm env}$. The second term is proportional to $(R_s C)^{-1}$, which is in practice the relaxation rate of the circuit, and is called the dissipative term. The last one (the diffusive term) is proportional to the temperature and describes thermal fluctuations.

The conditions for the Born-Markov approximation to be valid are as we said the weak coupling between the charge degree of freedom and the LC-oscillators bath and a fast decay of the bath correlation functions with respect to the scale over which the charge dynamics varies appreciably. More precisely this corresponds to the requirement (see Ref. [131])

$$\frac{\hbar}{R_s C} \ll \mathrm{Min}\{\hbar\Omega_c, k_B T\}\,. \tag{3.2.28}$$

We consider an ideally flat impedance R_s, assuming the cutoff Ω_c to be at very high frequency, so that we have always $(R_s C)^{-1} \ll \Omega_c$. The relevant requirement for the Born-Markov approximation to apply is then in our case $\hbar/(R_s C) \ll k_B T$, i.e. $k_B T \gg \alpha E_c$. For $\alpha = R_Q/R_s \ll 1$ there is thus a large range of validity.

We can now write (3.2.27) in the charge representation:

$$\begin{aligned}\frac{d}{dt}\rho_S(Q,Q',t) =& \frac{d}{dt}\langle Q|\hat{\rho}_S(t)|Q'\rangle = -\frac{i}{\hbar}\langle Q|\left[\frac{\hat{Q}^2}{2C}, \hat{\rho}_S(t)\right]|Q'\rangle + \\ &- \frac{i}{2\hbar R_s C}\langle Q|\Big[\hat{\varphi}, \Big\{\hat{Q}, \hat{\rho}_S(t)\Big\}\Big]|Q'\rangle - \frac{k_B T}{\hbar^2 R_s}\langle Q|\Big[\hat{\varphi}, \Big[\hat{\varphi}, \hat{\rho}_S(t)\Big]\Big]|Q'\rangle\,,\end{aligned} \tag{3.2.29}$$

which becomes:

$$\begin{aligned}\frac{d}{dt}\rho_S(Q,Q',t) =& -\frac{i}{2\hbar C}\left(Q^2 - Q'^2\right)\rho_S(Q,Q',t) + \\ &+ \frac{1}{2R_s C}\left(\frac{\partial}{\partial Q} + \frac{\partial}{\partial Q'}\right)(Q+Q')\,\rho_S(Q,Q',t) + \\ &+ \frac{k_B T}{R_s}\left(\frac{\partial}{\partial Q} + \frac{\partial}{\partial Q'}\right)^2 \rho_S(Q,Q',t)\,.\end{aligned} \tag{3.2.30}$$

We note that the current source term can be easily added to this picture by including a term $-I_b\hat{\varphi}$ in the Hamiltonian as part of the system, which leads to a contribution to the previous equation in the form

$$-I_b\left(\frac{\partial}{\partial Q} + \frac{\partial}{\partial Q'}\right)\rho_S(Q,Q',t)\,. \tag{3.2.31}$$

Eq. (3.2.30) represents the Markovian version of Eq.(13) in Ref. [76]. As is there stated, in the limit $\alpha \ll 1$ the nondiagonal elements decay with a time constant at worst of order $\sim R_s C$ and Eq. (3.2.30) reduces to the classical diagonal ME (2.1.1), see appendix 3.B for a sketch of proof and an estimation of the decay constant.

3.3 Combining the ME with the $P(E)$ theory

After recalling the bases of the Master Equation and the $P(E)$ approaches, we have now the necessary ingredients to tackle the problem presented in the introduction: describing at the same time SETOs and quantum fluctuations of the environment. A full treatment of the problem is not an easy task. In order to take into account quantum charge fluctuations one needs to solve the full quantum Master Equation out of equilibrium. This could be done for weak coupling to the environment, but the Coulomb blockade is a strong coupling effect, and requires an exact solution of the coupling with the environment. The $P(E)$ theory avoids dealing with a Master Equation, since all the quantities are calculated at equilibrium. We have not succeeded so far in obtaining a full quantum description of this regime, but as a preliminary exploration attempt we have combined the $P(E)$ theory with the classical Master Equation, implementing the first one to calculate the tunneling rates that enter in the second one. Our aim is to provide a simple tool to obtain a lower bound on the effect of quantum fluctuations.

The $P(E)$ tunneling rates [Eq. (3.1.8)] account for quantum fluctuations which are due to the environmental coupling and start to be important as soon as the condition $R_s \gg R_Q$ is relaxed. When the condition $R_t \gg R_s$ [Eq. (3.1.7)] drops and the environment has not the time to thermalize between tunneling events the equilibrium condition required by the $P(E)$ is no more valid. This is of course the case of the ideal SETOs regime but also of the intermediate regime we are interested in (see Fig. 3.0.2 in the introduction), where weakened SETOs and quantum fluctuations are both present. Here the out-of equilibrium behavior of the charge and the delay in the response of the environment to an abrupt charge change due to tunneling are essential features of the transport mechanism. However, the charge is actually the only variable which needs a special treatment, the equilibrium assumption for the rest of the bath degrees of freedom of $H_{\rm env}$ [Eq. (3.1.2)] continuing to be perfectly satisfied. It is then reasonable to imagine the $P(E)$ description of environmental quantum fluctuations to remain fairly good, and on the other hand the classical part of the full time dynamics of the charge is taken into account by the Master Equation. Exploiting the ME with the $P(E)$-improved rates seems thus to be the most natural idea to describe at the same time quantum fluctuations of the environment and SETOs.

As we will see in Sec. 3.3.1 the results of standard (orthodox theory) ME and of the pure $P(E)$ theory are correctly retrieved by our method in the limits $\alpha \to 0$ and $\rho = R_s/R_t \to 0$ respectively, so that the very basic condition for a good description of the crossover between the two limits is satisfied. A source of approximation which needs to be considered is the fact

that the *classical* Master Equation neglects the *quantum* contribution to charge fluctuations which arise from the discrete charge transfer across the junction. We have however illustrated in Sec. 3.2 the condition for a classical diagonal ME to hold: the full quantum ME can be always reduced to the form (2.2.3) if $k_BT \gg \alpha E_c$ [see Eq. (3.2.28)]. At high enough temperature the classical description works thus well, and in particular it is valid in the interesting region $\alpha E_c < k_BT < E_c$, with $\alpha < 1$. For $k_BT \lesssim \alpha E_c$ the effects of out-of-equilibrium quantum fluctuations of the charge are instead underestimated and the results have to be interpreted as a lower-bound limit.

3.3.1 Numerical results

Following the idea introduced in Sec. 3.3, we show the numerical results obtained by applying the same technique of Sec. 2.1 to solve the ME and calculate the charge noise but using here the prediction of the $P(E)$ theory for the rates. Specifically, the ME (2.1.1) is now implemented with the tunneling rates $\overleftarrow{\Gamma}$ and $\overrightarrow{\Gamma}$ given in Eq. (3.1.8) instead of the orthodox ones $\Gamma^{\pm}$. It reads explicitly:

$$\begin{aligned}\frac{\partial\sigma(Q,t)}{\partial t} = -I_b\frac{\partial\sigma(Q,t)}{\partial Q} + \frac{1}{R_s}\frac{\partial}{\partial Q}\left(k_BT\frac{\partial\sigma(Q,t)}{\partial Q} + \frac{Q}{C}\sigma(Q,t)\right) + \\ - \left(\overleftarrow{\Gamma}(Q) + \overrightarrow{\Gamma}(Q)\right)\sigma(Q,t) + \overrightarrow{\Gamma}(Q+\mathrm{e})\sigma(Q+\mathrm{e},t) + \overleftarrow{\Gamma}(Q-\mathrm{e})\sigma(Q-\mathrm{e},t)\,.\end{aligned} \tag{3.3.1}$$

In Fig. 3.3.1 the I-V characteristics are displayed. As in Fig. 2.3.1, we chose the case $\rho = 10$ and $\kappa = 1$, for which SETOs are still quite sharp and the back-bending is evident. For comparison we report in the same figure the zero-temperature (Monte Carlo) curve, the result obtained with the orthodox rates and also the result of the bare $P(E)$ theory. It clearly appears first of all that in this case the $P(E)$ alone fails to describe the transport: treating the charge as if at equilibrium completely misses the back-bending. Secondly, we have that the curves obtained for finite α display a further smearing of the 'nose' with respect to the ($\alpha = 0$) result of chapter 2. This is what we expect, since in the tunneling rates the threshold is further smoothened. Surprisingly though, the difference is already clearly visible for α as small as 0.01. This indicates that although the $P(E)$ alone misses the main transport feature, the quantum contributions introduced by the $P(E)$-provided tunneling rates are significant even at values of α which one may tend to consider as still deep in the orthodox limit $\alpha \ll 1$.

Fig. 3.3.2 shows the charge noise spectrum for the same parameters. A finite α acts against the SETOs analogously to what happens for the I-V characteristics: here for increasing α the peak is smeared more and more compared to the $\alpha = 0$ case. We also show for completeness in the same figure the bare $P(E)$ spectrum, which can be obtained for example directly from Eq. (3.1.10). By defining for shortness the left-hand side of Eq. (3.1.10) as

$$\int_{-\infty}^{+\infty} dt\, e^{-i\omega t}\,\langle\tilde{\phi}(0)\tilde{\phi}(t)\rangle \equiv \langle\tilde{\phi}\tilde{\phi}\rangle_\omega\,, \tag{3.3.2}$$

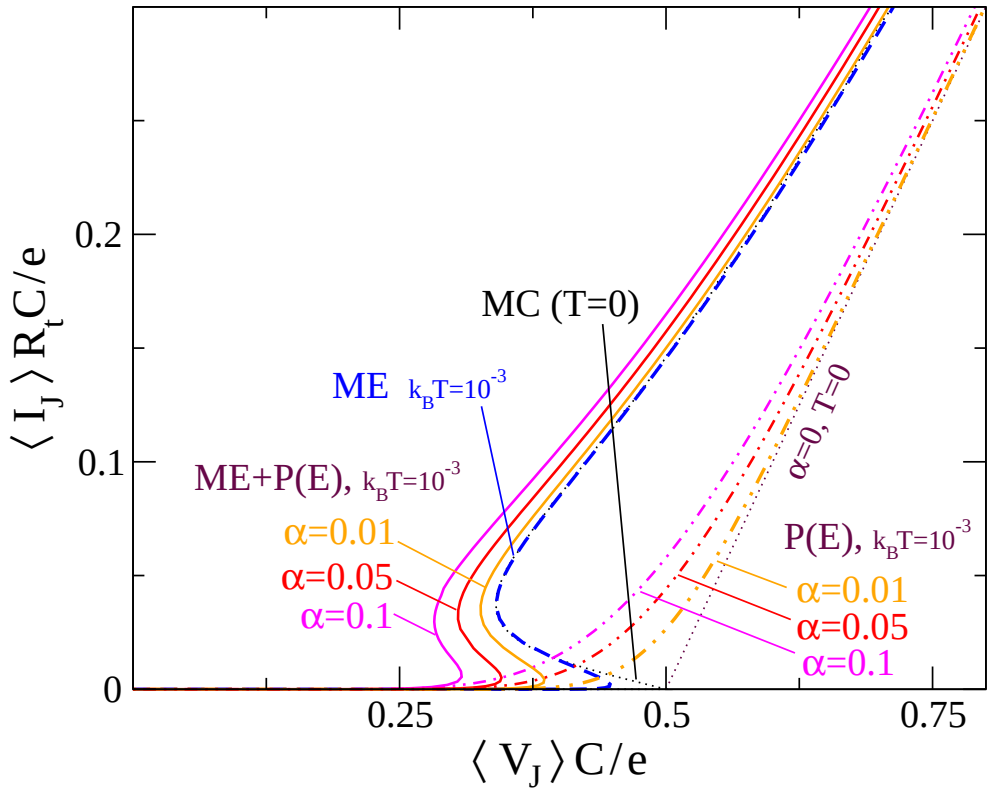

Figure 3.3.1: The I-V characteristics computed for $\rho = 10$ by combining the ME with the $P(E)$ theory for $\alpha = 0.01, 0.05, 0.1$ (solid lines). The Monte Carlo $T = 0$ curve and the pure ME calculation at $k_B T = 10^{-3}$ are reported for comparison (dotted and dashed respectively). The pure $P(E)$ computations as from Eq. (3.1.28) are also shown for the same values of α (dot-dashed lines), together with the $\alpha = 0$, $T = 0$ limit (dotted).

we can in fact calculate the spectrum of the charge fluctuations given by the $P(E)$ theory as

$$S(\omega)_{\mathrm{P(E)}} = \frac{C^2\hbar^2}{\mathrm{e}^2}\,\omega^2\,\frac{\langle\tilde{\phi}\tilde{\phi}\rangle_\omega + \langle\tilde{\phi}\tilde{\phi}\rangle_{-\omega}}{2}\,. \tag{3.3.3}$$

It contains only the equilibrium charge fluctuations and therefore remains blind to the SETOs peak.

If we choose a value of the ratio $R_Q/R_t = \alpha\rho = 0.2$ and then change R_s/R_t we obtain the evolution of the I-V characteristics shown in Fig. 3.3.3. We can see that the curves cross over from the result of the orthodox ME to the result of the bare $P(E)$ as α increases, i.e. the $P(E)$ is also retrieved for large α, as the orthodox theory is for $\alpha \to 0$. Conversely to what happens in the upper-left panel, which is analogous to Fig. 3.3.1, in the lower-right panel with $\alpha = 2$ and $\rho = 0.1$ the orthodox ME this time does not work well, as it pictures a threshold unrealistically sharp and sees the current blocked where it is actually already flowing. For intermediate values of α and ρ, neither of the two theories alone prove to be efficient in describing transport. We note that the constraint $R_t \gg R_Q$ limits the range of

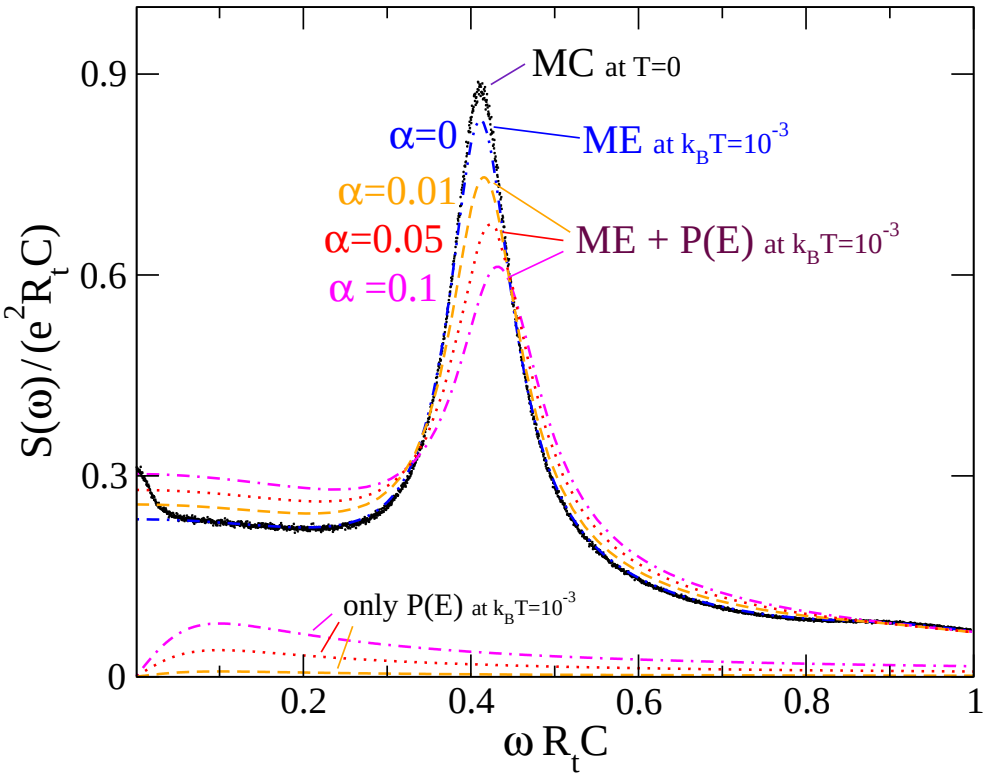

Figure 3.3.2: The charge noise $S(\omega)$ computed for $\rho = 10$ and $\kappa = 1$ with the different techniques considered so far: 1) the Monte Carlo zero-temperature calculation of chapter 1; 2) the orthodox ME technique at finite temperature of chapter 2 ($k_BT = 0.001\,e^2/C$), i.e. equivalent to $\alpha = 0$; 3) the ME with the tunneling rates predicted by the $P(E)$ theory, given by Eq. (3.1.8) (at the same temperature). The values $\alpha = 0.01$, $\alpha = 0.05$ and $\alpha = 0.1$ are shown; 4) the equilibrium spectrum obtained by the $P(E)$ theory alone for the same values of α.

values that can be spanned by the product $\alpha\rho$: in Fig. 3.3.1 and Fig. 3.3.2 for example we chose $\rho = 10$, for which the back-bending of I-V curves is fairly marked and a clear peak is still visible in the noise spectrum, and we must then have $\alpha \lesssim 0.1$. As we have seen in the introduction, this limitation is intrinsically related to the fact that in the perturbation-theory regime $\alpha_t \ll 1$ the more clear-cut are the SETOs the less important become the effects of quantum fluctuations.

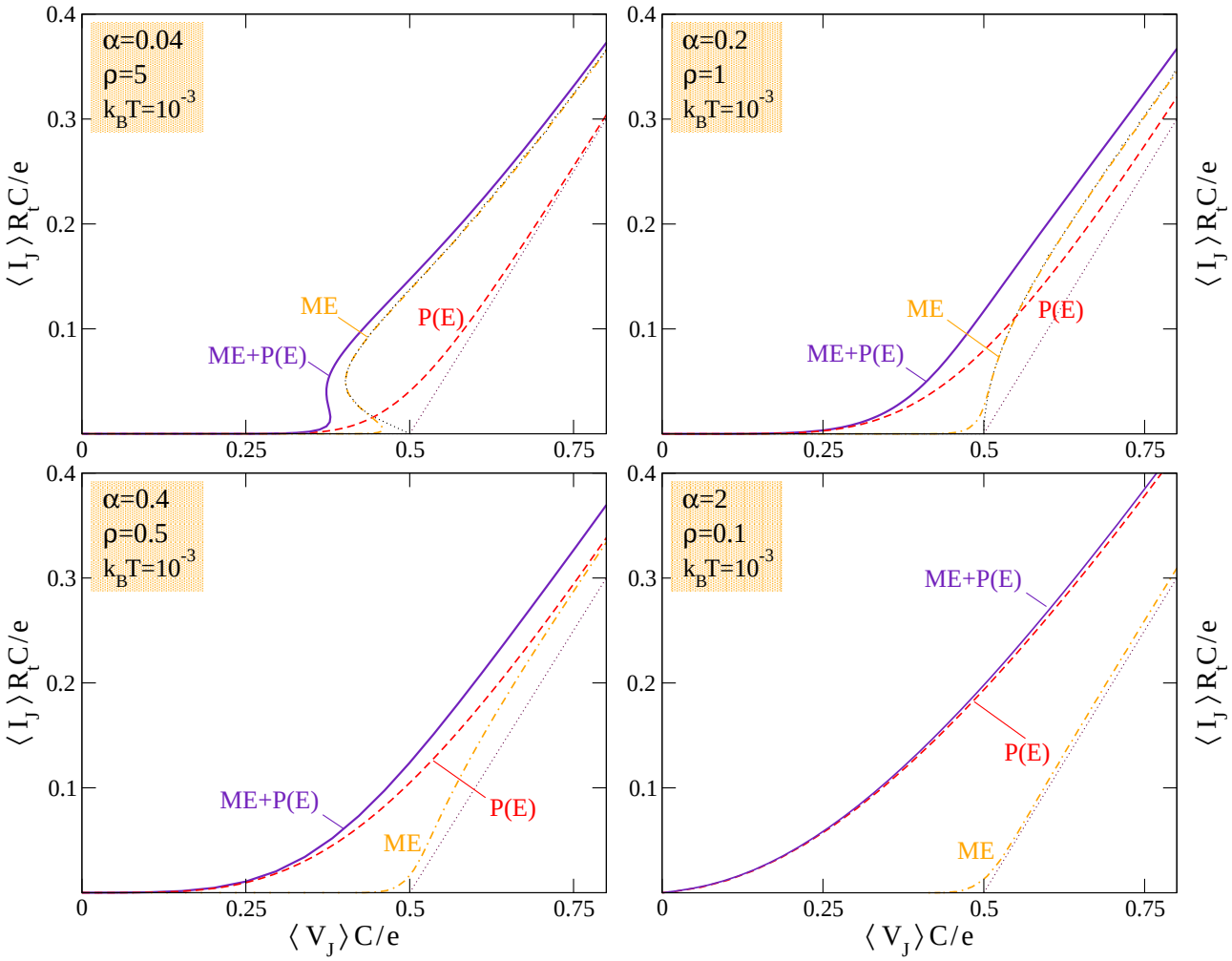

Figure 3.3.3: I-V characteristics obtained combining the ME with $P(E)$ for varying α and ρ at fixed $\alpha\rho = 0.2$. The results of the bare ME and the bare $P(E)$ are reported for comparison. We see that the mixed approach merges between the two with a crossover from the former to the latter as α increases and as the voltage decreases for α fixed. k_BT in units of e^2/C.

3.4 Conclusions and perspectives

We have provided an approximate method to describe the transport through a tunnel junction in the presence of both single-charge effects such as SETOs and quantum fluctuations of the environmental degrees of freedom. It has allowed us to explore a region of the phase-diagram scheme of Fig. 3.0.2 left aside by the standard theoretical tools so far, but eventually very appealing from the experimental point of view. The results are quite interesting. On the one hand the effect of quantum fluctuations has proven to be visible for values of α (as small as 0.01) which one could expect to be lying still in the orthodox limit. This suggests that quantum effects, however small, should not be neglected in a description of single-charge effects which wants to be complete. On the other hand, in the intermediate region where $\alpha \sim 1$ and $\rho \sim 1$ it clearly appears that transport fails to be described by the $P(E)$ theory alone, meaning in practice that the delay in the response of the environment to the tunneling is indeed important and the out-of-equilibrium behavior of the charge must be taken into account. Our method is far from being rigorous, but first of all it points out a hole in the standard perturbation-theory theoretical approach, which is not able to fully cover the crossover from $\alpha \to 0$ to $\alpha \to \infty$ at fixed value of $\alpha_t \ll 1$; and secondly it starts to shed some light on it, providing lower-bound estimations of the effects at play.

To summarize part II on the whole, we have given a complete description of the phenomenon of SETOs. In chapter 1 we focused at first on the standard, ideal zero temperature and $R_s \gg R_t \gg R_Q$ case, where standard means that it is the one addressed by the bulk of the existing literature. We have here fully characterized the SETOs, providing numerical results and an analytical approach to describe the noise peak which represent their main signature. The picture has then enlarged in chapter 2 to thermal effects, and in chapter 3 to the effects of quantum fluctuations. Thermal effects have proven to be quite important and we have shown how they start to affect SETOs even for $k_B T/E_c \ll 1$. Also quantum effects appear to be non-negligible. Nevertheless, even within this enriched picture, the phenomenon should possess strong enough features to be detected and exploited experimentally in some realistic system.

In view of possible experimental development, more theoretical effort is however called for. A full quantum description of transport through a tunnel junction in a realistic environment, accounting for the out-of-equilibrium dynamic of the charge, is not available and not easily concealed, due to the fact that the coupling with the environment cannot be considered small and an exact solution is required. In the literature, studies of the quantum dynamics of tunnel junctions are carried out with Feynman-Vernon or Keldysh-action techniques and have to deal with different degrees of approximation: in Ref. [133] for example, the quantum fluctuations due to charge transfer are taken into account, but as if originated by the continuous charging of a resistor R_t, thus neglecting the discreteness of the charge, which is a good approximation only in the weak coupling limit $R_t \gg \{R_Q, R_s\}$ and does not describe well the interesting $R_s \sim R_t \gtrsim R_Q$ regime. A computational approach would perhaps be the best way to start

tackling the problem. In Ref. [134] the explicit and exact form of the generating functional for a generic circuit composed by a quantum conductor in series with an Ohmic conductor is given. This can be straightforwardly specialized to the case of a tunnel junction in series with a dissipative element (impedance). One could then for example think of writing an equation for the exact dynamics of the phase quantum variable of the circuit and solving it numerically by quantum Monte Carlo technique. This would be in practice the quantum extension of the numerical approach of chapter 1. Such a numerical implementation should be feasible, though possibly demanding in terms of computational efforts.

Appendix

3.A Details of the $P(E)$ numerical implementation

We give here technical details about how the numerical computation of the $P(E)$ function is actually carried out. We need to solve Eq. (3.1.23). We first discretize the integral in Eq. (3.1.23) in energy steps of width Δ:

$$E\,P(E) - \sum_{j=0}^{j_{\max}} \Delta\, \frac{E_c}{\pi} \left(\arctan\left(\frac{\pi x_j}{\alpha E_c}\right) - \arctan\left(\frac{\pi x_{j+1}}{\alpha E_c}\right)\right) \times \\ \times \left[P(E-x_j) + P(E+x_j) + \coth\left(\frac{\beta x_j}{2}\right)\left(P(E-x_j) - P(E+x_j)\right)\right] = 0\,, \qquad (3.A.1)$$

where we have carried out analytically the integration of the function $\zeta(x)$ in each step $x_j - x_{j+1}$:

$$\int_{x_j}^{x_{j+1}} \zeta\left(\frac{x}{\hbar}\right) = \frac{E_c}{\pi}\left(\arctan\left(\frac{\pi x_{j+1}}{\alpha E_c}\right) - \arctan\left(\frac{\pi x_j}{\alpha E_c}\right)\right)\,, \qquad (3.A.2)$$

since $\zeta(x)$ quickly diverges for $x \to 0$ and it is inconvenient to assume it constant on the same scale Δ as the rest of the integrand. We then solve an equation in matrix form $\mathbf{MP} = \mathbf{b}$, where the vector $\mathbf{b}$ has just one [5] nonzero entry $\mathbf{b}[i_\star] = 1$ and the matrix $\mathbf{M}$ has nonzero entries

$$M_{i,i} = E_i \\ M_{i,i+j} = -\sum_{j=0}^{j_{\max}} \Delta\, \frac{E_c}{\pi}\left(\arctan\left(\frac{\pi x_j}{\alpha E_c}\right) - \arctan\left(\frac{\pi x_{j+1}}{\alpha E_c}\right)\right)\left(1 - \coth\left(\frac{\beta x_j}{2}\right)\right) \\ M_{i,i-j} = -\sum_{j=0}^{j_{\max}} \Delta\, \frac{E_c}{\pi}\left(\arctan\left(\frac{\pi x_j}{\alpha E_c}\right) - \arctan\left(\frac{\pi x_{j+1}}{\alpha E_c}\right)\right)\left(1 + \coth\left(\frac{\beta x_j}{2}\right)\right)\,, \qquad (3.A.3)$$

and we then put all the elements of the $i_\star$th row equal to Δ, i.e. $\mathbf{M}[i_\star][j] = \Delta$ for all j, so that the normalization condition $\sum_i \Delta P_i = 1$, which corresponds to Eq. (3.1.13), is automatically satisfied.

5. the position of which is not important as soon as it is not on the borders.

3.B Vanishing of the quantum component of the density matrix

We show here how the density matrix $\rho_S(Q,Q',t)$ in Eq. (3.2.30) reduces to a diagonal form in the basis $\{Q,Q'\}$ after a time at worst of the order of τ_s. We introduce the variables $u \equiv (Q+Q')/(2\mathrm{e})$ and $v \equiv (Q-Q')/\mathrm{e}$, which are maximized and minimized for $Q = Q'$ and represent then the 'classical' and 'quantum' variables respectively. In terms of u and v Eq. (3.2.30) becomes:

$$\frac{d}{d\tau}\rho_S(u,v,t) = -\frac{iuv}{\alpha}\rho_S(u,v,t) + \frac{\partial}{\partial u}\left[u\rho_S(u,v,t) + \lambda\frac{\partial}{\partial u}\rho_S(u,v,t)\right], \tag{3.B.1}$$

where $\alpha = R_Q/R_s$ and we introduced the dimensionless time $\tau \equiv t/(R_sC)$ and the dimensionless temperature $\lambda \equiv k_BT/(\mathrm{e}^2/C) \ll 1$. We want to show that for v different from zero the time evolution dictated by Eq. (3.B.1) predicts that the density matrix vanishes on a time scale smaller or of the order of τ_s. We focus first on the limit $\alpha \ll 1$ and $v/\alpha \gg 1$, which is also the relevant one for the SETOs regime. In this limit the first term of the equation is very large and will induce rapid oscillations of the density matrix. It is therefore convenient to eliminate this rapid oscillations by defining $\rho_S \equiv \exp\{-iuv\tau/\alpha\}\tilde{\rho}$, so that we can write

$$\frac{d}{d\tau}\rho_S = -\frac{iuv}{\alpha}\rho_S + e^{-\frac{iuv}{\alpha}\tau}\frac{d}{d\tau}\tilde{\rho} = -\frac{iuv}{\alpha}\rho_S + \frac{\partial}{\partial u}\left[e^{-\frac{iuv}{\alpha}\tau}\left(u\tilde{\rho} - \frac{i\lambda v\tau}{\alpha}\tilde{\rho} + \lambda\frac{\partial}{\partial u}\tilde{\rho}\right)\right], \tag{3.B.2}$$

and the equation for $\tilde{\rho}$ reads

$$\begin{aligned}\frac{d}{d\tau}\tilde{\rho} =& e^{\frac{iuv}{\alpha}\tau}\frac{\partial}{\partial u}\left[e^{-\frac{iuv}{\alpha}\tau}\left(u\tilde{\rho} - \frac{i\lambda v\tau}{\alpha}\tilde{\rho} + \lambda\frac{\partial}{\partial u}\tilde{\rho}\right)\right] = \\ =& -\frac{iv\tau}{\alpha}\left(u\tilde{\rho} - \frac{i\lambda v\tau}{\alpha}\tilde{\rho} + \lambda\frac{\partial}{\partial u}\tilde{\rho}\right) + \frac{\partial}{\partial u}\left(u\tilde{\rho} - \frac{i\lambda v\tau}{\alpha}\tilde{\rho} + \lambda\frac{\partial}{\partial u}\tilde{\rho}\right).\end{aligned} \tag{3.B.3}$$

The dominant term of the previous equation in the limit $\frac{v}{\alpha} \gg 1$ is $-(\lambda v^2\tau^2/\alpha^2)\tilde{\rho}$. Neglecting the other terms in the equation, this leads to the following solution for $\tilde{\rho}$:

$$\tilde{\rho} \sim \exp\{-\lambda v^2\tau^3/(3\alpha^2)\}. \tag{3.B.4}$$

We have thus $\rho_S \sim \exp\{-iuv\tau/\alpha - \lambda v^2\tau^3/(3\alpha^2)\}$, showing that for any fixed value of u, $\rho_S(v)$ decays to zero on a scale $\sim \tau_s \sqrt[3]{\alpha^2/\lambda} \ll \tau_s$.

We can actually prove the decay of the off-diagonal contribution also in the opposite limit of large α, more precisely $v/\alpha \ll 1$. We introduce in this case the moments of the distribution $\rho_S(u,v,\tau)$ with respect to the variable u as:

$$A_n \equiv \int_{-\infty}^{+\infty} du\ \rho_S(u,v,\tau)\ u^n. \tag{3.B.5}$$

To show the off-diagonal decay of the density matrix it is enough proving that the solution of Eq. 3.B.1 in the $\{u,v\}$ space squeezes towards the u axis, which is equivalent to ask that

for any finite v the integral $\int_{-\infty}^{+\infty} du\, \rho_S(u,v,t)$ must go to zero. Our goal is then to show that A_0 decays exponentially in time if $v > 0$. To do so we can write a differential equation for A_0, but this will couple to A_1. The same can be done for A_1, the series of equations form an infinite set of linear differential equations and for small v/α it is sufficient to include a few moments since higher moments vanish rapidly. Let us show that explicitly. Using Eq. (3.B.1) we have:

$$\begin{aligned}
\dot{A}_0 &= \int_{-\infty}^{+\infty} du\, \frac{d}{d\tau}\rho_S(u,v,\tau) = \\
&= \int_{-\infty}^{+\infty} du\, \left\{ -\frac{iuv}{\alpha}\rho_S(u,v,t) + \frac{\partial}{\partial u}\, \left[u\rho_S(u,v,t) + \lambda \frac{\partial}{\partial u}\rho_S(u,v,t) \right] \right\} = \\
&= -\frac{iv}{\alpha} \int_{-\infty}^{+\infty} du\, u\, \rho_S(u,v,t) = -\frac{iv}{\alpha} A_1\,, \\
\dot{A}_1 &= \int_{-\infty}^{+\infty} du\, \frac{d}{d\tau}\rho_S(u,v,\tau)\, u = \\
&= \int_{-\infty}^{+\infty} du\, \left\{ -\frac{iu^2v}{\alpha}\rho_S(u,v,t) + u\, \frac{\partial}{\partial u}\, \left[u\rho_S(u,v,t) + \lambda \frac{\partial}{\partial u}\rho_S(u,v,t) \right] \right\} = \\
&= -\frac{iv}{\alpha} A_2 - \int_{-\infty}^{+\infty} du\, \left[u\rho_S(u,v,t) + \lambda \frac{\partial}{\partial u}\rho_S(u,v,t) \right] = -\frac{iv}{\alpha} A_2 - A_1\,, \\
\dot{A}_2 &= \int_{-\infty}^{+\infty} du\, \frac{d}{d\tau}\rho_S(u,v,\tau)\, u^2 = \\
&= \int_{-\infty}^{+\infty} du\, \left\{ -\frac{iu^3v}{\alpha}\rho_S(u,v,t) + u^2\, \frac{\partial}{\partial u}\, \left[u\rho_S(u,v,t) + \lambda \frac{\partial}{\partial u}\rho_S(u,v,t) \right] \right\} = \\
&= -\frac{iv}{\alpha} A_3 - \int_{-\infty}^{+\infty} du\, 2\, u\, \left[u\rho_S(u,v,t) + \lambda \frac{\partial}{\partial u}\rho_S(u,v,t) \right] = \\
&= -\frac{iv}{\alpha} A_3 - 2A_2 + 2\lambda A_0\,,
\end{aligned} \tag{3.B.6}$$

and so on. We thus easily derive the general equation for all the moments:

$$\begin{aligned}
\dot{A}_n &= \int_{-\infty}^{+\infty} du\, \frac{d}{d\tau}\rho_S(u,v,\tau)\, u^n = \\
&= \int_{-\infty}^{+\infty} du\, \left\{ -\frac{iu^nv}{\alpha}\rho_S(u,v,t) + u^n\, \frac{\partial}{\partial u}\, \left[u\rho_S(u,v,t) + \lambda \frac{\partial}{\partial u}\rho_S(u,v,t) \right] \right\} = \\
&= -\frac{iv}{\alpha} A_{n+1} - nA_n + n(n-1)\lambda A_{n-2}\,.
\end{aligned} \tag{3.B.7}$$

Eq. (3.B.7) is best handled by putting it in matrix form as

$$\dot{\mathbf{A}} = (\dot{A}_0, \dot{A}1, \ldots, \dot{A}_n, \ldots) = \mathbf{W}(A_0, A1, \ldots, A_n, \ldots) = \mathbf{WA}\,, \tag{3.B.8}$$

with

$$\mathbf{W} = \begin{pmatrix} 0 & -iv/\alpha & 0 & 0 & 0 & 0 & \dots \\ 0 & -1 & -iv/\alpha & 0 & 0 & 0 & \dots \\ 2\lambda & 0 & -2 & -iv/\alpha & 0 & 0 & \dots \\ 0 & 6\lambda & 0 & -3 & -iv/\alpha & 0 & \dots \\ 0 & 0 & 12\lambda & 0 & -4 & -iv/\alpha & \dots \\ \vdots & \vdots & \vdots & \ddots & \vdots & \ddots & \ddots \\ \vdots & \vdots & \vdots & \vdots & \ddots & \vdots & \ddots \end{pmatrix} . \tag{3.B.9}$$

Since the coupling λ is small and we are in the limit $v/\alpha \ll 1$ we see that $\mathbf{W}$ is almost diagonal and has eigenvalues which at the lowest order in lambda are given by $0, -1, -2, -3, -4, \dots$. Including lambda perturbatively will modify the eigenvalues slightly, but in particular the 0 eigenvalue will acquire a small negative real part controlled by λ and v/α.

We now just need to show that the solution of Eq. (3.B.8) decays in time for finite v, that is, all the moments and in particular A_0 go to zero for long enough time. The slowest decay contribution is given by the minimum eigenvalue, which is close to zero but does not vanish at finite λ and v/α. By solving numerically for the eigenvalues of a finite-size $\mathbf{W}$ ($N \times N$ with $N = 4$ is actually enough for convergence in this $\lambda \ll 1$, $v/\alpha \ll 1$ limit), we find that the minimum eigenvalue actually decays as $\sim -\lambda v^2/\alpha^2$.

This shows that as far as v is finite the off-diagonal part of the density matrix vanishes exponentially, but it also tells that for $v \to 0$ the decay time becomes longer the more we approach the diagonal part, giving a clear picture of the crossover between the classical (diagonal part) and quantum (off-diagonal part) in the density matrix. As a last comment, we note that this time is also controlled by the temperature, as one could expect for decoherence.

List of Figures

0.1 Pumping VS SETOs 2

Part I

1.1 Thouless adiabatic pump 7

2.1 Scheme of the three-site model 9

2.2 Sketch of the vibrational modes of the trimer 11

3.1 Solution in the spin space 14

3.2 Direct current for the isolated system 15

4.2.1 Circulating direct current for several temperatures 23

4.3.1 Analytical-numerical comparison of the pumped current 24

4.3.2 Time evolution of the current 25

4.4.1 Experimental setup of a triple quantum dot 26

4.4.2 Experimental setup of a symmetric triple quantum dot 27

Part II

1.1.1 Tunnel junction scheme 33

1.1.2 Influence of the environment in a tunnel-junction circuit 35

1.2.1 Basic scheme of the junction circuit 37

1.2.2 I-V characteristics of the junction 38

1.3.1 Average voltage through the junction versus bias current 39

1.3.2 Direct visualization of the time behavior of the charge 40

1.3.3 Scheme of the tunneling process . . . 42
1.3.4 Analytical-numerical comparisons for the I-V 'nose' . . . 45
1.3.5 Scheme of the transport regimes . . . 46
1.4.1 Width of the noise peak as a function of κ/ρ . . . 51
1.5.1 Width-scaled spectra for varying ρ . . . 54
1.5.2 Numerical-analytical comparison of the charge-fluctuation spectrum . . . 55
1.5.3 MC spectra for different bias conditions κ . . . 56
1.5.4 MC spectra for different resistive environments . . . 57
1.A.1 $Q_1(t)$ and $Q_2(t)$ displayed . . . 60
1.A.2 Plots of the distribution $\sigma_{n_0+1}(Q,t)$ . . . 60
1.A.3 Plots of the distribution $\sigma_{n_0+1}(Q,t)$ at small times . . . 61
1.B.1 Current contributions in the tunnel junction circuit . . . 62
1.B.2 High-bias noise . . . 64

2.1.1 Finite temperature tunneling rates . . . 66
2.3.1 Finite temperature I-V characteristics . . . 71
2.3.2 Charge noise for different temperatures . . . 72
2.3.3 Current noise for different temperatures . . . 73
2.5.1 Fano factor as a function of V_J . . . 79
2.5.2 Theoretical high-bias Fano factor for different temperatures . . . 80
2.5.3 High-bias Fano factor: numerical/analytical comparison . . . 80

3.0.1 Scheme of the behavior of the realistic environmental impedance . . . 83
3.0.2 Phase-diagram scheme of the transport regimes . . . 84
3.0.3 Zoom on the relevant area of the phase-diagram . . . 85
3.1.1 Circuit scheme for the $P(E)$ theory . . . 86
3.1.2 $P(E)$ function at $T = 0$ . . . 91
3.1.3 $P(E)$ function for $\alpha = 0.1$ at different temperatures . . . 92
3.1.4 I-V characteristics at $T = 0$ for different values of α . . . 92
3.3.1 Effects of quantum fluctuations on I-V characteristics . . . 100

3.3.2 Effects of quantum fluctuations on charge noise 101
3.3.3 I-V characteristics with ME and $P(E)$ 102

Index of Notations

Part I

ω pumping frequency 4

e electron charge 6

ϵ_i on-site energy at the site i 10

γ_{ij} tight-binding hopping integrals between sites i and j 10

$|x\rangle$,$|y\rangle$ basis spanning the 2×2 subspace 10

d_{ij} instantaneous distance between atoms i and j 10

u_0 equilibrium separation of trimer atoms in the equilateral geometry 10

k coupling constant in the dependence of the hopping terms on the displacement 10

$\mathbf{R}_i$ displaced atomic positions 10

Δ constant determining energy gap between states $|x\rangle$ and $|y\rangle$ 11

σ^i Pauli matrix 11

$\mathcal{H}_S$ pumping Hamiltonian in the 2×2 space 11

$\tilde{\mathcal{H}}_{\text{eff}}$ effective Hamiltonian in the rotating frame 13

$\hat{\mathbf{n}}$ $= (0, -\omega/\omega', \Delta/\omega')$ 13

ω' the Larmor frequency $\sqrt{\Delta^2 + \omega^2}$ 13

J dimensionless current I/I_0 14

$J_\xi(\omega)$ baths spectral density 17

α_ξ coupling constant to the bath ξ, assumed weak 17

$\mathcal{C}(t)$ baths autocorrelation function 17

T temperature 22

Part II

R_Q quantum of resistance 30

R_t tunneling resistance 30

C junction capacitance 30

e	electron charge 30
E_c	charging energy 33
T	temperature 33
$\Gamma(\,)$	tunneling rate 36
R_s	shunt resistance 36
I_b	bias current 36
$Z(\omega)$	impedance 37
τ_s	$= R_sC$, relaxation time 37
ρ	the ratio R_s/R_t 37
$I_{\rm th}$	$= \mathrm{e}/2\tau_s$, current threshold 37
κ	relative distance of the bias current from the threshold $(I_b - I_{\rm th})/I_{\rm th}$ 37
$Q_{\rm s}$	$= I_b\tau_s$, charge saturation value 40
$t_\star$	the time needed to charge the capacitance from $Q = -\mathrm{e}/2$ to $Q = \mathrm{e}/2$ 41
τ_n	time at which the nth hopping event takes place 41
t_n	time at which the threshold $Q(t) = \mathrm{e}/2$ is reached before the nth hopping event 41
$\delta\tau_n$	delay time before the nth hopping event after threshold 41
$\mathfrak{F}(\delta\tau)$	$= t_n - t_{n-1}$ 42
$P_n(t)$	probability that n electrons have tunneled through the junction at the time t 42
$\mathcal{P}(t)$	probability density that a hopping event takes places at time t 42
$\langle\delta\tau\rangle$	the average delay time for an electron to hop after threshold 43
$\mathcal{T}$	$= \langle\mathfrak{F}\rangle$, period of the SETOs 43
$S(\omega)$	charge noise 47
Ω_n	pole giving the nth peak in the charge-noise spectrum 50
Γ_n	FWHM of the Lorentzian for the nth charge-noise peak 50
$\mathbb{F}$	Fano factor 53
$S_J(\omega)$	current noise 53
$\sigma(Q,t)$	probability density that at time t the charge on the capacitance is Q 65
$\Gamma^{\pm}(\,)$	backward (+) and forward (−) tunneling rates, orthodox-theory style 66
Γ_0	typical tunneling rate $(R_tC)^{-1}$ 75
α	the ratio R_Q/R_s 84
α_t	the ratio R_Q/R_t 84
$\Gamma^{\rightleftarrows}(\,)$	backward (←) and forward (→) tunneling rates, $P(E)$-theory style 88
$\mathcal{J}(t)$	$P(E)$ phase-phase correlation function 88
$J(\omega)$	spectral density for the bath of the dissipatative Hamiltonian model 95

Bibliography

[1] A. D. O'Connell, M. Hofheinz, M. Ansmann, R. C. Bialczak, M. Lenander, E. Lucero, M. Neeley, D. Sank, H. Wang, M. Weides, J. Wenner, J. M. Martinis, A. N. Cleland, *Quantum ground state and single-phonon control of a mechanical resonator*, Nature **464**, 697 (2010).

[2] F. Santandrea, L. Y. Gorelik, R. I. Shekhter, M. Jonson, *Cooling of nanomechanical resonators by thermally activated single-electron transport*, Phys. Rev. Lett. **106**, 186803 (2011).

[3] R. Landauer, *Conductance from transmission: common sense points*, Phys. Scripta. T **42**, 110 (1992).

[4] A.-P. Jauho, N. S. Wingreen, Y. Meir, *Time-dependent transport in interacting and noninteracting resonant-tunneling systems*, Phys. Rev. B **50**, 5528 (1994).

[5] S. Datta, *Electronic Transport in Mesoscopic Systems* (Cambridge University Press, Cambridge, 1995).

[6] Ya. M. Blanter, M. Büttiker, *Shot noise in mesoscopic conductors*, Phys. Rep. **336**, 1 (2000).

[7] T. H. Oosterkamp, T. Fujisawa, W. G. van derWiel, K. Ishibashi, R. V. Hijman, S. Tarucha, L. P. Kouwenhoven, *Microwave spectroscopy of a quantum-dot molecule*, Nature **395**, 873 (1998).

[8] W. G. van der Wiel, S. De Franceschi, J. M. Elzerman, T. Fujisawa, S. Tarucha, L. P. Kouwenhoven, *Electron transport through double quantum dots*, Rev. Mod. Phys. **75**, 1 (2003).

[9] G. Platero, R. Aguado, *Photon-assisted transport in semiconductor nanostructures*, Phys. Rep. **395**, 1 (2004).

[10] M. Switkes, C. M. Marcus, K. Campman, A. C. Gossard, *An adiabatic quantum electron pump*, Science **283**, 1905 (1999).

[11] J. M. Martinis, M. Nahum, H. D. Jensen, *Metrological accuracy of the electron pump*, Phys. Rev. Lett. **72**, 904 (1994).

[12] J. P. Pekola, J. J. Vartiainen, M. Möttönen, O.-P. Saira, M. Meschke, D. V. Averin, *Hybrid single-electron transistor as a source of quantized electric current*, Nature Phys. **4**, 120 (2008).

[13] A. Fuhrer, C. Fasth, L. Samuelson, *Single electron pumping in InAs nanowire double quantum dots*, Appl. Phys. Lett. **91**, 052109 (2007).

[14] M. R. Buitelaar, V. Kashcheyevs, P. J. Leek, V. I. Talyanskii, C. G. Smith, D. Anderson, G. A. C. Jones, J. Wei, D. H. Cobden, *Adiabatic charge pumping in carbon nanotube quantum dots*, Phys. Rev. Lett. **101**, 126803 (2008).

[15] B. Kaestner, V. Kashcheyevs, G. Hein, K. Pierz, U. Siegner, H. W. Schumacher, *Single-parameter quantized charge pumping in high magnetic fields*, Appl. Phys. Lett. **92**, 192106 (2008).

[16] V. I. Talyanskii, J. M. Shilton, M. Pepper, C. G. Smith, C. J. B. Ford, E. H. Linfield, D. A. Ritchie, G. A. C. Jones, *Single-electron transport in a one-dimensional channel by high-frequency surface acoustic waves*, Phys. Rev. B **56**, 15180 (1997).

[17] N. E. Fletcher, J. Ebbecke, T. J. B. M. Janssen, F. J. Ahlers, M. Pepper, H. E. Beere, D. A. Ritchie, *Quantized acoustoelectric current transport through a static quantum dot using a surface acoustic wave*, Phys. Rev. B **68**, 245310 (2003).

[18] J. Ebbecke N. E. Fletcher, T. J. B. M. Janssen, F. J. Ahlers, M. Pepper, H. E. Beere, D. A. Ritchie, *Quantized charge pumping through a quantum dot by surface acoustic waves*, Appl. Phys. Lett. **84**, 4319 (2004).

[19] F. Giazotto, P. Spathis, S. Roddaro, S. Biswas, F. Taddei, M. Governale, L. Sorba, *A Josephson quantum electron pump*, Nature Phys. **7**, 857 (2011).

[20] R. Aguado, L. P. Kouwenhoven, *Double quantum dots as detectors of high-frequency quantum noise in mesoscopic conductors*, Phys. Rev. Lett. **84**, 1986 (2000).

[21] E. Zakka-Bajjani, J. Ségala, F. Portier, P. Roche, D. C. Glattli, A. Cavanna, Y. Jin, *Experimental test of the high-frequency quantum shot noise theory in a quantum point contact*, Phys. Rev. Lett. **99**, 236803 (2007).

[22] J. Gabelli, B. Reulet, *Dynamics of quantum noise in a tunnel junction under ac excitation*, Phys. Rev. Lett. **100**, 026601 (2008).

[23] J. Basset, H. Bouchiat, R. Deblock, *Emission and absorption quantum noise measurement with an on-chip resonant circuit*, Phys. Rev. Lett. **105**, 166801 (2010).

[24] J. P. Pekola, V. Brosco, M. Möttönen, P. Solinas, A. Shnirman, *Decoherence in adiabatic quantum evolution: application to cooper pair pumping*, Phys. Rev. Lett. **105**, 030401 (2010).

[25] A. Russomanno, S. Pugnetti, V. Brosco, R. Fazio, *Floquet theory of Cooper pair pumping*, Phys. Rev. B **83**, 214508 (2011).

[26] Yu. Makhlin, A. D. Mirlin, *Counting statistics for arbitrary cycles in quantum pumps*, Phys. Rev. Lett. **87**, 276803 (2001).

[27] O. Entin-Wohlman, A. Aharony, Y. Levinson, *Adiabatic transport in nanostructures*, Phys. Rev. B **65**, 195411 (2002).

[28] M. Moskalets, M. Büttiker, *Floquet scattering theory of quantum pumps*, Phys. Rev. B **66**, 205320 (2002).

[29] I. L. Aleiner, A. V. Andreev, *Adiabatic charge pumping in almost open dots*, Phys. Rev. Lett. **81**, 1286 (1998).

[30] B. L. Hazelzet, M. R. Wegewijs, T. H. Stoof, Yu. V. Nazarov, *Coherent and incoherent pumping of electrons in double quantum dots*, Phys. Rev. B **63**, 165313 (2001).

[31] L. Arrachea, A. Levy Yeyati, A. Martin-Rodero, *Nonadiabatic features of electron pumping through a quantum dot in the Kondo regime*, Phys. Rev. B **77**, 165326 (2008).

[32] J. Splettstoesser, M. Governale, J. König, R. Fazio, *Adiabatic pumping through interacting quantum dots*, Phys. Rev. Lett. **95**, 246803 (2005).

[33] E. Sela, Y. Oreg, *Adiabatic pumping in interacting systems*, Phys. Rev. Lett. **96**, 166802 (2006).

[34] P. W. Brouwer, *Scattering approach to parametric pumping*, Phys. Rev. B **58**, R10135 (1998).

[35] D. Cohen, *Quantum pumping in closed systems, adiabatic transport, and the Kubo formula*, Phys. Rev. B **68**, 155303 (2003).

[36] M. Möttönen, J. P. Pekola, J. J. Vartiainen, V. Brosco, F. W. J. Hekking, *Measurement scheme of the Berry phase in superconducting circuits*, Phys. Rev. B **73**, 214523 (2006).

[37] D. Fioretto, A. Silva, *Phase coherence, inelastic scattering, and interaction corrections in pumping through quantum dots*, Phys. Rev. Lett. **100**, 236803 (2008).

[38] M. Hiller, T. Kottos, D. Cohen, *Control of atomic currents using a quantum stirring device*, Europhys. Lett. **82**, 40006 (2008).

[39] J. Salmilehto, P. Solinas, J. Ankerhold, M. Möttönen, *Adiabatically steered open quantum systems: Master equation and optimal phase*, Phys. Rev. A **82**, 062112 (2010).

[40] F. Pellegrini, *Quantum dissipation at the nanoscale*, PhD Thesis 2011, SISSA/ISAS, `http://www.sissa.it/cm/thesis/2011/pellegrini.pdf`.

[41] F. Pellegrini, C. Negri, F. Pistolesi, N. Manini, G. E. Santoro, E. Tosatti, *Crossover from adiabatic to antiadiabatic quantum pumping with dissipation*, Phys. Rev. Lett. **107**, 060401 (2011).

[42] D. Cohen, *Quantum pumping and dissipation in closed systems*, Physica E: Low-dimensional Systems and Nanostructures **29**, 308 (2005). Proceedings of Frontiers of Quantum and Mesoscopic Thermodynamics.

[43] D. J. Thouless, *Quantization of particle transport*, Phys. Rev. B **27**, 6083 (1983).

[44] Q. Niu, *Quantum adiabatic particle transport*, Phys. Rev. B **34**, 5093 (1986).

[45] B. L. Altshuler, L. I. Glazman, *Pumping electrons*, Science **283**, 1864 (1999).

[46] M. V. Berry, *Quantal phase factors accompanying adiabatic changes*, Proc. Roy. Soc. Lond. A **392**, 45 (1984).

[47] M. Büttiker, H. Thomas, A. Prêtre, *Current partition in multiprobe conductors in the presence of slowly oscillating external potentials*, Z. Phys. B Condensed Matter **94**, 133 (1994).

[48] G. B. Lubkin, *Adiabatic quantum electron pump produces DC current*, Physics Today **52**, 19 (1999).

[49] F. Zhou, B. J. Spivak, B. Altshuler, *Mesoscopic mechanism of adiabatic charge transport*, Phys. Rev. Lett. **82**, 608 (1999).

[50] T. A. Shutenko, I. L. Aleiner, B. L. Altshuler, *Mesoscopic fluctuations of adiabatic charge pumping in quantum dots*, Phys. Rev. B **61**, 10366 (2000).

[51] M. L. Polianski, P. W. Brouwer, *Pumped current and voltage for an adiabatic quantum pump*, Phys. Rev. B **64**, 075304 (2001).

[52] M. L. Polianski, M. G. Vavilov, P. W. Brouwer, *Noise through quantum pumps*, Phys. Rev. B **65**, 245314 (2002).

[53] M. Moskalets, M. Büttiker, *Dissipation and noise in adiabatic quantum pumps*, Phys. Rev. B **66**, 035306 (2002).

[54] M. Moskalets, M. Büttiker, *Magnetic-field symmetry of pump currents of adiabatically driven mesoscopic structures*, Phys. Rev. B **72**, 035324 (2005).

[55] L. P. Kouwenhoven, S. Jauhar, K. McCormick, D. Dixon, P. L. McEuen, Yu. V. Nazarov, N. C. van der Vaart, C. T. Foxon, *Photon-assisted tunneling through a quantum dot*, Phys. Rev. B **50**, 2019 (1994).

[56] L. P. Kouwenhoven, S. Jauhar, J. Orenstein, P. L. McEuen, Y. Nagamune, J. Motohisa, H. Sakaki, *Observation of photon-assisted tunneling through a quantum dot*, Phys. Rev. Lett. **73**, 3443 (1994).

[57] L. J. Geerligs, V. F. Anderegg, P. A. M. Holweg, J. E. Mooij, H. Pothier, D. Esteve, C. Urbina, M. H. Devoret, *Frequency-locked turnstile device for single electrons*, Phys. Rev. Lett. **64**, 2691 (1990).

[58] L. P. Kouwenhoven, A. T. Johnson, N. C. van der Vaart, C. J. P. M. Harmans, C. T. Foxon, *Quantized current in a quantum-dot turnstile using oscillating tunnel barriers*, Phys. Rev. Lett. **67**, 1626 (1991).

[59] H. Pothier, P. Lafarge, C. Urbina, D. Esteve, M. H. Devoret, *Single-electron pump based on charging effects*, Europhys. Lett. **17**, 249 (1992).

[60] P. W. Brouwer, *Rectification of displacement currents in an adiabatic electron pump*, Phys. Rev. B **63**, 121303(R) (2001).

[61] L. DiCarlo, C. M. Marcus, J. S. Harris,Jr., *Photocurrent, rectification, and magnetic field symmetry of induced current through quantum dots*, Phys. Rev. Lett. **91**, 246804 (2003).

[62] S. Russo, J. Tobiska, T. M. Klapwijk, A. F. Morpurgo, *Adiabatic quantum pumping at the Josephson frequency*, Phys. Rev. Lett. **99**, 086601 (2007).

[63] P. Solinas, M. Möttönen, J. Salmilehto, J. P. Pekola, *Decoherence of adiabatically steered quantum systems*, Phys. Rev. B 82, 134517 (2010).

[64] W. H. Gerber, E. Schumacher, *The dynamic Jahn-Teller effect in the electronic ground state of Li_3. An ab initio calculation of the BO hypersurface and the lowest vibronic states of Li_3*, J. Chem. Phys. **69**, 1692 (1978).

[65] G. Delacrétaz, E. R. Grant, R. L. Whetten, L. Wöste, J. W. Zwanziger, *Fractional quantization of molecular pseudorotation in Na_3*, Phys. Rev. Lett. **56**, 2598 (1986).

[66] Ph. Dugourd, J. Chevaleyre, J. P. Perrot, M. Broyer, *Jahn-Teller analysis of the Na_3 A state*, J. Chem. Phys. **93**, 2332 (1990).

[67] C. Negri, *Phonon-induced nonadiabatic rotating currents around nonchiral carbon nanotubes*, MSc Thesis 2010, Universitá degli Studi di Milano, `www.mi.infm.it/manini/theses/negriMag.pdf`.

[68] R. Englman, *The Jahn-Teller Effect in Molecules and Crystals* (Wiley, London, 1972).

[69] N. W. Ashcroft, M. D. Mermin, *Solid State Physics* (Holt-Saunders, Philadelphia, 1976).

[70] L. Gaudreau, A. S. Sachrajda, S. Studenikin, A. Kam, F. Delgado, Y. P. Shim, M. Korkusinski, P. Hawrylak, *Coherent transport through a ring of three quantum dots*, Phys. Rev. B **80**, 075415 (2009).

[71] M. Seo, H. K. Choi, S.-Y. Lee, N. Kim, Y. Chung, H.-S. Sim, V. Umansky, D. Mahalu, *Charge frustration in a triangular triple quantum dot*, unpublished, (2012).

[72] R. P. Feynman, F. L. Vernon Jr. , *The theory of a general quantum system interacting with a linear dissipative system*, Ann. Phys. **24**, 118 (1963).

[73] A. O. Caldeira, A. J. Leggett, *Quantum tunnelling in a dissipative system*, Ann. Phys. **149** 374 (1983).

[74] M. A. Schlosshauer, *Decoherence and the Quantum-To-Classical Transition* (Springer, 2007).

[75] L. Gaudreau, S. A. Studenikin, A. S. Sachrajda, P. Zawadzki, A. Kam, J. Lapointe, M. Korkusinski, P. Hawrylak, *Stability diagram of a few-electron triple dot*, Phys. Rev. Lett. **97**, 036807 (2006).

[76] D. V. Averin, K. K. Likharev, *Coulomb blockade of single-electron tunneling, and coherent oscillations in small tunnel junctions*, J. Low Temp. Phys. **62**, 345 (1986).

[77] T. A. Fulton, G. J. Dolan, *Observation of single-electron charging effects in small tunnel junctions*, Phys. Rev. Lett. **59**, 109 (1987).

[78] *Single Charge Tunneling*, Vol. 294 of NATO ASI Series B: Physics, edited by H. Grabert and M. Devoret (Plenum Press, New York, 1992).

[79] E. Ben-Jacob, Y. Gefen, *New quantum oscillations in current driven small junctions*, Phys. Lett. A **108**, 289 (1985).

[80] D. V. Averin, K. K. Likharev, *New results of the theory of SET and Bloch oscillations in small tunnel junctions*, IEEE Trans. Magn. **23**, 1138 (1987).

[81] K. K. Likharev, *Correlated discrete transfer of single electrons in ultrasmall tunnel junctions*, IBM J. Res. Dev. **32**, 144 (1988).

[82] D. Popović, C. J. B. Ford, J. M. Hong, A. B. Fowler, *Effect of quantum fluctuations of the environment on the Coulomb blockade in a single barrier*, Phys. Rev. B **48**, 12349 (1993).

[83] F. Pierre, H. Pothier, P. Joyez, N. O. Birge, D. Esteve, M. H. Devoret, *Electrodynamic dip in the local density of states of a metallic wire*, Phys. Rev. Lett **86**, 1590 (2001).

[84] T. T. Hongisto, A. B. Zorin, *Single-charge transistor based on the charge-phase duality of a superconducting nanowire circuit*, Phys. Rev. Lett. **108**, 097001 (2012).

[85] J. Haruyama, I. Takesue, Y. Sato, *Coulomb blockade in a single tunnel junction directly connected to a multiwalled carbon nanotube*, Appl. Phys. Lett. **77**, 2891 (2000).

[86] J. M. Martinis, R. L. Kautz, *Classical phase diffusion in small hysteretic Josephson junctions*, Phys. Rev. Lett. **63**, 1507 (1989).

[87] L. S. Kuzmin, Yu. V. Nazarov, D. B. Haviland, P. Delsing, T. Claeson, *Coulomb blockade and incoherent tunneling of Cooper pairs in ultrasmall junctions affected by strong quantum fluctuations*, Phys. Rev. Lett. **67**, 1161 (1991).

[88] A. N. Cleland, J. M. Schmidt, J. Clarke, *Charge fluctuations in small-capacitance junctions*, Phys. Rev. Lett. **64**, 1565 (1990).

[89] A. N. Cleland, J. M. Schmidt, J. Clarke, *Influence of the environment on the Coulomb blockade in submicrometer normal-metal tunnel junctions*, Phys. Rev. B **45**, 2950 (1992).

[90] L. S. Kuzmin, Yu. A. Pashkin, *Single electron tunnelling oscillations in a current-biased josephson junction*, Physica B: Condensed Matter **194**, 1713 (1994).

[91] W. Zheng, J. R. Friedman, D. A. Averin, S. Han, J. E. Lukens, *Observation of strong Coulomb blockade in resistively isolated tunnel junctions*, Solid State Commun. **108**, 839 (1998).

[92] P. Delsing, K. K. Likharev, L. S. Kuzmin, T. Claeson, *Time-correlated single-electron tunneling in one-dimensional arrays of ultrasmall tunnel junctions*, Phys. Rev. Lett. **63**, 1861 (1989).

[93] P. Delsing, T. Claeson, K. K. Likharev, L. S. Kuzmin, *Observation of single-electron-tunneling oscillations*, Phys. Rev. B **42**, 7439 (1990).

[94] K. K. Likharev, N. S. Bakhvalov, G. S. Kazacha, S. I. Serdyukova, *Single electron tunnel junction array: An electrostatic analog of the Josephson transmission line*, IEEE Trans. Magn. **25**, 1436 (1989).

[95] J. Bylander, T. Duty, P. Delsing, *Current measurement by real-time counting of single electrons*, Nature **434**, 361 (2005).

[96] K. K. Likharev, A. B. Zorin, *Theory of the Bloch-wave oscillations in small Josephson junctions*, J. Low Temp. Phys. **59**, 347 (1985).

[97] L. S. Kuzmin, D. B. Haviland, *Observation of the Bloch oscillation in an ultrasmall tunnel junction*, Phys. Rev. Lett. **67**, 2890 (1991).

[98] L. S. Kuzmin, *Experimental evidence for the autonomous Bloch oscillations in single Josephson junctions*, IEEE Trans. Magn. **3**, 1983 (1993).

[99] S. Corlevi, W. Guichard, F. W. J. Hekking, D. B. Haviland, *Phase-charge duality of a josephson junction in a fluctuating electromagnetic environment*, Phys. Rev. Lett. **97**, 096802 (2006).

[100] I. S. Beloborodov, F. W. J. Hekking, F. Pistolesi, *Influence of thermal fluctuations on an underdamped Josephson tunnel junction*, in *New Directions in Mesoscopic Physics (Towards Nanosciences)*, p. 339, R. Fazio, V. F. Gantmakher and Y. Imry ed., (Kluwer Academic Publishers, New York, 2003).

[101] M. Watanabe, D. B. Haviland, R. L. Kautz, *Control of the electromagnetic environment for single Josephson junctions using arrays of dc SQUIDs*, Supercond. Sci. Technol. **14**, 870 (2001).

[102] M. Watanabe, D. B. Haviland, *Coulomb blockade and coherent single-Cooper-pair tunneling in single josephson junctions*, Phys. Rev. Lett. **86**, 5120 (2001).

[103] S. Corlevi, W. Guichard, F. W. J. Hekking, D. B. Haviland, *Coulomb blockade of Cooper pair tunneling and parity effects in the Cooper pair transistor*, Phys. Rev. B **74**, 224505 (2006).

[104] F. Maibaum, S. V. Lotkhov, A. B. Zorin, *Towards the observation of phase locked Bloch oscillations in arrays of small Josephson junctions*, Phys. Rev. B **84**, 174514 (2011).

[105] J. S. Lehtinen, K. Zakharov, K. Yu. Arutyunov, *Coulomb blockade and Bloch oscillations in superconducting Ti nanowires*, arXiv:1209.4259.

[106] M. Ueda, *Probability-density-function description of mesoscopic normal tunnel junctions*, Phys. Rev. B **42**, 3087 (1990).

[107] M. Ueda, Y. Yamamoto, *Exact time-domain description of the crossover from random to Coulomb-regulated single-electron tunneling in ultrasmall normal tunnel junctions*, Phys. Rev. B **41**, 3082 (1990).

[108] M. Ueda, N. Hatakenaka, *Theory of mesoscopic tunnel junctions: From shot noise to the standard quantum limit*, Phys. Rev. B **43**, 4975 (1991).

[109] C. Negri, F. Pistolesi, *Charge fluctuations in single-electron tunneling oscillations*, Phys. Rev. B **85**, 115416 (2012).

[110] G.-L. Ingold, Yu. V. Nazarov, in *Single Charge Tunneling*, Vol. 294 of NATO ASI Series B: Physics, edited by H. Grabert and M. Devoret (Plenum Press, New York, 1992).

[111] C. Wasshuber, *Computational Single-Electronics* (Springer-Verlag, Wien, 2001).

[112] G. Schön, A. D. Zaikin, *Quantum coherent effects, phase transitions, and the dissipative dynamics of ultra small tunnel junctions*, Phys. Rep. **198**, 237 (1990).

[113] P. G. Kirton, A. D. Armour, M. Houzet, F. Pistolesi, *Quantum current noise from a Born-Markov master equation*, Phys. Rev. B **86**, 081305(R) (2012).

[114] C. Flindt, T. Novotný, A.-P. Jauho, *Current noise spectrum of a quantum shuttle*, Physica E **92**, 411 (2005).

[115] C. Emary, D. Marcos, R. Aguado, T. Brandes, *Frequency-dependent counting statistics in interacting nanoscale conductors*, Phys. Rev. B **76**, 161404(R) (2007).

[116] M. H. Devoret, D. Esteve, H. Grabert, G.-L. Ingold, H. Pothier, C. Urbina, *Observability of the Coulomb blockade in single tunnel junctions*, Physica B: Condensed Matter **165-166**, 977 (1990).

[117] S. M. Girvin, L. I. Glazman, M. Jonson, D. R. Penn, M. D. Stiles, *Quantum fluctuations and the single-junction Coulomb blockade*, Phys. Rev. Lett. **64**, 3183 (1990).

[118] J. S. Penttilä, Ü. Parts, P. J. Hakonen, M. A. Paalanen, *Effect of quantum noise on Coulomb blockade in normal tunnel junctions at high voltages*, Phys. Rev. B **61**, 10890 (2000).

[119] S. V. Panyukov, A. D. Zaikin, *Coulomb blockade and nonperturbative ground-state properties of ultrasmall tunnel junctions*, Phys. Rev. Lett. **67**, 3168 (1991).

[120] G. Falci, G. Schön, G. T. Zimanyi, *Unified scaling theory of the electron box for arbitrary tunneling strength*, Phys. Rev. Lett. **74**, 3257 (1995).

[121] X. Wang, H. Grabert, *Coulomb charging at large conduction*, Phys. Rev. B **53**, 12621 (1996).

[122] W. Hofstetter, W. Zwerger, *Single-electron box and the helicity modulus of an inverse square XY model*, Phys. Rev. Lett. **78**, 3737 (1997).

[123] D. S. Golubev, J. König, H. Schoeller, G. Schön, A. D. Zaikin, *Strong electron tunneling through mesoscopic metallic grains*, Phys. Rev. B **56**, 15782 (1997).

[124] G. Y. Hu, R. F. O'Connell, *Environmental effects on Coulomb blockade in a small tunnel junction: A nonperturbative calculation*, Phys. Rev. B **56**, 4737 (1997).

[125] J. König, H. Schoeller, *Strong tunneling in the single-electron box*, Phys. Rev. Lett. **81**, 3511 (1998).

[126] P. Joyez, D. Esteve, M. H. Devoret, *How is the Coulomb blockade suppressed in high-conductance tunnel junctions?*, Phys. Rev. Lett. **80**, 1956 (1998).

[127] D. Chouvaev, L. S. Kuzmin, D. S. Golubev, A. D. Zaikin, *Strong tunneling and Coulomb blockade in a single-electron transistor*, Phys. Rev. B **59**, 10599 (1999).

[128] X. Wang, R. Egger, H. Grabert, *Coulomb charging energy for arbitrary tunneling strength*, Europhys. Lett. **38**, 545 (1997).

[129] A. D. Zaikin, S. V. Panyukov, *Transport properties of mesoscopic tunnel junctions: nonperturbative analysis*, Phys. Lett. A **183**, 115 (1993).

[130] D. S. Golubev, A. D. Zaikin, *Quantum dynamics of ultrasmall tunnel junctions: Real-time analysis*, Phys. Rev. B **46**, 10903 (1992).

[131] H.-P. Breuer, F. Petruccione, *The Theory Of Open Quantum Systems*, Oxford University Press, Oxford, 2002.

[132] G.-L. Ingold, H. Grabert, *Finite-temperature current-voltage characteristics of ultrasmall tunnel junctions*, Europhys. Lett. **14**, 371 (1991).

[133] K. Flensberg, M. Jonson, *Quantum fluctuations and charging effects in small tunnel junctions*, Phys. Rev. B **44**, 7586 (1991).

[134] Yu. V. Nazarov, *Full counting statistics and field theory*, Annalen der Physik **16**, 15 (2007).

Controlling electron transport: quantum pumping and single-electron tunneling oscillations

Exploiting time-dependent effects to induce and control currents through mesoscopic and nanoscopic conductors is a major challenge in the field of quantum transport. In this dissertation we consider two nanoscale systems in which a current can be induced through intriguing mechanisms of coupling between excitations by external fields and electron transport. We first study a quantum pumping problem, analyzing the possibility to induce a DC response to an AC parametric driving through a three-site system in a ring configuration. We are interested in particular in the crossover between adiabatic and antiadiabatic driving regimes and in the presence of dissipation, which is accounted for by coupling with an external bath. We show that for a clever choice of this coupling the dissipative model admits a full analytical solution for the steady state current valid at arbitrary frequency, which allows us to fully understand the pumping-frequency dependence of the induced current. We then focus on a different current-controlling scheme exploiting the phenomenon of single-electron tunneling oscillations (SETOs). In this case, opposite to what happens for pumping, an AC effect, an almost periodic current of single electrons, arises through a tunnel junction circuit as a consequence of a DC bias. We study the zero-temperature noise spectrum of a tunnel junction in different resistive environments with the aim to determine the boundaries of the SETOs regime and quantify their quality in terms of periodicity. We then discuss the finite-temperature generalization and the possibility to account for the effects of quantum fluctuations.

Keywords: Quantum transport, quantum pumping, dissipative two-level system, single-electron tunneling oscillations, current fluctuations, Coulomb blockade, tunnel junction.

Contrôle du transport électronique: pompage quantique et oscillations tunnel à un électron

Exploiter des effets dépendants du temps pour induire et contrôler des courants à travers des conducteurs mésoscopiques et nanoscopiques est un enjeu majeur dans le domaine du transport quantique. Dans cette thèse, nous considérons deux systèmes de taille nanométrique pour lesquels un courant est induit grâce au couplage entre champs extérieurs dépendants du temps et le transport d'électrons. Nous étudions d'abord un problème de pompage quantique au sein d'un système à trois sites en configuration d'anneau, en considérant la possibilité d'induire un courant continu par modulation temporelle des paramètres de contrôle. Nous nous intéressons en particulier à la transition entre régime adiabatique et antiadiabatique en présence d'un mécanisme de dissipation modélisé par un couplage entre le système et un bain extérieur. Nous montrons que le modèle dissipatif admet une solution analytique complète valable pour la composante DC du courant à fréquence arbitraire. Ceci nous permet de bien comprendre comment le courant induit dépend de la fréquence de pompage. Nous nous concentrons ensuite sur un autre système de contrôle du courant exploitant le phénomène des oscillations tunnel á un électron (SETOs). Contrairement au cas précédent, ici la circulation d'un courant continu à travers un circuit comportant une jonction tunnel produit, pour le régime approprié, un courant quasi-périodique d'électrons. On étudie le spectre de bruit à température nulle d'une jonction tunnel dans différents environnements résistifs dans le but de déterminer les limites du régime des SETOs et de quantifier leur degré de périodicité. Nous généralisons par la suite les résultats à température finie et discutons des effets des fluctuations quantiques.

Mots-clefs: Transport quantique, pompage quantique, système dissipatif à deux niveaux, oscillations tunnel à un électron, fluctuations de courant, blockage de Coulomb, jonction tunnel.